Fall 10-21-2024

Ferroptotic Cardiomyocytes Regulate Angiogenesis in the Regenerative Mouse Heart after Myocardial Infarction through Direct and Indirect Mechanisms

Rebecca Stairey
Medical University of South Carolina

Ferroptotic Cardiomyocytes Regulate Angiogenesis in the Regenerative Mouse Heart after Myocardial Infarction through Direct and Indirect Mechanisms

Rebecca Ashley Stairley

A dissertation submitted to the faculty of the Medical University of South Carolina in partial fulfillment of the requirements for the Doctor of Philosophy in the College of Graduate Studies.

Department of Regenerative Medicine and Cell Biology

2024

Approved by:

Chairman, Advisory Committee

_____

Henry Sucov

Ge Tao

Kristine Deleon-Pennell

Russell Norris

Danyelle Townsend

ACKNOWLEDGEMENTS

This work and completion of this project would not have been possible without the guidance of Dr. Ge Tao, who took a chance by letting me into his lab. He helped me to develop resilience, independence, and confidence I will need to succeed as a scientist. I am truly grateful for the mentorship he provided me with during my time in his lab. Somewhere I also picked up his habit of classical music and tea during writing, which is most certainly healthier than the triple shot Frappuccinos I had been used to.

The members of my committee deserve acknowledgement for the support they provided:

Dr. Henry Sucov, the chair of my committee, I always describe as having high standards and a firm but fair attitude. He was always willing to provide advice and feedback not just for my scientific development, but for times I needed an outside perspective. I am grateful for his assistance, and for when he's reading this: Happy Monday!

Dr. Russell "Chip" Norris, who was my first introduction to the amazing research community at MUSC. Working for him before joining the program gave me an up close and personal look at the life of a PhD student. My time in his lab fostered the earlier stages of my career. Since then, he has continued to provide valuable feedback for my development as a scientist, along with encouraging words when they were sorely needed.

Dr. Kristine Deleon-Pennell, who introduced me to and guided me through the world of cardiac immunology when I had no idea what I was doing. She provided

direction I otherwise would not have had and shared resources, expertise, and advice on not just experimental design, but life and career advice. I found a real passion for the cardiovascular immune population thanks to her support.

Dr. Danyelle Townsend, who identified areas I was lacking in and provided training opportunities. She again gave insightful advice and a much-needed perspective when evaluating my progress, and suggested ways to improve. I always found her presence on my committee grounding as a voice of reason.

To my lab mates, Shuang Li, Allison, and Mary- we toughed out some really rough times together, and that made the highs that much better. I could always count on all of them to bounce ideas around, double check work, vent about research, and make grad school not just tolerable but enjoyable. They kept me sane and I have been so lucky to have them with me on this journey

None of this would have ever been possible without the support of my amazing family. My parents worked tirelessly for decades to provide me with the best education available and always encouraged my passion for science. My brother William, for always telling me how cool my work is and how smart I am for doing it exactly when I needed the encouragement. My family built me up, from the ground up.

And finally, my husband and the love of my life, Joey. I could not find a more supportive husband if I tried. He took over countless chores when I had late lab nights, cooked for me when I was too tired to cook for myself, let me cry on his shoulder when I needed too, and celebrated my successes with me. I can’t express with words how much

his love and support allowed me to get to this point. I could not have done this without him, simple as that.

TABLE OF CONTENTS

List of Figures

List of Abbreviations

accidental cell death (ACD)
acute ST-segment elevation myocardial infarction (STEMI)
Acyl-CoA synthetase long-chain family member 4 (ACSL4)
arachidonate lipoxygenase 15 (ALOX-15)
arachidonic acid (AA)
arginase 1 (Arg1)
arginase 1 (Arg1)
Cardiovascular diseases (CVDs)
CD206
CD86
chitinase-like 3 (Chil3, or Ym1)
cleaved caspase 3 (cCas3)
congenital heart disease (CHD)
coronary artery disease (CAD)
danger-associated molecular patterns (DAMPs)
deferoxamine (DFO)
diphtheria toxin A (DTA)
divalent metal transporter 1 (DMT1, or SLC11A2)
Electron transport chain (ETC)
Endomucin (EMCN)
Endoplasmic Reticulum (ER)
endothelial–mesenchymal transition (EndMT)
Endotoxin-induced myocardial dysfunction (EIMD)
F4/80
Ferric iron(Fe^{3+})
ferritin heavy chain 1 (FTH1)
ferritin light chain (FTL)
ferrous (Fe^{2+})
from postnatal day 1 (P1) to postnatal day 7 (P7)
glutaredoxin (GRX)
glutathione peroxidase (GPXs)
heme oxygenase 1 (HO-1)
heme oxygenase-1 (HMOX-1)
heme oxygenase-1 (HO-1)
Human induced pluripotent stem cells (iPSCs)
hypoxia inducible factor 1 alpha (HIF1-alpha)
interferon gamma (IFNy)
Interleukin-12 (IL-12)
Interleukin-19 (IL-19)
Interleukin-20 (IL-20)
Interleukin-22 (IL-22)
iPSC-derived cardiomyocytes (iCMs)

left anterior descending coronary artery ligation (LAD-O)
Ly6C
mitogen-activated protein kinase (MAPK)
monocyte chemoattractant protein (MCP)
myocardial infarction (MI)
NADPH Oxidase (NOX)
nitric oxide (NO)
percutaneous coronary intervention (PCI)
peripheral artery disease (PAD)
phosphatidylserine (PtdSer)
polyunsaturated fatty acids (PUFAs)
Polyunsaturated fatty acyl moieties (PUFAs)
regulated cell death (RCD)
sarcoplasmic/endoplasmic reticulum calcium ATPase (SERCA)
serum uric acid (SUA)
superoxide dismutases (SODs)
thioredoxin (TRX)
transferrin receptor 1 (Tfr1)
tumor necrosis factor (TNF)
vascular endothelial growth factor (VEGF)
xanthine oxidase (XO)

REBECCA ASHLEY STAIRLEY. Ferroptotic Cardiomyocytes Regulate Angiogenesis in the Regenerative Mouse Heart after Myocardial Infarction through Direct and Indirect Mechanisms (Under the direction of GE TAO)

ABSTRACT

Cardiovascular diseases (CVDs) are the leading cause of death in the United States, and heart attack occurs every 40 seconds in the US. A myocardial infarction (MI), or heart attack, results in ischemic injury and cardiomyocyte (CM) death. Mature mammalian CM renewal in the heart is insufficient to repopulate the lost tissue. However, the neonatal mouse heart retains its regenerative capacity through the first week of life, providing a valuable model to identifying regenerative factors.

Recent work by our lab revealed that the main mechanism of CM death in the heart post-MI is ferroptosis. In this study, we investigate the effects of ferroptosis by subjecting regenerative postnatal day 1 (P1) and non-regenerative postnatal day 7 (P7) mice to permanent left anterior descending coronary artery occlusion (LAD-O) and treatment with Ferrostatin-1 (Fer-1), a commercially available ferroptosis inhibitor. Echocardiography and histology revealed impaired cardiac function accompanied by an insignificant increase in infarct size. Immunostaining showed decreased endothelial cell (EC) density alongside reduced macrophage infiltration and M2 polarization. Flow cytometry of ventricular tissue confirmed the macrophage phenotype.

To elucidate CM-derived signaling, we differentiated human induced pluripotent stem cells (hiPSCs) into CMs (iCMs). iCMs were exposed to either Erastin or Staurosporine to induce ferroptosis or apoptosis. Human umbilical vein endothelial cells (HUVECs) were treated with conditioned media from treated iCMs for assays

characterizing survival, migration, proliferation, and tube formation. HUVECs treated with conditioned media from ferroptotic iCMs exhibited increased survival and angiogenic activity over apoptotic iCM conditioned media treated HUVECs.

Cytokine array analysis allowed characterization of the ferroptotic iCM secretome, leading to the identification of a potential mechanism involving interleukin-19 (IL-19). We utilized computational modeling of publicly available single-cell RNA sequencing data to predict signaling networks between subpopulations of CMs, ECs, and macrophages that included IL-19. Further, IL-19 administration in P7 LAD-O mice lead to improved EC density and proliferation in the infarct, decreased CM ferroptosis, and improved cardiac function.

This project has led to a better understanding of the beneficial effects ferroptotic cardiomyocytes exert on cardiac remodeling after MI, and the role that regulated CM death plays on the wound healing process.

Introduction

1.1 Myocardial Infarction and Heart Failure

Cardiovascular diseases (CVDs) are the leading cause of death in the United States, with a heart attack occurring every 40 seconds [1,2]. CVDs are a broad category of heart diseases that includes coronary artery disease (CAD), congenital heart disease (CHD), peripheral artery disease (PAD), heart failure, arrythmias, stroke, and myocardial infarction, or heart attack (MI)[3]. CVDs contribute heavily to both premature mortality and rising health care costs, representing a national economic burden of over $400 billion [1,3]. Globally, ischemic heart disease has remained the number one cause of death for decades [4]. Risk factors associated with CVDs include hypertension, diabetes, high cholesterol, obesity, inadequate sleep and/or physical activity, tobacco use, and poor diet[5]. Many of these risk factors are behavioral, environmental, or social[3]. The prevalence of these risk factors is unfortunately projected to increase markedly over the next several decades[5].

MI is predominantly caused by a rupture of an atherosclerotic plaque that results in clot formation in the coronary arteries[6]. Therapies such as percutaneous coronary intervention (PCI) and thrombolytic therapy have led to improved outcomes, but pose their own unique challenges[6]. For example, thrombolytic therapy is associated with increased risk of bleeding complications[6]. Similarly, PCI may present logistical challenges associated with delays in obtaining medical attention[6]. The timing of PCI is also still under scrutiny. One trial documented that a delay of 4-16 hours can be introduced to the clinical PCI protocol in order to prevent no-reflow complications[7], while another documented the opposite and reported increased mortality in PCI delays

greater than 1 hour[8]. More recently, a third study reported no significant difference in major adverse cardiovascular events over a 6-month period between delayed and immediate PCI patients [9]. These discrepancies highlight how urgently new therapies are needed that go beyond current myocardial injury mitigation strategies.

During an MI, blood flow is first occluded to the cardiac muscle tissue, and clinical standards are to re-perfuse the hypoxic tissue as quickly as possible to mitigate damage[10]. This rapid reoxygenation causes a burst of ROS production, resulting in further damage and cardiomyocyte death[11]. This type of ischemia/reperfusion injury, or I/R injury, is a major hurdle that promotes cardiomyocyte death and strongly affects patient prognosis [11]. Mature human cardiomyocytes are unable to regenerate following injury due to the low annual turnover of between 0.2-2% in adults [12]. This limitation prevents recovery for MI patients in the truest sense, as lost cardiomyocytes cannot be replaced to support cardiac function (Figure 1.1). Thus, inducing cardiomyocyte regeneration after injury represents one of the ultimate goals of cardiovascular research.

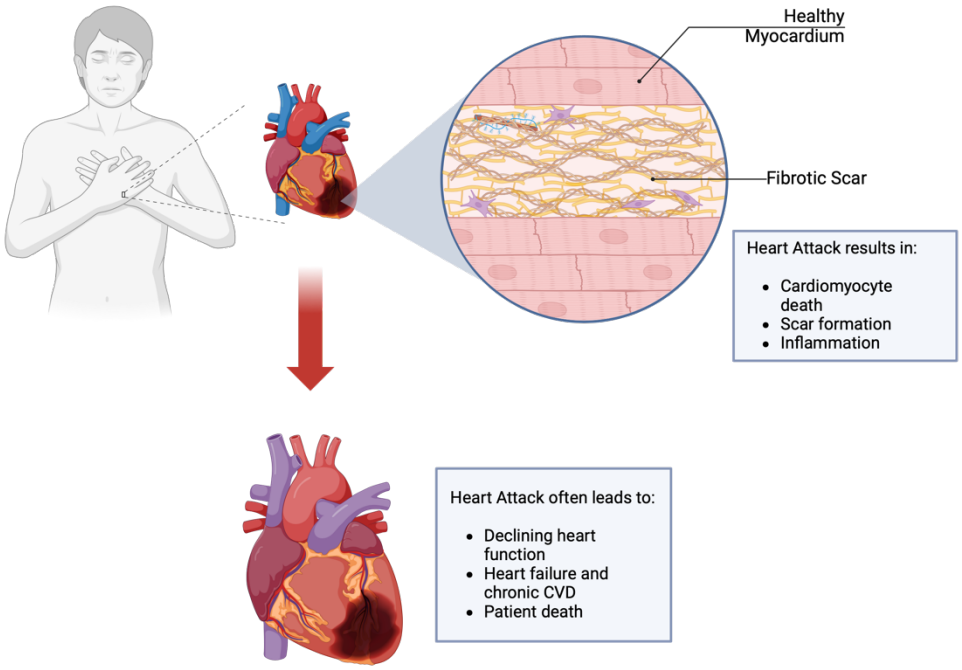

Figure 1.1 MI leads to heart failure. A heart attack occurs in the US every 40 seconds. Lack of cardiomyocyte proliferation after an MI leads to deposition of fibrotic ECM to prevent cardiac rupture but compromises cardiac function, often leading to heart failure.

1.2 Models of Cardiac Regeneration

Cardiac regeneration in zebrafish was first described in 2002 with the apical resection model, and as a popular model species for studying cardiac injury, it has since progressed to include other injury types[13]. While the adult zebrafish can completely regenerate resected myocardium without scar formation through cardiomyocyte proliferation[14], the zebrafish heart is morphologically and functionally distinct from the mammalian heart[15]. The two-chamber zebrafish heart is more anatomically similar to the embryonic, pre-septation mammalian heart than the fully developed four chamber mammalian heart[15]. This two-chamber structure results in the mixing of arterial and venous blood[13]. Zebrafish hearts have much lower pressure than the mammalian heart, which increases the feasibility of the resection model[13]. It should also be noted that the hypoxic zebrafish environment likely accounts for a substantial portion of their ability to regenerate cardiac tissue, as hypoxia has been shown to promote cardiac proliferation[13].

While these anatomical differences are significant, the zebrafish remains a useful tool for studying cardiac regeneration in a mature heart where growth and development have essentially ceased [14]. When apex resection is performed and approximately 20% of the ventricular myocardium is surgically removed from an adult zebrafish, the surgical hearts were indistinguishable from the control hearts by one week following the procedure[14]. Initially, a blood clot forms at the site of resection, but is replaced by fibrin, reaching intensity around one week post procedure[14]. Between this time point and 30 days post procedure, myofibers penetrate and replace

the fibrin and reform the muscle wall, with the fibrin clot being completely replaced by healthy, functional muscle tissue by 60 days post procedure[14]. Proliferation rates increase from a baseline of 3% in uninjured hearts to up to 32% in the resected hearts, peaking at 14 days post procedure[14]. Beyond the zebrafish model of apex resection, cryoinjury and genetic ablation were also introduced[13]. The cryoinjury model more accurately reflects cardiac injury in humans in the initial stages, with a large amount of cell death followed by a fibrotic scar; however, this scar is replaced by functional myocardium, although this process takes up to 180 days[13,16]. This suggests that the presence of a fibrotic scar itself is not sufficient to prevent cardiomyocyte proliferation in zebrafish, a mechanism that might be leveraged to develop strategies for similar regeneration in mammalian hearts[13]. Genetic ablation in the zebrafish model is carried out via tamoxifen-inducible Cre-recombinase under the cardiomyocyte specific promoter *cmcl2* to remove a *loxP* -flanked STOP cassette and thusly express cytotoxic diphtheria toxin A (DTA) upon tamoxifen administration[17]. Using this model cardiomyocyte-specific cell death is performed, removing otherwise healthy cardiomyocytes without primary to other cell types in the heart. This model is most useful for investigating cardiomyocyte proliferation in the context of cell signaling derived from non-myocyte populations in the heart, rather than inflammation or specific types of cell death, such as necrosis, apoptosis, etc[13].

The neonatal mouse model of cardiac injury, which was first demonstrated to possess a potent regenerative capability following apical resection in 2011, is more analogous to the human heart and remains one of the more prevalent animal models in

the field of cardiovascular regeneration[13]. Like the zebrafish model, cryoinjury has also been utilized in the neonatal mouse heart, which was again able to regenerate with the stipulation that more severe transmural cryoinjuries result in incomplete regeneration[13,18]. This upper threshold on the injury severity for complete regeneration was again reported in the apical resection model, with studies showing resection of less than 15% of heart tissue results in complete regeneration while resection of 30% of heart tissue or greater results in incomplete regeneration[13,19,20]. Complete regeneration has since been demonstrated in the left anterior descending coronary artery ligation (LAD-O) model, which is more clinically relevant as it closely mirrors the ischemic injury suffered by myocardial infarction patients[13].

While the LAD-O model is more clinically relevant, it comes with the hurdle of variation of the surgical technique resulting in discrepancies in the severity of the ischemic injury that must be accounted for experimentally[13]. Further complicating neonatal mouse model is the aptly termed “regenerative window”, of which the current consensus has established exists from postnatal day 1 (P1) to postnatal day 7 (P7), with P7 mice exhibiting a similar fibrotic injury seen in adult mice[13,19,21]. Studies repeatedly confirm that the P1 mouse is regenerative, but for how long this ability persists and why remains a topic of debate[13]. Apex resection in P1 mice is variable, resulting in waves of immune infiltration, CM proliferation, fibrosis, and thorough remodeling that ultimately alters as well as restores ventricular physiology that is evident based on restored cardiac function combined with cardiac hypertrophy[22]. Apex resection in P2 mice is poorly tolerated compared to P1 mice and results in a fibrotic response, even when the

severity of the resection is controlled for[19,20]. These models are summarized in figure 1.3. This timeline correlates with the conversion from anaerobic glycolysis to oxidative phosphorylation that neonatal mice undergo immediately following birth as they switch from the low oxygen environment of the womb to the high oxygen environment outside of the womb[13,23]. This sudden rush of reactive oxygen species is thought to be largely responsible for cell cycle arrest and inhibition of cardiac regeneration, which was supported by studies showing that the switch from hyperplastic to hypertrophic cardiomyocyte growth was at least partially mediated by reactive oxygen species activity[13,17,23].

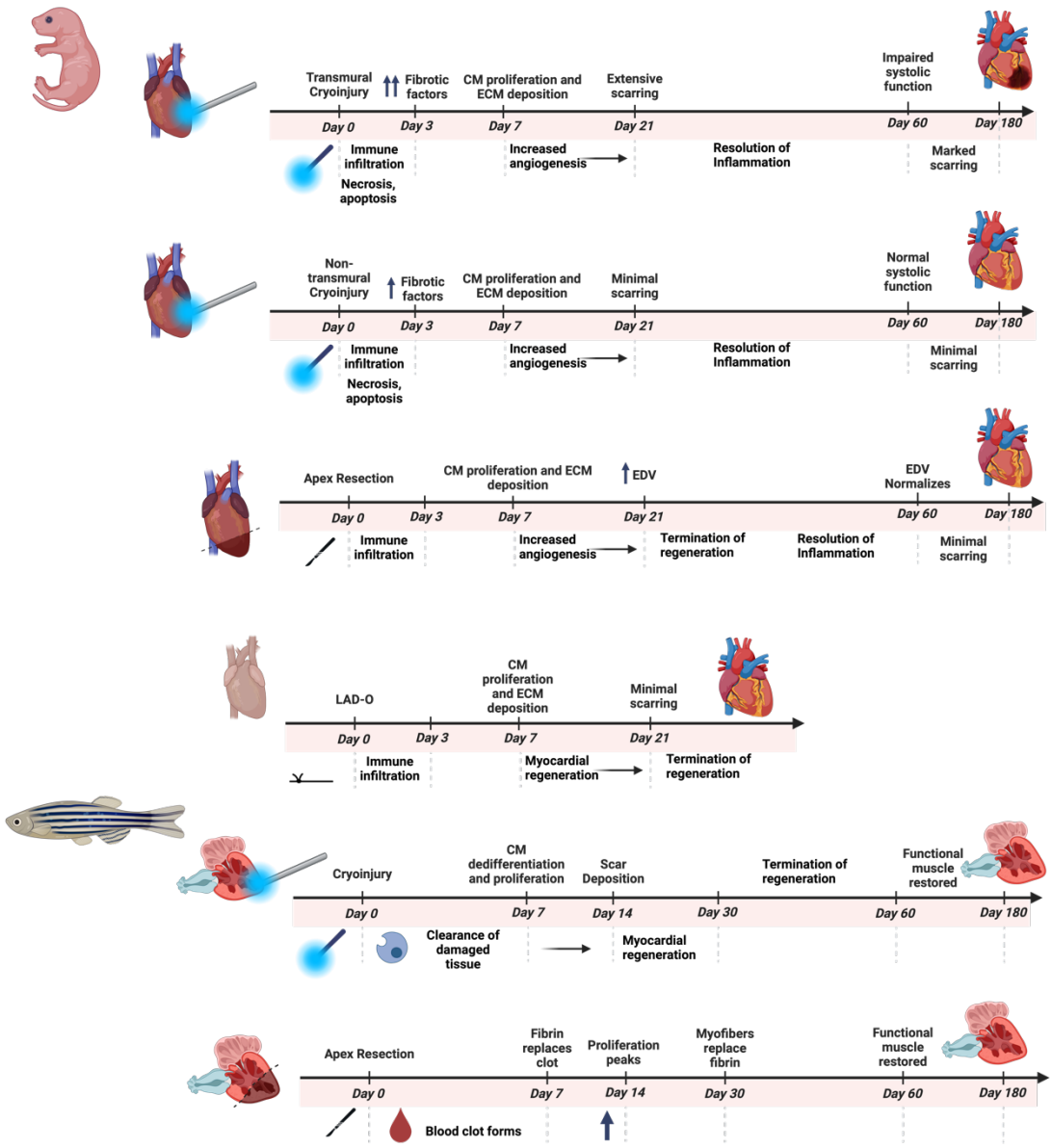

Figure 1.2 Models of cardiac regeneration. Despite its 2-chamber heart, the zebrafish model of regeneration is often utilized with the apex resection and cryoinjury models. When apex resection is performed and approximately 20% of the ventricular myocardium is surgically removed the surgical hearts were indistinguishable from the control hearts by one week following the procedure. Cryoinjury more accurately reflects injury in the human adult heart but takes up to 180 days to fully heal. The mouse heart is more anatomically similar to the human heart, although the ability of the neonatal murine heart to regenerate is both short-lived and highly variable depending on the severity of the injury.

1.3 Reactive Oxygen Species

Reactive Oxygen Species, or ROS, are reactive molecules that are naturally produced by living cells, usually as byproducts of aerobic metabolism [24,25]. ROS comprise a majority of common oxidants in cells and include free radicals such as superoxide (O_2^-), non-radicals such as hydrogen peroxide (H_2O_2), lipid peroxides (ROOH), and the corresponding hydroxyl (HO^-) and peroxyl (ROO^-) radicals. [26,27]. In healthy cardiac muscle tissue, ROS are largely generated by mitochondria, as well as xanthine oxidase (XO), and NAPDH oxidase (NOX)[28]. Cardiomyocytes have a very energy cost, and the heart consumes around 8% of total ATP consumption as the most metabolically active organ in the body[29]. As such, cardiomyocytes are very mitochondrial dense[29]. Mitochondrial ROS production is dependent on the membrane potential, and increased ROS production in cardiomyocytes is likely to be linked to compromised membrane potential or depletion of the NADPH pool[29]. Other organelles are similarly able to generate ROS, including but not limited to the sarcoplasmic reticulum, the endoplasmic reticulum, peroxisomes, and plasma membranes [25]. The physiological processes of healthy cells also produce ROS. NOX formation, arachidonic acid (AA) metabolism, and enzymatic activity of nitric oxide (NO) and xanthine oxidase (XO) are other major sources of ROS[25]. XO functions to oxidize xanthine to produce superoxide and uric acid[30].

Typically, ROS are kept at physiological levels by endogenous antioxidant defense systems[17,29]. Nuclear factor erythroid 2-related factor 2 (Nrf2), transcription

factor and master regulator of the antioxidant response, is bound by Keap1 to promote ubiquitination and degradation and prevent hyperactivation of antioxidants[31]. Upon induction of oxidative stress, Nrf2 is released from the degradation complex and translocates to the nucleus to activate transcription of antioxidant genes[31]. ROS can also induce activation of nuclear factors kappa-light-chain-enhancer of activated B cell (NF-kB), which influences DNA transcription[25]. Downstream effects of these regulators of the antioxidant response include catalases, glutathione peroxidase (GPXs), heme oxygenase 1 (HO-1), and superoxide dismutases (SODs)[25]. Superoxide is rapidly scavenged by various SODs, including cytosolic, mitochondrial, and extracellular SODs, to generate H_2O_2, which is then available for conversion to H_2O by catalases, glutathione peroxidases (GPXs), and peroxiredoxins (PRXs)[26]. Three types of SODs have been identified based on their location in the cell, with SOD1 in the cytoplasm, SOD2 in the mitochondria, and SOD3 in the extracellular space[25]. SOD1, the most common and therefore most studied isoform, uses Cu-Zn cofactors to scavenge superoxide[25]. The copper is cycled through the following reduction-oxidation reaction[25]:

Reduction: $Cu^{2+}Zn^{2+}SOD + O_2^- \rightarrow Cu^{+}Zn^{2+}SOD + O_2$

Oxidation: $Cu^{+}Zn^{2+}SOD + O_2^-(+2H^+) \rightarrow Cu^{2+}Zn^{2+}SOD + H_2O_2$

Overall:

$$2O_2^-(+2H^+) \xrightarrow{SOD} O_2 + H_2O_2$$

Therefore, a copper chelator can inactivate SOD by removing the copper from the active site[25]. GPXs, a family consisting of GPX1-8, are responsible for scavenging hydrogen peroxide and are most active within the aqueous areas of the cell[25,32]. GPX4 is the only GPX that directly reduces lipid peroxides, using reduced glutathione as a cofactor and converting it to oxidized glutathione[32]. Through these mechanisms, the balance of ROS in the cell is maintained, preventing oxidative damage.

Lipid peroxides are highly reactive and can propagate further generation of ROS, resulting in accumulation of lipid peroxides that compromise the integrity of cellular membranes if left unchecked[27]. Cellular membranes are vulnerable to oxidative damage and are composed of a phospholipid bilayer, where the hydrophilic heads are oriented towards the aqueous interior and exterior of the cell and the hydrophobic tails comprise the inner layer of the membrane[33]. Polyunsaturated fatty acyl moieties (PUFAs) incorporated in phospholipids are specific sites of iron-dependent oxidation due to their readily abstractable bis-allylic hydrogens[34]. There have been contrasting reports published on whether or not lipid peroxidation of the membrane results in increased membrane permeability and resultant loss of membrane integrity[35,36]. Lipid molecular dynamics simulations suggest that the migration of the hydroperoxide site towards the hydrophilic region of the membrane is responsible for expansion of the lipid and subsequent decrease in membrane thickness[36]. Models have also shown that while alteration of the mechanical and structural membrane properties following lipid peroxidation is inevitable, but the changes are oxidation site-dependent[36]. The

membrane will expand regardless of the oxidation site, but C12 and C15 peroxidation will soften the membrane, where C5 and C8 peroxidation will increase membrane rigidity[36]. This is likely due to the location of C12 and C15 being nearer to the hydrophobic interior of the bilayer, where peroxidation destabilizes the membrane, and C5 and C8 being nearer to the membrane-water interface[36] (**Figure 1.3**).

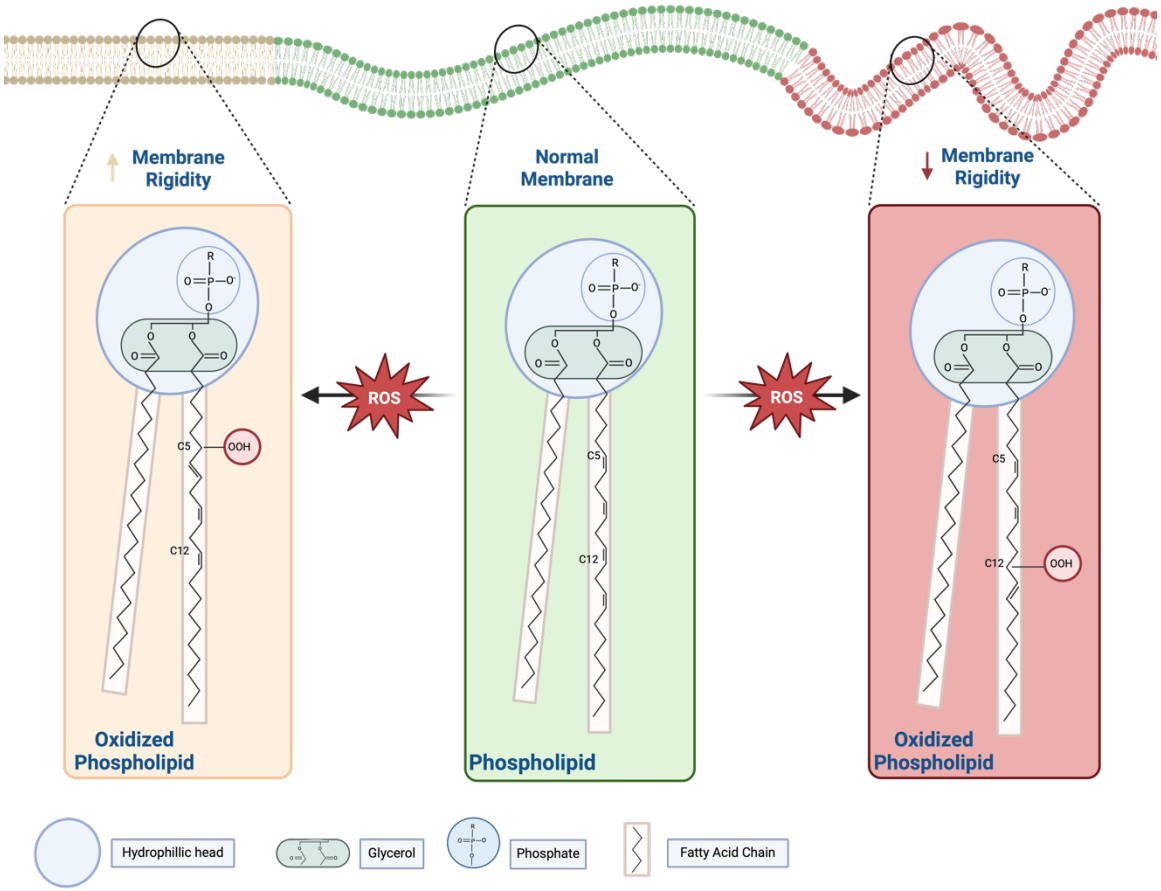

Figure 1.3 Oxidation of phospholipids can compromise membrane function. Depending on the location of the peroxidation, membrane fluidity may be affected differently. As membrane structure is inherently connected to its function, excessive lipid peroxidation can compromise and kill a cell if not countered by antioxidant mechanisms in a timely manner.

ROS are capable of causing other types of damage within the cell beyond loss of membrane integrity and can also degrade into smaller compounds that result in protein and DNA damage[27,31]. Under physiological conditions, ROS oxidation of the thiolate anion to sulfenic acid and subsequent formation of disulfide bonds are reversable by disulfide reductases thioredoxin (TRX) and glutaredoxin (GRX)[26]. During periods of oxidative stress, however, irreversible hyperoxidation of cysteine residues can occur, permanently altering protein function[26]. Protein modification, such fragmentation, cross-linking, and denaturation, as potential consequences of oxidative stress on amino acids[25]. Aromatic or Sulphur containing molecules are more sensitive to oxidation, and guanine is more susceptible to oxidation that results in DNA damage[25].

The consequences of oxidative damage have been a topic of interest in many diseases, and many attempts have been made to decrease ROS therapeutically. Increased ROS alters calcium handling in heart failure through modification of micro RNAs that lead to the inhibition of the sarcoplasmic/endoplasmic reticulum calcium ATPase (SERCA) 2a transcription[29]. Major sources of ROS in the heart include the mitochondria, NOX formation, arachidonic acid (AA) metabolism, and enzymatic activity of nitric oxide (NO) and xanthine oxidase (XO). Mitochondria dysfunction during oxidative stress may be due to disruptions in the membrane phospholipids that disturb the electron transport chain (ETC)[29]. Inner mitochondrial membrane phospholipid cardiolipin, which is essential for ETC activity, membrane transporters, mitochondrial iron homeostasis, and ROS production[29], is redistributed to the outer mitochondrial

membrane upon oxidation, resulting in formation of mitochondrial pores that trigger cell death in cardiomyocytes[37]. Left untreated, this eventually progresses to cardiac dysfunction as an early stage complication of Endotoxin-induced myocardial dysfunction (EIMD)[37]. XO oxidizes xanthine to produce superoxide and uric acid[30], the latter of which is upregulated in heart failure, making serum uric acid (SUA) a prognostic marker and XO an attractive target for pharmaceutical intervention[30]. However, while XO inhibitors seemed promising based on preclinical data, there have been obstacles in clinical trials[30]. XO inhibitor Allopurinol consistently demonstrated no benefit over placebo groups in at least 4 separate heart failure clinical trials, while XO inhibitor Oxypurinol produced mixed results[30]. At a dose of 600 mg/day, Oxypurinol produced an improvement in secondary outcomes such as ejection fraction, but still did not report consistent improvements in primary outcomes[30]. While it has been theorized that this apparent disconnect is caused by the interconnected nature of the nitroso-redox pathways, it is equally like likely that inhibiting ROS production significantly impacts the surrounding tissue more than originally thought. Supporting this concept is the continued lack of evidence from ROS scavenging compounds in repeated heart failure clinical trials[29]. While it could also be argued that the lack of benefit is due to poor bioavailability of tested ROS scavenging compounds[29], the body of research to date suggests that there is an ideal concentration of ROS for optimal function that is disrupted when either ROS production or antioxidant activity out paces the other.

While they have been traditionally considered negative due to their involvement in various diseases, ROS have more recently been shown to have crucial roles in

beneficial and necessary signaling pathways[29]. They have become more prevalent in a variety of research subjects, including cancer signaling, neurodegenerative disorders, and aging[24]. Lower levels of ROS are known to be beneficial in many contexts, including transient sympathetic drive, preconditioning paradigms, mitochondria quality control, and exercise[29]. Exercise training, for example, is known to modify cardiac antioxidant activity and improve quality of life in heart failure patients, but this benefit can be negated with the addition of high doses of ROS scavengers, such as vitamin C or E[29]. In both experimental and clinical trials, antioxidant administration has yielded mixed results[28]. Another example is angiogenesis, the process of new blood vessel formation to revascularize tissues, occurs in response to various growth factors [26]. In response to hypoxia, ischemic tissues produce ROS that stimulate vascular endothelial growth factor (VEGF) production from various cell types, including macrophages and fibroblasts [26]. This ROS-induced VEGF expression stimulates proliferation and migration of endothelial cells[26]. Similarly, H_2O_2 produced by endothelium are required for neovascularization following ischemic injury[26]. ROS interact with mitogen-activated protein kinase (MAPK), resulting in increased expression VEGF [38], further highlighting the complex nature of ROS signaling.

During an MI, blood flow is first occluded to the cardiac muscle tissue, and clinical standards are to re-perfuse the hypoxic tissue as quickly as possible to mitigate damage[10]. This rapid reoxygenation causes a burst of ROS production, resulting in further damage and cardiomyocyte death[11]. This type of ischemia/reperfusion injury, or I/R injury, is a major hurdle that promotes cardiomyocyte death and strongly affects

patient prognosis [11]. However, ROS damage does not only occur upon reperfusion. ROS have been shown to accumulate quickly at the onset of cardiac ischemia-reperfusion injury [28] [24]. A rapid increase in superoxide production was observed within minutes of the onset of ischemia in the rodent heart [39]. Oxymyoglobin was identified as a source of superoxide generation[40], but multiple mechanisms for ROS generation during ischemia have been identified or postulated. An increase of succinate in the heart during ischemia of rat hearts was reported[41], and this increase was supported in further mouse studies[42]. Succinate accumulation was localized to ischemic regions of the heart and levels were proportional to the duration of ischemia[42], driven by reversal of succinate dehydrogenase that reduces fumarate to succinate[43]. Succinate-driven reverse electron transport of the mitochondria then results in increased superoxide production upon reperfusion by acting as a terminal electron sink [24,43]. Inhibition of succinate dehydrogenase reduced ROS production after ischemia-reperfusion injury [43], further supporting this mechanism. During the period of ischemia, electron carrier pools such as NADH and Coenzyme Q and other redox active enzymes become highly reduced, while the mitochondria become more damaged[44]. Residual oxygen from myoglobin combined with electron leakage of the mitochondrial electron transport chain facilitates production of superoxide[39,45]. The damaged mitochondria are then primed for further oxidative damage upon reperfusion, during which oxygen is quicky reintroduced[24,28,42]. It has also been shown that periods of hypoxia trigger an increase in ferrous iron in the ER and lipid peroxidation via arachidonate lipoxygenase 15 (ALOX-15) in response to heme oxygenase-1 (HMOX-1) in

the myocardium, both of which further prime the cell for a burst of damage upon reperfusion[11].

Clinical standards for treating ischemic tissues are to restore blood flow to resolve the initial injury; however, this reperfusion itself exacerbates the tissue injury caused by ischemia[38]. The specific type of injury caused by restoring blood flow to ischemic tissues is termed ischemia-reperfusion injury [38]. While the initial ischemia will cause accumulation of ROS and necrosis if left untreated, the reperfusion itself may cause more tissue damage than the period of ischemia already had [46]. During reperfusion, the reintroduction of oxygen is itself a large source of oxidation that results in the production of large quantities of ROS [38]. This rapid increase of oxygen and nutrients also drives oxidative metabolism and increases mitochondrial function[46]. However, ischemia-induced mitochondria membrane and ETC damage increases the likelihood that electrons may “slip” nonspecifically to generate superoxide, which would be a large source of ROS production upon reperfusion[46]. Additionally, cardiolipin is both highly sensitive to peroxidation and increasingly oxidized during reperfusion, causing mitochondrial membrane damage that promotes further ETC damage in a ROS-induced ROS production cycle[46,47]. Left unchecked, damage resulting from ROS accumulation can culminate in ferroptosis, a type of regulated cell death[48].

1.4 Regulated Cell Death

Many types of regulated cell death (RCD) have been implicated in cardiovascular disease[49]. RCD differs from accidental cell death (ACD) in that it is regulated by signaling cascades and represent a measured response to maintain order in the surrounding environment[50]. Therefore, understanding the mechanisms that govern each type is crucial to understanding their contributions to disease progression. It was previously assumed that most, if not all, RCD in mammalian cells resulted from apoptosis; however, among the currently known types of RCD, some of the most commonly studied types include apoptosis, necroptosis, and more recently, ferroptosis[50,51].

Apoptosis was initially described in the context of insect development and has since been implicated as a key factor in development and homeostasis[50,52]. Apoptotic cells exhibit characteristics of blebbing and shrinkage, during which the chromatin is condensed, DNA is fragmented into nucleosomal units, and phosphatidylserine (PtdSer) is exposed on the cell surface[50,52]. These cells are then targeted for efferocytosis by macrophages that identify apoptotic cells by the PtdSer signal that has been exposed on the outer surface of the cell membrane[52]. Two distinct apoptosis-initiating pathways have been identified; the intrinsic and extrinsic signaling pathways[49,52]. The intrinsic pathway, also referred to as the mitochondrial or Bcl-2 mediated pathway, is triggered as a consequence of genotoxic agents, cytokine withdrawal, or developmental cues[52]. These events result in the oligomerization of Bax/Bak which trigger the mitochondria to release pro-apoptotic cytochrome c, resulting in the cleavage of procaspase 9 to caspase

9[49,52]. Caspase 9 activates caspase 3, which cleaves over 1,300 substrates to execute apoptotic cell death[52]. The extrinsic pathway, also called the death receptor pathway, is triggered by external death factors of the tumor necrosis factor (TNF) family, such as FasL, Fas Ligand, TNF-alpha, TRAIL, and TNF-related apoptosis-inducing ligand[49,52]. In cardiomyocytes, these factors trigger a similar signaling cascade that culminates in caspase 8 cleaving and activating caspase 3[49,52]. Studies have shown that decreasing expression of apoptotic signaling proteins, namely Bcl-2 and caspase 3, improves cardiac function in models of I/R, highlighting that myocardial apoptosis can have deleterious effects on cardiac function[49]. Interestingly, it has been shown in glioma cell models of cancer that Ampelopsin, a flavonoid shown to alter tubulin handling in the cell, triggers apoptosis through ROS generation[50,53]. Research has also discovered a timeline of RCD and demonstrated that not only does ferroptosis occur before apoptosis, but that ferroptosis promotes susceptibility to apoptosis, suggesting a strong connection between apoptosis and ferroptosis [54].

1.5 Ferroptosis, Inhibitors, and Ferrostatin-1

Ferroptosis is a type of regulated cell death that was first identified in 2012 by the Stockwell lab and is characterized by the iron-dependent accumulation of cytotoxic lipid peroxides[51]. Oxidized lipids may occur though enzymatic activity or spontaneously[27]. Spontaneous lipid peroxide formation, or Fenton chemistry, is catalyzed by labile iron[27]. Therefore, regulators of iron homeostasis, antioxidants, and lipid synthesis are all key players in ferroptotic pathways. Ferric (Fe^{3+}) iron binds to

transferrin and is then imported into the cardiomyocyte via transferrin receptor 1 (Tfr1)[55]. Ferric iron is then reduced to ferrous (Fe^{2+}) iron in the endosome and released from the endosome by divalent metal transporter 1 (DMT1, or SLC11A2)[55]. Excess iron is sequestered by an iron storage protein complex comprised of ferritin light chain (FTL) and ferritin heavy chain 1 (FTH1)[55]. Increased TfR1 expression results in iron accumulation that triggers ferroptosis[56], whereas ferroptosis can be suppressed with iron chelator deferoxamine (DFO)[51]. Labile iron reacts with ROS to produce oxidative damage, which is mitigated utilizing antioxidants. GPX4 is the only GPX that directly reduces lipid peroxides, using reduced glutathione as a cofactor and converting it to oxidized glutathione[32]. Reduced glutathione is imported into the cell via System Xc, a cystine/glutamate antiporter[55]. Small molecular compound Erastin can induce ferroptosis pharmacologically by inhibiting System Xc and preventing its import of reduced glutathione, depleting the intracellular pool and preventing GPX4 activity[32,55,57]. Acyl-CoA synthetase long-chain family member 4 (ACSL4) is required or ferroptosis, as it synthesizes the polyunsaturated fatty acids (PUFAs) that are converted to lipid peroxides[58] (**Figure 1.4).**

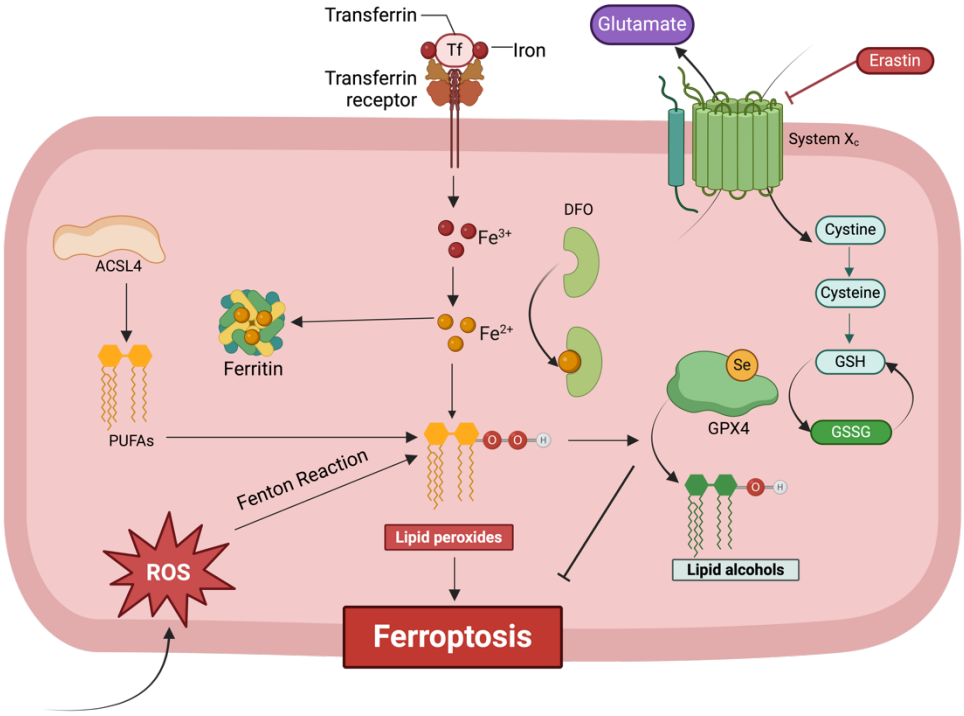

Figure 1.4 Key regulators of ferroptosis. Ferroptosis is characterized by the accumulation of both intracellular iron and ROS that culminates in cell death and can be suppressed by iron chelating agents such as deferoxamine (DFO) and antioxidants. Ferroptosis itself is a result of the accumulation of cytotoxic lipid hydroperoxides within the membranes of the cell, which can be triggered in multiple ways. Lipid peroxidation can occur via the Fenton reaction, wherein ferrous (Fe+2) iron reacts with ROS to produce hydroxyl radicals while propagating lipid peroxidation and increasing damage to cellular membranes. Because of this, ROS and iron are key players in the ferroptotic pathways, and modulators of iron storage and oxidative stress are key regulators of these pathways. ACSL4 contributes to ferroptotic pathways as a PUFA synthesizer, a does the transferrin receptor, which imports iron into the cell. The fight against ferroptosis has several key players: enzymes, antioxidants, and iron chelators. Selenoenzyme Glutathione Peroxidase 4 (GPX4) converts cytotoxic lipid hydroperoxides into non-toxic lipid alcohols by utilizing reduced glutathione (GSH) as a cofactor. GSH synthesis requires cysteine as a substrate, which is imported into the cell by the cysteine/glutamate antiporter System X_C. By inhibiting System XC the intracellular pool of cysteine is depleted, leading to a reduction of GSH and a decrease in GPX4 activity. Through this disruption of redox homeostasis, ROS continue to react with lipids and the resulting lipid hydroperoxides build up until ferroptotic cell death is triggered.

The elucidation of these mechanisms has allowed for the manipulation of key factors to investigate the effects of ferroptosis in the heart. In mouse models, cre-mediated deletion of FTH1 and subsequent inability to store labile iron caused an increase in cardiac ferroptosis[59]. This increase resulted in significant left ventricular hypertrophy and impaired cardiac function that eventually culminated in heart failure[59]. In this same study, it was noted that elevated free iron levels amplified ROS production[59]. The stability of hypoxia inducible factor 1 alpha (HIF1-alpha), which is responsible for activating transcription of various genes mediating the cellular response to hypoxia, is reliant on the activity of iron-dependent prolyl-hydroxylases[60,61]. In the presence of iron and oxygen, these hydroxylases modify proline residues on HIF-1alpha that target them for degradation[60,61], demonstrating the connection between iron concentration and ROS handling. In the heart alone, ferroptosis has been linked to diabetic cardiomyopathy, heart transplantation, sepsis-induced cardiac injury, and Doxorubicin-induced cardiomyopathy, to name a few [62-65]. It also being investigated currently in hypertrophic and dilated cardiomyopathy [66]. These studies are also possible due to the commercially available inhibitors of ferroptosis.

Among the more potent inhibitors of ferroptosis is Ferrostatin-1. Ferrostatin-1 (Fer-1) is a synthetic small molecule that scavenges hydroperoxyl radicals in the presence of iron [67]. Because it is not consumed during this process it is an efficient inhibitor of ferroptosis, comparable to GPX4[67]. Fer-1 forms a complex with ferrous iron, which acts as the electron donor[67]. Using this mechanism, it is able to scavenge the initiating alkoxyl radicals that are produced by ferrous iron from lipid peroxides and

acts as a radical trapping antioxidant[67] (**figure 1.5**). Since its discovery, Fer-1 has been used repeatedly to investigate the role of ferroptosis in various diseases.

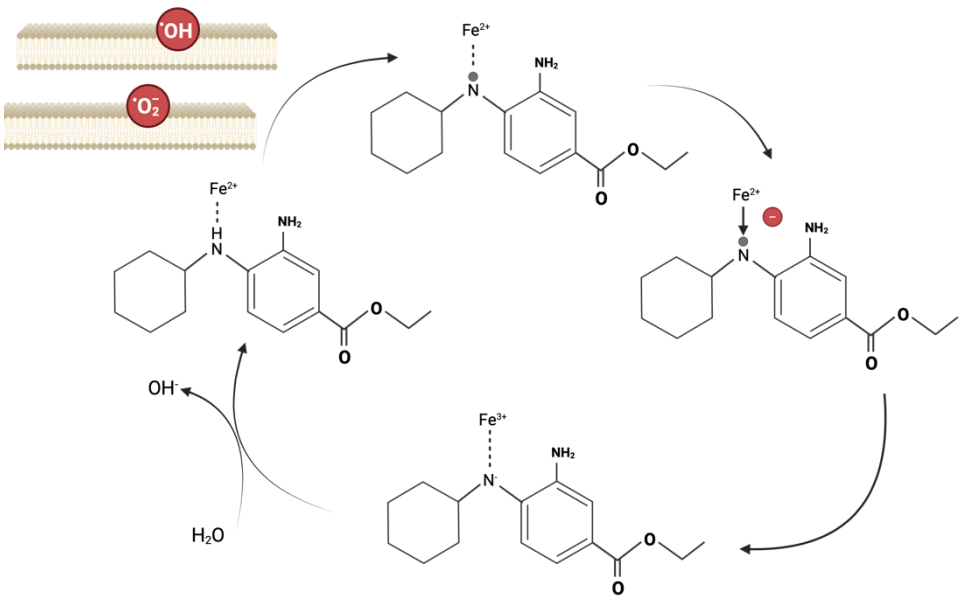

Figure 1.5 Mechanism of action of Ferrostatin-1. Ferrostatin-1 (Fer-1), a synthetic antioxidant and small molecule inhibitor of ferroptosis, prevents erastin-induced accumulation of lipid ROS. Fer-1 is a hydroperoxyl radical scavenger and while it does require reduced iron, is not consumed while exerting its antioxidant activity, making it a highly efficient option for preventing ferroptosis.

Morphologically, ferroptosis is distinct from other forms of RCD and does not result in cell blebbing, chromatin condensation, organelle swelling, etc.[51]. The only morphological feature currently associated with ferroptosis is mitochondria shrinkage with increased cristae density[51]; however, this phenomenon may be cell-type specific and merits further investigation[40]. This was initially thought to indicate that ferroptosis involved excessive ROS production caused by mitochondria ETC defects, but the Stockwell lab demonstrated that ferroptosis could still occur in cells lacking a functional ETC. [34,51]. Oxidized PUFAs can induce intracellular aggregation of misfolded proteins, and the Endoplasmic Reticulum (ER) has been shown to be the main essential site of ferroptosis as lipid hydroperoxides primarily accumulate in the ER[34,68]. While current research supports the ER as the main target of ferroptosis, lipid peroxides also interact with calcium channels, resulting in dysregulation of calcium homeostasis of the cell[68]. These effects are equally crucial to understand as calcium handling is central the excitation-contraction coupling mechanism in cardiomyocytes[69]. This is just one example of how ferroptotic pathways can affect cardiac function in more nuanced ways than the death of muscle tissue.

1.6 Immune System and Landscape in MI

Cell death is a key event that triggers sterile inflammation in response to MI, and macrophages are involved in every stage of the process [70,71]. Macrophages are a part of a subgroup of leukocytes called myeloid cells that also includes granulocytes, monocytes and dendritic cells [72]. It has been shown through clodronate liposome-

mediated cell depletion of macrophages that their participation is necessary for neonatal heart regeneration[71]. Distinct populations of macrophages exist in the heart, including tissue resident cardiac macrophages and monocyte-derived, circulating macrophages [72,73].

Infiltrating macrophages are primarily pro-inflammatory and produce higher levels of inflammatory cytokines and chemokines [73]. They are typically identified by low expression of F4/80 and high expression of Ly6C, and positive expression of CCR2[74,75]. CCR2 is a receptor for monocyte chemoattractant protein (MCP) and facilitates monocyte infiltration into tissues[76]. Circulating monocytes are recruited into the tissue by resident cells, then differentiate into macrophages once exposed to local cytokines and growth factors[75,77]. Infiltrating macrophages exhibit higher rates of proliferation once present in the heart which must be tightly regulated by resident cardiac macrophages, as an influx of inflammatory immune cells into the heart leads to decreased contractility [77]. This is one of the largest reasons why infiltrating macrophages are considered maladaptive, and experimental inhibition of MCP and CCR2 signaling has been shown to reduce inflammation and improve cardiac function in mouse models of heart injury, providing strong evidence to support this theory [75].

Resident macrophages are primarily derived from embryonic yolk sac and fetal liver monocytes, and are mainly anti-inflammatory [73]. They are involved in clearing apoptotic cells and damaged mitochondria, promoting tissue repair, and regulating myocardial fibrosis and hypertrophy[73]. Resident cardiac macrophages are typically identified by high expression of F4/80 and low expression of Ly6C and have been largely

considered CCR2-, but in recent years, a subpopulation of CCR2+ resident cardiac macrophages have been identified[74,78]. Therefore they can be further divided into subsets of populations with differing roles in tissue repair based on CCR2 expression[75]. CCR2- resident cardiac macrophages reduce inflammation by decreasing monocyte and macrophage recruitment after injury, and depletion of CCR2- resident cardiac macrophages prior to IR injury diminished LV systolic function, LV dilation, and increased akinetic myocardium [75]. Conversely, CCR2+ resident cardiac macrophages increase monocyte and macrophage recruitment and subsequently fibrosis, and depletion of CCR2+ resident cardiac macrophages prior to IR injury improved LV systolic function, smaller LV chamber dimensions, and reduced akinetic myocardium[75] (**figure 1.6**). However, these CCR2+ resident cardiac macrophages are distinct from CCR2+ infiltrating macrophages. They produce inflammatory chemokines such as Cxcl1, Cxcl2, Ccl2, Cc17, and Cc19, cytokines such as Il1beta and Il19, and express genes implicated in adverse cardiac remodeling such as Arg1, Mrc1, and Hif1α, on a smaller scale than infiltrating CCR2+ macrophages[75]. CCR2+ resident cardiac macrophages are not able to repopulate once depleted after MI, unlike infiltrating CCR2+ macrophages[75].

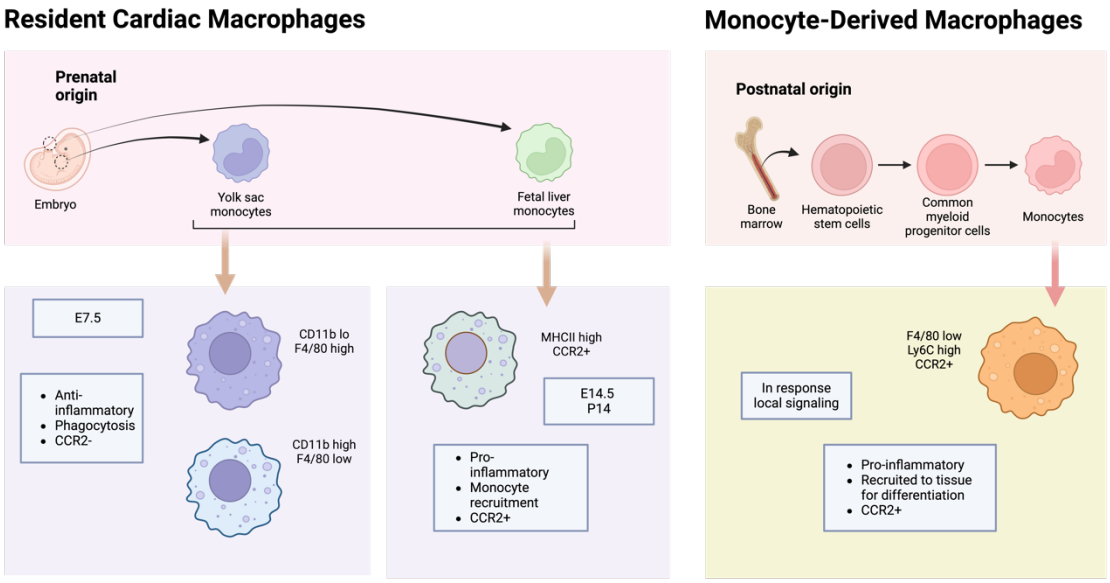

Figure 1.6 Schematic of macrophage differentiation in the heart. Injury to cardiac tissues mobilizes non-cardiac cell types to the site of the injury, including endothelial cells and macrophages, both of which are crucial for myocardial repair[79]. Under physiological conditions, these cell types communicate with each other to maintain normal heart function. Macrophages do not all support regeneration and are categorized in several ways. Resident neonatal cardiac macrophages contribute significantly to angiogenesis and cardiomyocyte proliferation while producing minimal inflammation. Conversely, infiltrating monocyte-derived macrophages recruited to the injured heart in the adult mouse strongly promote inflammation and exhibit limited angiogenic and regenerative capability

The M1 and M2 states are used to describe degrees of polarization towards either a pro-inflammatory or pro-regenerative state, which can be induced by certain cytokines[80]. The M1 pro-inflammatory macrophages rely on glycolysis, while the M2 pro-regenerative macrophages utilize oxidative phosphorylation[74,81]. The M1 macrophages demonstrate increased phagocytosis, antigen presentation, inflammatory cytokine production, and ROS generation[80]. The M2 macrophages produce anti-inflammatory cytokines and growth factors that stimulate fibroblast-mediated ECM production, cell proliferation, and angiogenesis, contributing to tissue repair[80]. However, research has repeatedly emphasized that this distinction is not strictly binary and should be thought of as a gradient[80]. RNA sequencing and flow cytometry have shown that many macrophages involved in cardiac injury, though polarized more towards either state, may express canonical markers of both M1 and M2 genes[80]. This emphasizes that macrophages play multiple and overlapping roles during the wound healing process post-MI.

The macrophage population in the infarct exhibits high plasticity and heterogeneity [74,75]. In the adult infarcted mouse heart, there is a distinct pattern of macrophage polarization that correlates with the stages or injury[74]. At 1 day post-MI, macrophages primarily express genes related to the inflammatory response, including ECM disassembly, glycolysis, and response to hypoxia [74]. The resident macrophage population as identified via high expression of F4/80 and low expression of Ly6C decreases from roughly 78% to 14%, indicating rapid depletion of the resident macrophage population after MI[74]. Conversely, infiltrating monocytes as identified via

low expression of F4/80 and high expression of Ly6C increased from roughly 12% to 74%, indicating that lost resident cardiac macrophages are replaced by infiltrating macrophages[74]. These day 1 macrophages display a strong pro-inflammatory and matrix-degrading phenotype, likely due at least in part to the large influx of infiltrating monocytes[74]. However, several genes that repress inflammation were also highly expressed, likely as a mechanism to prevent excessive inflammation[74]. By day 3, the macrophage population expresses genes related to mitochondrial function, including termination of mitochondrial translation, electron transport, complex I assembly, cristae formation, and ATP synthesis-coupled proton transport[74]. They simultaneously downregulate genes related to ECM organization and cell migration[74]. Together this indicates an overall phenotype shift away from leukocyte extravasation and towards phagocytosis, proliferation, and metabolic reprogramming towards oxidative phosphorylation, the latter of which is a metabolic signature of M2 macrophages[74,81]. Additionally, resident cardiac macrophage proliferation has been re-initiated by day 3[74]. By day 7, the macrophages take on a more pro-reparative phenotype, with the top upregulated pathways including ECM disassembly and collagen fibril organization, and inflammatory response being the top downregulated pathway[74].

Many cytokines have been implicated in mediating both the immune response and tissue remodeling processes after MI, and the expression of both pro and anti-inflammatory cytokines must be carefully balanced to orchestrate the wound healing process. Many cytokines have been implicated in immune polarization as cytokine signaling is one of the predominant methods of macrophage polarization in the microenvironment [82]. Macrophage migration inhibitory factor (MIF) is expressed by both immune and non-immune cell types to modulate immune recruitment, and is used as a biomarker as it correlates positively with infarct size in MI patients[83]. Notably, it is also produced by cardiomyocytes in culture in response to hypoxia or stretching [83].Cardiomyocytes also produce cytokines to stimulate angiogenesis after MI, including VEGFs, FGFs, HGF, Angiopoietin 1, etc. [84]. Certain cytokines implicated in macrophage polarization have also been implicated in angiogenesis, such as Interleukin-19 (IL-19) [85].

IL-19 has been implicated in both angiogenesis and immune signaling during and post-MI. IL-19 is part of the IL-10 subfamily that also includes IL-20, IL-22, and IL-24, and signals through a heterodimer of IL-20ralpha and IL-20rbeta receptor subunits, targeting both immune and vascular cell types [85-87]. IL-19 promotes endothelial migration and spreading, mitosis, and tube formation, and can accelerate revascularization in mice[87-90]. Similarly, IL-19 knockout mice exhibit significantly decreased reperfusion, which can be rescued by administration of recombinant IL-19 protein[87,91].IL-19 signaling has been identified in macrophages, endothelial cells, vascular smooth muscle cells (VSMCs), lymphocytes, peripheral blood mononuclear cells (PBMCs), and T cells [91,92].

Due to the strong pro-reparative function it exerts on a broad range of cell types, it is regarded as a crucial mediator of inflammation and angiogenesis[89,90,92].

In the adult mouse model of MI, IL-19 treatment decreased infarct size and myocardial apoptosis while improving cardiac function, measured by ejection fraction and fractional shortening [93]. Microvascular density, VEGF expression, and heme oxygenase-1 (HO-1) were also increased post-MI[93]. Secreted IL-19 also polarizes macrophages towards the M2 phenotype[94]. IL-19 knockout mice with exogenous IL-19 protein administration exhibited increased expression of canonical M2 macrophage markers from isolated monocytes, along with increased VEGF-A expression and decreased IL-12 expression, indicating both an increase in angiogenesis and a decrease in inflammatory response [87]. In MI mouse models, exogenous IL-19 protein delivery increased mRNA expression of pro-regenerative CD206, arginase 1 (Arg1), and chitinase-like 3 (Chil3, or Ym1), while also decreasing mRNA expression of inflammatory marker interferon gamma (IFNy) [93]. IL-19 administration also increased the percentage of M2-like macrophages in the heart by over 25% [93], highlighting the ability of IL-19 to limit maladaptive inflammatory remodeling and bolster a regenerative response in the heart after infarction[93]. Further supporting these mouse studies, IL-19 was investigated as a biomarker in acute ST-segment elevation myocardial infarction (STEMI) patients [95]. Circulating IL-19 levels were elevated after injury and correlated negatively with left ventricular ejection fraction (LVEF), suggesting that circulating IL-19 represents the anti-inflammatory response to cardiac IR Injury[95]. As IL-19 was also elevated after emergency percutaneous coronary intervention (PCI), it may also act as a metric to

evaluate successful coronary opening following STEMI [95]. Taken together, the body of research points to IL-19 being both a potent regulator of immune function and cardiac remodeling, as well as a promising therapeutic target.

Inhibiting Ferroptosis in regenerating hearts does not improve cardiac function post-MI

2.1 Introduction

Heart failure caused by myocardial infarction, or MI, is the leading cause of death in the United States as reported by the American Heart Association. An MI, or heart attack, is typically induced by coronary artery occlusion that deprives the myocardium of oxygen and nutrients, resulting in cell death. Mammalian cardiomyocyte turnover rate is insufficient to replace the lost cell population, so clinical strategies focus on timely angioplasty to re-perfuse the infarcted myocardium to minimize the loss of cardiomyocytes [10,96]. As such, there is an urgent need for effective therapeutic strategies to repair damaged myocardium efficiently.

In the infarcted myocardium, ischemia and increased levels of reactive oxygen species (ROS) promote cardiomyocyte death and maladaptive fibrosis[23,97]. Under physiological conditions, various cell types communicate with each other to maintain normal heart function[84]. During the remodeling and repair process of the injured cardiac tissue, cell death and injury responses are tightly regulated to maintain cardiac function[17]. Thus, we need to understand the mechanisms that govern regulated cell death (RCD) in order to understand the mechanisms that govern cardiac regeneration.

In recent studies, our lab has shown that cardiomyocytes primarily undergo ferroptosis as opposed to other forms of regulated cell death[98]. Ferroptosis is a non-apoptotic form of RCD caused by excessive lipid hydroperoxide production in the presence of iron [51]. Morphologically, ferroptosis causes shrinkage of mitochondrial crista, increased membrane density, and outer membrane rupture [40,99,100]. Cellular iron, normally stored in a protein complex composed of ferritins, is required for the

onset of ferroptosis [59]. Notably, pediatric oncology patients often suffer from cardiac toxicity caused by chemotherapy drug doxorubicin[101,102], which is known to both induce oxidative stress and increase levels of labile iron, two key players in the ferroptotic pathways[103,104]. Ferrostatin-1 (Fer-1), a radical trapping antioxidant, has been shown to selectively inhibit ferroptosis by scavenging free radicals and stop the propagation of lipid peroxidation, making it an excellent tool for studying ferroptotic pathways[57,105].

While adult mouse hearts are considered non regenerative, the neonatal mouse is capable of regenerating the damage myocardium after MI, a transient ability that is gradually lost during the first week of life[106]. This makes the neonatal mouse heart a valuable tool to study cardiac regeneration. This study aimed to elucidate the effects of ferroptotic CMs on infarct remodeling and wound healing using the regenerative murine model of MI and ferroptosis inhibiting reagent Fer-1.

2.2 Results

Previous work investigating the types of RCD in cardiomyocytes after an MI revealed that cardiomyocytes primarily undergo ferroptosis[98]. To investigate the role of ferroptosis in regenerative mouse hearts post-MI, ferroptosis was inhibited after MI via injection of Fer-1[57]. LAD-O was performed at postnatal day 1 or day 7, and subcutaneous injection of Fer- was administered immediately following surgery and continued every 24 hours until the last dose was administered at 3 days post-MI (**Figure 2.1A**). As previously reported data showed that cardiomyocyte ferroptosis peaked at 3 days post-MI, hearts were collected at the 3 days post-MI timepoint [98]. By using this timepoint, we aimed to observe the largest possible impact on the infarcted heart as a result of inhibition of ferroptosis. Fer-1 activity was assessed via analysis of 4HNE, a byproduct of lipid peroxidation and established marker of ferroptosis[40]. Immunohistochemical staining for 4HNE revealed notable reductions in lipid peroxidation (**Figure 2.1B-H**), confirming that Fer-1 injections at a dosage of 2mg/kg sufficiently lowered lipid peroxidation in the post-MI heart. While Fer-1 has been utilized in recent years to study the effects of ferroptosis in adult mice models of MI[107,108], it has not yet been studied in the regenerative MI mouse model. To begin investigating the effects of inhibiting ferroptosis on cardiac function in the regenerative MI mouse model we assessed cardiac function after MI. At two weeks post-MI, echocardiography was performed on both MI and sham mice to determine whether cardiac function was compromised. Surprisingly, no significant change was observed in the Fer-1 treated regenerative P1 MI hearts. In DMSO treated control animals given

LAD-O, the mean ejection fraction was 59.58 and fractional shortening was 31.16. In the Fer-1 treated animals given LAD-O, ejection fraction was 64.59, and fractional shortening was 34.42 (P- value of .420 for EF and .455 for FS) (**Figure 2.2C**). Similarly, the infarct size, while trending downward, was not significantly different from the vehicle treated MI hearts, with the DMSO LAD-O animals (**Figure 2.2B**). Infarct size decreased from 2.24% in the DMSO treated MI hearts to 1.20% in the Fer-1 treated hearts (P = .437).

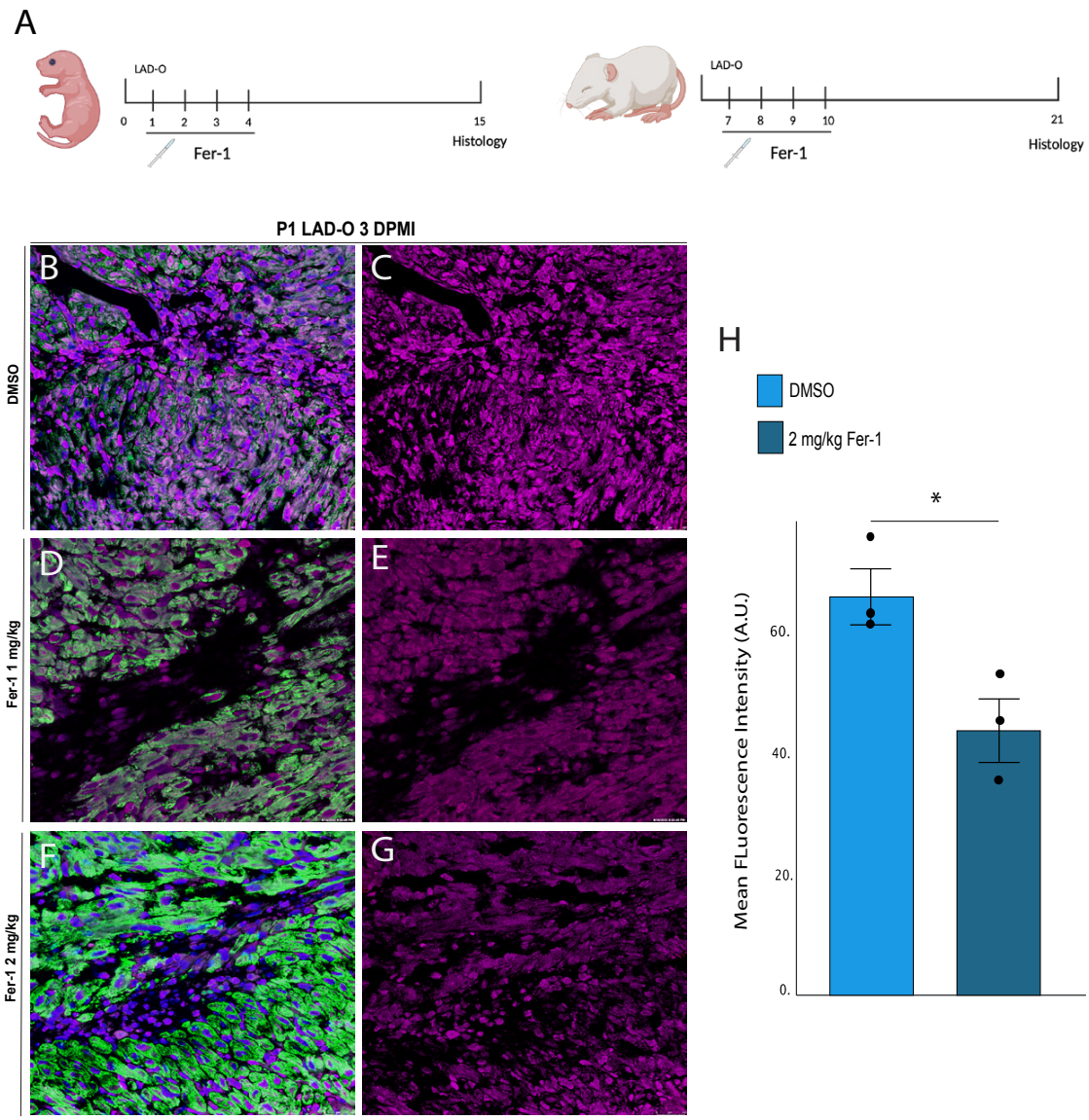

Figure 2.1 Fer-1 administration after MI reduces lipid peroxidation in mice. Mice were treated with either Fer-1 or DMSO immediately after P1 LAD-O, and again every 24 hours until 3 days post-MI for histology. **(A)** Diagram of experimental design showing timeline of Fer-1 or DMSO administration via subcutaneous injection immediately following LAD-O in P1 or P7 mice. P1 LAD-O hearts were stained for cTnT (green), Dapi (blue), and 4HNE (purple). **(B-C)** DMSO treated hearts staining depicting lipid peroxidation in the infarct in tissue sections of the infarct region. **(D-E)** Fer-1 (1 mg/kg) treated hearts staining depicting lipid peroxidation in the infarct. **(F-G)** Fer-1 (2 mg/kg) treated hearts staining depicting lipid peroxidation in the infarct. **(H)** Quantification of intensity of 4HNE staining in DMSO and Fer-1 treated hearts as measured by fluorescence intensity.

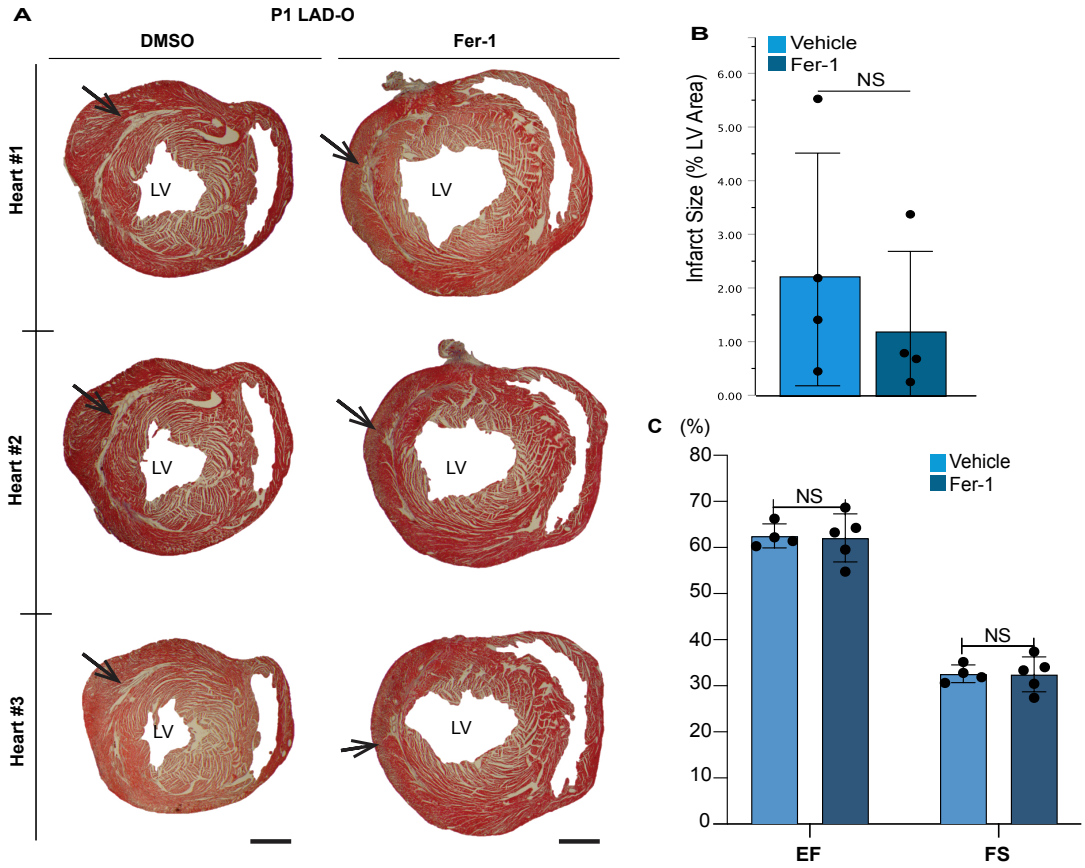

Figure 2.2 Fer-1 administration does not improve cardiac function or infarct size in P1 MI mice. Fer-1 or DMSO as vehicle control was administered subcutaneously at 0, 1, 2, and 3 days post-surgery and hearts were analyzed at 14 days post surgery. **(A)** Masson's trichrome staining to visualize infarcted/fibrotic area in blue (arrows) in heart sections of three representative hearts from each group 14 days after P1 LAD-O. **(B)** Quantification of infarct size in DMSO and Fer-1 treated hearts in P1 MI mice, as percent of total left ventricular area. **(C)** Quantification of ejection fraction and fractional shorting in DMSO and Fer-1 treated hearts in P1 MI mice, as measured by echocardiography.

We then pivoted to the non-regenerative P7 mouse model of MI to determine whether Fer-1 administration after MI would improve cardiac function. Contrary to our expectations and the current body of research, the non-regenerative P7 MI hearts deteriorated as a result of Fer-1 administration at a dose of 2 mg/kg. The increase in infarct size was both minimal and non-significant, increasing from 3.09 % in the DMSO group to 3.58 in the Fer-1 group ($p = .665$); however, assessment of ejection fraction and fractional shortening showed that both were significantly worse in the Fer-1 treated animals ($p < 0.05$) (**Figure 2.4**). These data contradict previously established paradigms that show inhibiting ferroptosis is beneficial for the post-MI mouse heart. Our data suggest that ferroptosis plays some unknown but crucially beneficial role in the remodeling and wound healing process.

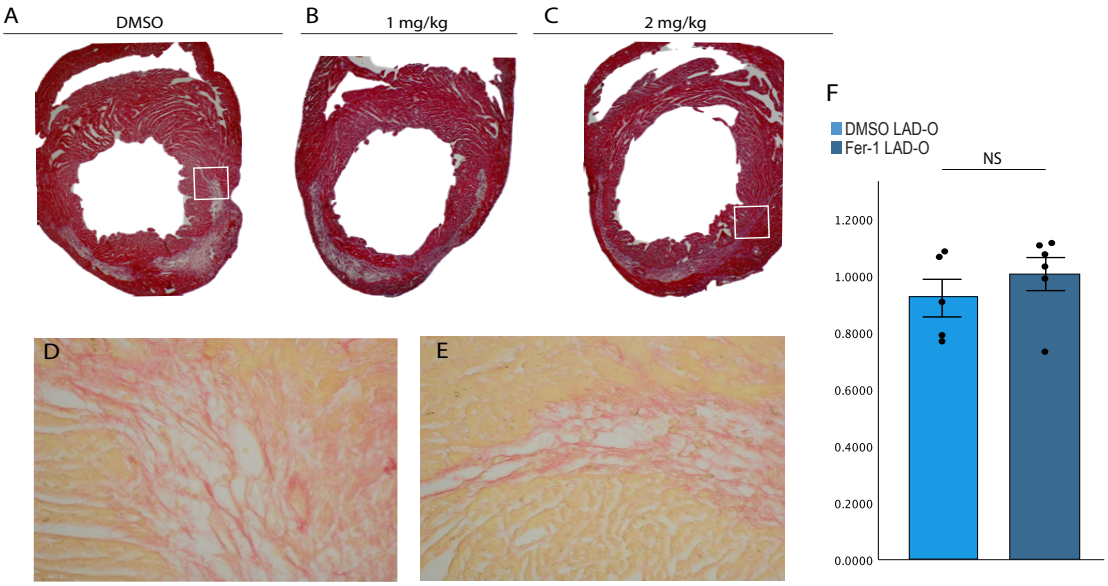

Figure 2.3 Fer-1 administration does not result in significant hypertrophy at P1 3DPMI. **(A-C)** Trichrome staining was performed on LAD-O animals treated with either DMSO or Fer-1 (1 or 2 mg/kg). **(D-E)** Representative images of the infarct region after picrosirius red staining to visualize collagen deposition in the infarct of **(D)** DMSO or **(E)** 2 mg/kg Fer-2 treated hearts. No apparent changes to collagen deposition or composition are seen. **(F)** Heart weight to body weight ratios of DMSO (0.92) and 2 mg/kg Fer-1 (1.00) treated hearts reveal no changes to cardiac hypertrophy at this timepoint ($p = .385$)

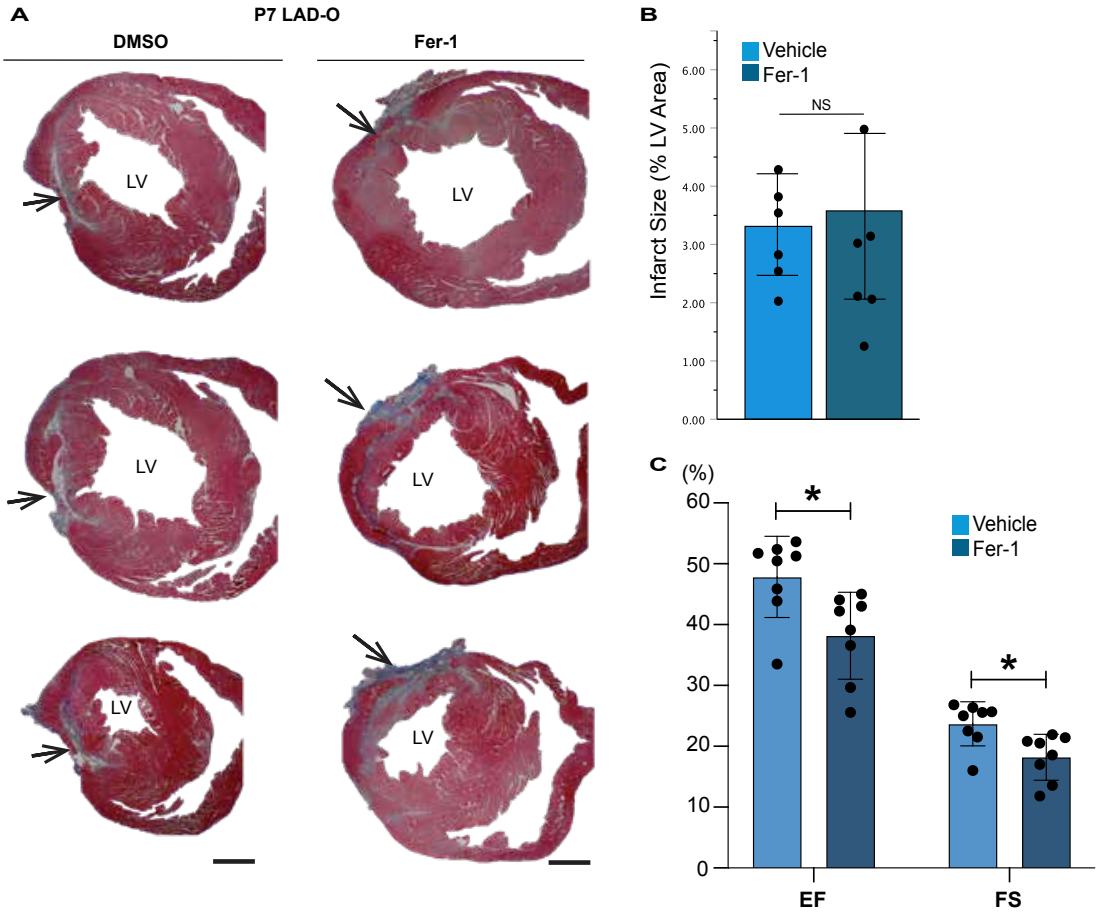

Figure 2.4: Fer-1 administration worsens outcomes in P7 MI mice. Fer-1 or DMSO as vehicle control was administered subcutaneously at 0, 1, 2, and 3 days post-surgery and hearts were analyzed at 21 days post-surgery. **(A)** Masson's trichrome staining to visualize infarcted/fibrotic area in blue (arrows) in heart sections of three representative hearts from each group 21 days after P7 LAD-O. **(B)** Quantification of infarct size in DMSO and Fer-1 treated hearts in P7 MI mice, as percent of total left ventricular area. **(C)** Quantification of ejection fraction and fractional shorting in DMSO and Fer-1 treated hearts in P1 MI mice, as measured by echocardiography.

As previous research has hinted at connections between apoptosis and ferroptosis [54], we next evaluated whether the inhibition of ferroptosis would result in an increased rate of apoptosis. P1 3DPMI mouse hearts were probed for expression of cardiac troponin t to label cardiomyocytes and cleaved caspase 3 (cCas3) to identify apoptotic cells. Apoptotic cardiomyocytes were identified with double positive staining of both cardiac troponin t and cCas3. We observed that cardiomyocyte apoptosis occurred in low levels in the DMSO treated LAD-O animals, at 0.17%. While the variability of cardiomyocyte apoptosis was much greater in the Fer-1 treated animals, the average was still significantly higher at 0.46% ($P = .029$) (**Figure 2.5**), indicating that a suppression of ferroptosis after LAD-O yields an increase in cardiomyocyte apoptosis.

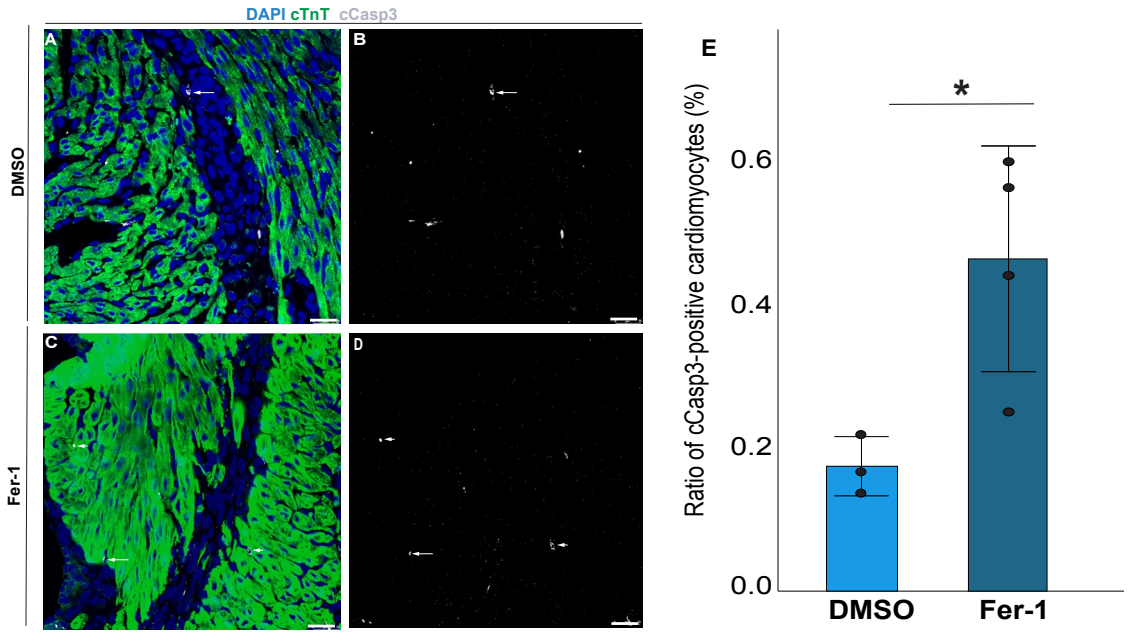

Figure 2.5 Inhibition of ferroptosis leads to increased apoptosis after LAD-O. (**A**–**D**) At 3 days after P1 LAD-O, tissue sections from hearts treated with vehicle control (DMSO, (**A**–**C**B) and Fer-1 (**C-D**) were stained for cleaved caspase-3 (cCas3) (grey) and cTnT (green). Arrows indicate cCas3-positive cardiomyocytes, quantified in **(E)** as the percent of total CMs per field. Percentage of apoptotic cardiomyocytes is significantly increased in the Fer-1 treated mice (0.46%) compared to vehicle control mice (0.17%) ($p = .029$).

To investigate the specific mechanisms by which cardiomyocyte ferroptosis influences the infarcted heart, we switched to a cell culture model. We differentiated iPSCs into iCMs to study the specific effects of cardiomyocyte ferroptosis (**figure 2.6A**). Once iCMs were beating spontaneously and uniformly (**figure 2.6B**), they were treated with either 30 μM Erastin as in inducer of ferroptosis [109], or DMSO as the vehicle control for a period of 6 hours. This timepoint was chosen as the amount of time Erastin takes to trigger ferroptosis via lipid peroxidation of the endoplasmic reticulum (ER)[34]. After the 6-hour treatment was completed, media was aspirated, iCMs were allowed to recover for a period of 16 hours in fresh media to generate conditioned media containing all the cytokines produced by the stressed cardiomyocytes (**Figure 2.6C)**. To characterize the paracrine factors released by healthy and ferroptotic cardiomyocytes, we performed a cytokine array analysis of the conditioned media to examine 105 cytokines and chemokines. Ferroptotic cardiomyocytes produced greater amounts of all but three secreted factors compared to the healthy DMSO control cardiomyocytes. Of the downregulated cytokines, the first was dipeptidyl peptidase IV (DPPIV), which was deceased by Log2FC 0.65 and reportedly contributes to cardiac dysfunction in rats[110]. The second was interleukin-5 (IL-5), which decreased by Log2FC 1.54 and contributes to M2 macrophage polarization and eosinophil recruitment in the infarcted heart[111]. The third was Fas ligand, which was decreased by Log2FC 6.53 and is expressed in response to I/R injury to trigger apoptosis[112].

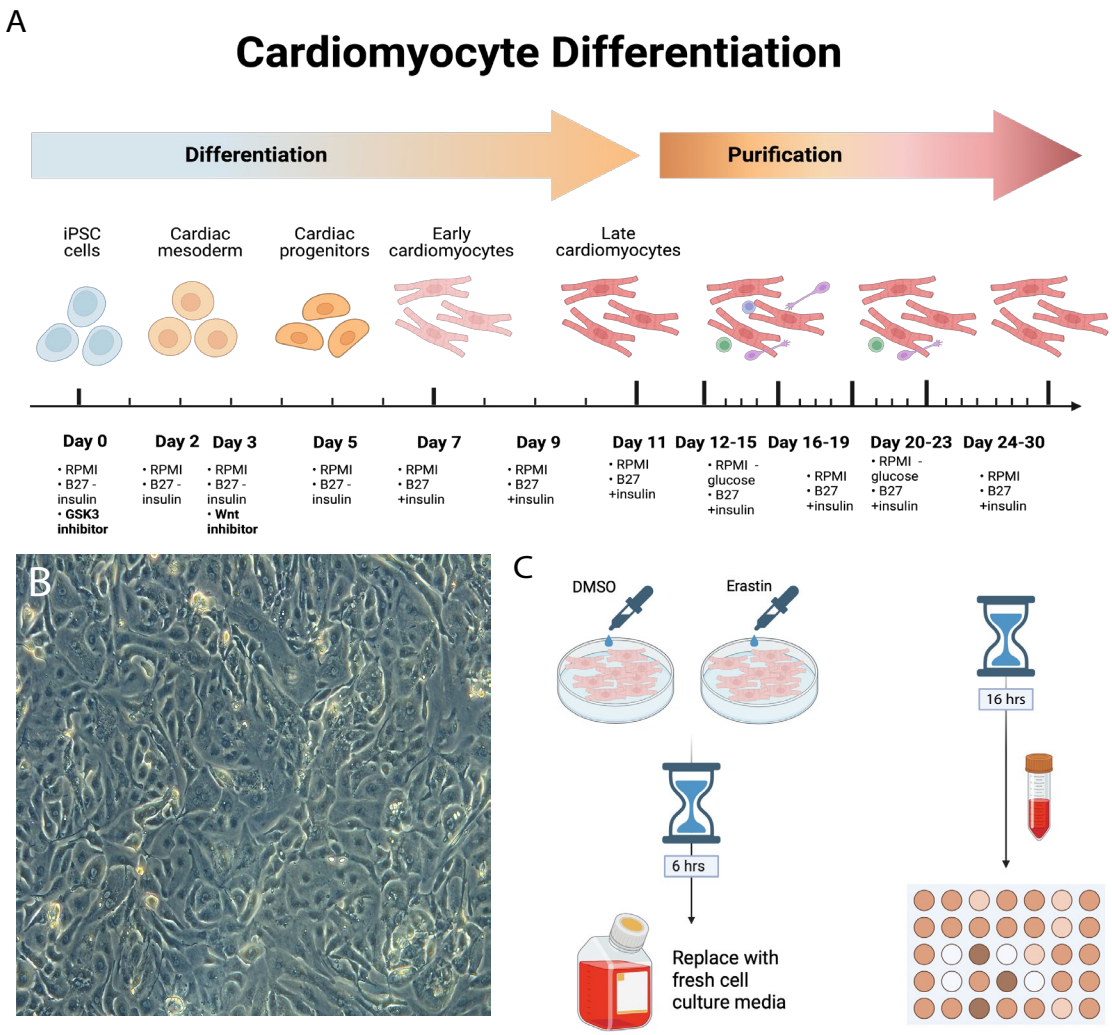

Figure 2.6 Generation of induced pluripotent stem cell-derived cardiomyocytes and conditioned media. (A) Schematic showing the timeline and reagents necessary for differentiation of iCMs from iPSCs. **(B)** Representative image of iCMs generated from iPSCs. **(C)** Diagram outlining experimental design for generation of conditioned media. iCMs were treated with either 30 μM Erastin or DMSO vehicle control 6 hours. Following treatment, iCMs were rinsed gently and thoroughly in PBS and allowed to recover in fresh media overnight for a period of 16 hours. Afterwards, conditioned media was collected and used for cytokine array analysis with a commercially available assay to examine expression of 105 different cytokines and chemokines.

The remaining cytokines were produced in greater amounts in the ferroptotic cardiomyocytes. Among the top hits of upregulated cytokines are Cripto-1, which has been implicated in stemness and muscle regeneration[113], interleukin 4 (IL-4), which is generally considered proliferative[114], and established pro-angiogenic factor VEGF. To investigate the major pathways involved in ferroptotic cardiomyocyte signaling, any cytokine that exhibited a Log2 fold change increase of 1 or greater was included in a Gene Ontology analysis through Metascape (**Figure 2.7A-C**). The top upregulated pathway was expectedly NABA secreted factors, which contains 343 genes primarily composed of cytokines and growth factors [115,116]. The second hit, positive regulation of protein phosphorylation, is not specific enough to provide any insight into the function of ferroptotic cardiomyocytes. The third hit, inflammatory response, contains 890 genes characterized by vasodilation, extravasation, and accumulation of white blood cells and macrophages into intercellular spaces [116], providing evidence for cardiomyocyte-derived immune signaling. The fourth hit was Interleukin-10 (IL-10) Signaling (**Figure 2.7F**). The IL-10 family of cytokines are crucial effector and regulatory molecules in immune system signaling [117], and has not been previously been reported as a cardiomyocyte-derived cytokine. Interestingly, IL-19, a member of the IL-10 cytokine family, has repeatedly been shown to be pro-angiogenic and anti-inflammatory, but has mainly been investigated in endothelial and macrophage populations[90,93,118].

To confirm that IL-19 is expressed by ferroptotic cardiomyocytes, we performed immunoblotting of the conditioned media produced by cardiomyocytes treated with DMSO, Erastin, or Staurosporine. Analysis of IL-19 expression shows a trending increase of IL-19 expression from the Erastin-treated iCMs compared to the controls, while the Staurosporine-treated iCMs produced significantly decreased amounts of IL-19 (**Figure 2.7D,E**). This provides further support for the hypothesis that ferroptotic cardiomyocytes possess uniquely beneficial secretome over other types of RCD.

Taken together, these results suggest a previously unappreciated role for cardiomyocytes in not only wound healing and regulation of the infarct after MI, but possibly in directly stimulating the cardiac immune population.

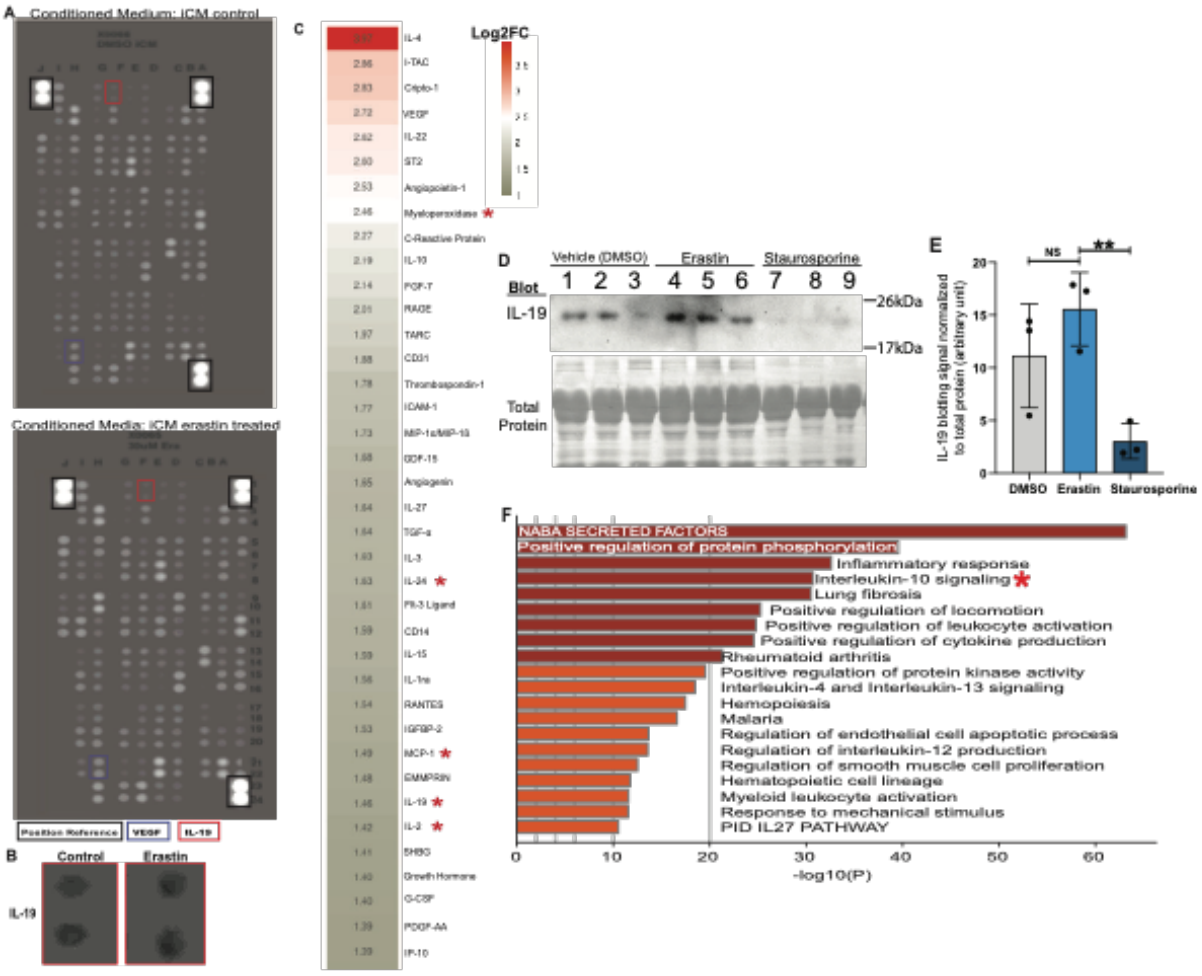

Figure 2.7 Ferroptotic cardiomyocytes secrete factors involved in immune regulation and angiogenesis. Cytokines and chemokines released by ferroptotic cardiomyocytes have distinct roles in immune modulation. (**A**) Inverted cytokine array blot image of conditioned media from iCMs treated with either vehicle control (DMSO) or erastin (30 μM). (**B**) Zoomed-in images of blotting spots of IL-19, highlighted by red boxes in A. (**C**) Heat map depicting levels of more highly secreted cytokines from ferroptotic iCMs as $\log_2$ of fold change (FC) in pixel intensity compared to DMSO-treated iCMs. Red asterisks mark factors associated with Interleukin-10 signaling. (**D**,**E**) Immunoblotting of IL-19 in conditioned medium samples from iCMs treated with vehicle (DMSO), erastin, or staurosporine, $n = 3$ (**D**). Signal intensity of the IL-19 blotting band normalized to total protein (Ponceau) and plotted in (**E**). (**F**) Gene Ontology (Metascape) analysis of cytokines that increased in conditioned media after erastin treatment. **, $p < 0.01$. NS, not significant.

2.3 Discussion

Heart disease and stroke take more lives annually than cancer and chronic lower respiratory disease combined, at over 19 million deaths globally caused by CVD[119]. This economic burden of CVD is in the hundreds of billions in the United States alone and climbing[119]. Thus, CVD represents not only a public health crisis but an economic one. Clinical treatment typically involves a surgical intervention such as coronary angioplasty or ventricular assist device implantation, which come with high cost to the patient, and the potential for complications, such as bleeding, infection, etc.[120]. However, lack of therapies to regenerate lost cardiac tissue and address the underlying cause of post-MI heart failure is a major hurdle that strongly affects patient prognosis [11]. Our research aims to identify factors that regulate cell death and wound healing after an MI as a basis to develop such therapies.

Previous work has demonstrated that cardiomyocytes preferentially undergo ferroptosis after LAD-O as opposed to other types of regulated cell death[98]. Here, we utilized ferroptosis inhibitor Fer-1 in both the regenerative P1 and the non-regenerative P7 postnatal mouse heart to investigate the role of ferroptosis after MI.

It has been reported that Fer-1 inhibits ferroptosis by scavenging the hydroperoxyl radical, thereby preventing accumulation of lipid peroxides[121]. To confirm this, we performed immunohistochemical analysis 4-Hydroxy-2-nonenal (4HNE), a commonly used marker of lipid peroxidation, [122,123] on both control and Fer-1 treated tissues. As expected, administration of Fer-1 decreased 4HNE staining in the

hearts of treated animals in (**Figure 2.1**). Next, we proceeded to investigate the effects of Fer-1 on the infarcted heart.

We found that pharmacological inhibition of ferroptosis via Ferrostatin-1 administration did not improve cardiac function in the regenerative P1 mouse heart, as there was no significant difference in either ejection fraction or fractional shortening between the Fer-1 and DMSO treated groups (**Figure 2.2**). We did observe a downward trend in infarct size in the P1 hearts, though this likely does not represent any impactful improvement. This finding was not completely unexpected, as inhibition of cell death in an already regenerative model is somewhat expected to yield a positive result in terms of cardiac function.

We then switched to the P7 non-regenerative model of MI to determine whether inhibiting ferroptosis would improve cardiac function. Unexpectedly, inhibiting ferroptosis after LAD-O resulted in deteriorating cardiac function. Echocardiography revealed worsening ejection fraction and fractional shortening in the Fer-1 treated animals. Analysis of infarct size showed only a downward trend in total infarcted LV area (**Figure 2.3 A,B**). Previously published data of the mouse MI model that utilized Fer-1 shows that cardiac function is improved with the inhibition of ferroptosis[107,108], which directly contradicts our findings.

There may be several explanations for this discrepancy. First, Fer-1 administration in a study by Li, et al. was performed as a pretreatment 24 hours prior to LAD-O at a dose of 1 mg/kg in adult mice, then performed echocardiography measurements 7 days post MI [107]. We utilized a higher dose with a younger mouse

model and chose to administer Fer-1 following LAD-O rather than as a pre-treatment and performed echocardiography measurements at 14 days post MI. Post-MI changes in ECM deposition, tissue remodeling, infarct size, and cardiac function are dynamic. As LV hypertrophy, fractional shortening, declining cardiac function, and diastolic LV dimension largely stabilize at 14 days post- MI in mice [124], it is crucial to allow these remodeling processes to resolve to observe the full effects of Fer-1 administration on cardiac function. At two weeks post-MI, we observed worsening ejection fraction and fractional shortening, indicative of declining cardiac function, in the non-regenerative P7 hearts. Alternatively, while the P7 mouse is considered non-regenerative, murine cardiomyocyte DNA synthesis persists until postnatal day 14 (P14), at which the heart switches to a hypertrophic growth phase[125,126]. This difference in the developmental timepoint of the mouse model used may be responsible for the difference in experimental results.

We hypothesized that, if ferroptosis is inhibited, cardiomyocytes may undergo an alternative form of cell death. As previous reports have suggested a strong connection between apoptosis and ferroptosis, we stained tissue sections for cleaved caspase-3, a marker of apoptosis[54]. The percentage of apoptotic cardiomyocytes, identified via double positive staining of cleaved caspase-3 and cardiac troponin t, was just under 0.2% in control P1 3DPMI hearts (**Figure 2.5**). This low rate of apoptotic cardiomyocytes at this timepoint agrees with previously published studies[98]. This number more than doubled, significantly increasing to a rate of 0.5% Fer-1 treated

hearts (P = .029), confirming that inhibition of ferroptosis results in an increased apoptotic rate in cardiomyocytes.

The consensus to date is that there is a correlation between ferroptosis and other forms of RCD, with emphasis on apoptosis. It has been hypothesized that in certain contexts, apoptosis may be converted to ferroptosis [54]. Supporting this concept, there are many overlaps in the organelles and signaling pathways involved in both[54]. Some studies have shown that ROS generation and intracellular glutathione depletion, key events in ferroptosis, result in caspase-3 dependent apoptosis[127,128]. Conversely, apoptosis-inducing factor (AIF), which is involved in caspase-dependent apoptosis, can be released in certain cell types when mitochondrial ROS accumulates, and this action can be blocked by Fer-1[129]. This study provides some further evidence to support this link between apoptosis and ferroptosis.

To investigate the specific effects of ferroptotic cardiomyocytes, we continued with an *in vitro* design of iCM cell culture (**Figure 2.6**). Human induced pluripotent stem cells (iPSCs) can be differentiated into cardiomyocytes (iCMs), resulting in a relevant cell culture model to study human cardiomyocytes where samples are otherwise scarce[130,131]. iCMs were treated with either DMSO as the vehicle control or 30μM Erastin for a period pf 6 hours before treated media was aspirated and fresh media added. iCMs incubated in the fresh media for a period of 16 hours to collect secreted factors from stressed cells, resulting in conditioned media that was then used for a cytokine array analysis (**Figure 2.7**). Three cytokines were downregulated compared to the healthy cardiomyocytes; DPPIV,IL-5, and Fas ligand.

DPPIV exists as either a plasma membrane protein present on epithelial cells, endothelial cells, and lymphocytes, but also as a serum protein[132]. Interestingly, elevated serum DPPIV has been reported in patients with cardiovascular disease, and DPPIV knockout mice exhibit increased survival post-MI[110]. The second was interleukin-5 (IL-5), which is elevated in STEMI patient serum samples[133]. IL-5 has also been shown to reduce infarct size and increase M2 polarization in mice treated with exogenous IL-5 protein[111]. While this seemingly supports a non-regenerative role for ferroptotic cardiomyocytes, IL-5 has been shown to exert this activity through interleukin-4 (IL-4) signaling, which was the most increased cytokine[111]. The third was Fas ligand, which is expressed in response to I/R injury to trigger apoptosis[112] via the extrinsic pathway of apoptosis, a highly studied pathway implicated in the pathogenesis of heart failure[134].

As the number of upregulated cytokines was high, we began investigating the signaling pathways involved by performing gene ontology analysis. The top upregulated pathways were NABA secreted factors, followed by Positive regulation of protein phosphorylation, and Inflammatory response. While the first two pathways provide only general information related to biological processes and responses to stress, inflammatory response (GO:0006954) includes regulation of molecular mediators of immune signaling as well as immune migration involved in the inflammatory response. This alludes to ferroptotic cardiomyocytes playing an active role in the remodeling process post-MI.

The first hit that gave us specific signaling pathway information was Interleukin-10 signaling (**Figure 2.7D**). The IL-10 family of cytokines contains 9 total interleukins that are known to be both potent and highly versatile, playing both pro and anti-inflammatory roles, and can be divided into three subgroups based on function [117]. The Interleukin-20 (IL-20) subgroup contains interleukin 19 (IL-19), interleukin 20 (IL-20), interleukin 22 (IL-22), interleukin 24 (IL-24), and interleukin 26 (IL-26)[117]. The interleukin 28 (IL-28) subgroup contains interleukin 28A (IL-28A), interleukin 28B (IL-28B), and interleukin 29 (IL-29), also known as type III interferons (IFNs) IFN λ2, 3, and 1, respectively[117]. The final member, interleukin 10 (IL-10), resides as its own subgroup[117]. As the IL-20 subfamily cytokines were collectively among the top hits in the Gene Ontology analysis (**Figure 2.6**), we focused on these cytokines.

The IL-20 subfamily interleukins are thought to act mainly on tissue epithelium and stroma cells while regulating proliferation, remodeling, and repair [117]. Interleukins 19, 20, and 24 signal through the IL-20 Type I receptor complex composed of a heterodimer of IL20 receptor Beta and IL20 receptor alpha [118]. IL-20 and IL-24 can also bind to the IL-20 Type II receptor comprised of IL-22Rα and IL-20Rβ, while IL-19 can only signal through IL-20 Type 1 Receptor[118]. IL-20 Type I Receptor binding initiates activation of the Janus Kinase (JAK) and signal transducer and activator of transcription (STAT) pathways, particularly STAT3[118], which heavily influences immune regulation and regulation of growth, differentiation, and apoptosis[135]. IL-19 has been thoroughly studied in the context of inflammatory vascular disease [118], providing context for cardiomyocyte-derived IL-19 signaling.

While it is recognized that cardiomyocytes produce danger-associated molecular patterns (DAMPs) in response to stress or injury[136], cardiomyocytes have not been traditionally considered as strong contributors to cardiac inflammation compared to immune and stromal cells[137]. In more recent years, they have been considered as larger players in crosstalk that results in chronic, low grade inflammation that is often characteristic of heart failure[137].

This study demonstrates that the inhibition of ferroptosis is not necessarily beneficial in all contexts and is certainly detrimental in the early postnatal infarcted mouse heart. We also provide evidence to suggest that ferroptotic cardiomyocytes play a more direct role in regulation of cardiac wound healing than previously thought. This adds needed context to ongoing research into cardiac injury and highlights the importance of understanding the mechanisms that modulate regulated cell death.

Ferroptotic Cardiomyocytes support the angiogenic response

3.1 Introduction

This study aimed to elucidate the effects of ferroptotic CMs on various cell populations in the infarcted heart. Cardiac cell populations participate in the ventricular remodeling process through mechanisms such as autocrine and paracrine signaling or direct cell-cell interactions [91,138]. We previously reported in a recent publication that cardiac fibroblasts protect cardiomyocytes from ferroptosis through both paracrine effects and direct interaction [98]. This further highlights the role of cell–cell interaction in the repair of damaged myocardium. As the wound healing response post-MI requires strict coordination of various processes, numerous studies have been conducted to characterize the roles each cell type play in the wound healing process.

One of the most crucial processes is revascularization of the ischemic area through angiogenesis. Angiogenesis involves highly coordinated signaling from multiple cell types, including various endothelial cell phenotypes[139]. For example, tip cells, which are characterized by filopodia and migratory behavior, and stalk cells, which are more proliferative, possess fewer filopodia, and express adherent and tight junctions, are both required to support the stability of nascent vasculature [140,141]. Angiogenesis is also supported by various cell types and conditions. Cardiac fibroblasts, macrophages, neutrophils, and regulatory T-cells have all been implicated in the regulation of angiogenesis, as has hypoxia [78,142-144].

The hypoxia in the infarct triggers activation of pro-angiogenic signaling[144]. HIF-1a, for example, is regulated by intracellular oxygen concentration and contributes

to angiogenesis via VEGF upregulation [140,145-148]. Other cardioprotective and proangiogenic factors in the post-MI heart include iNOS, HO-1, adiponectin, and insulin-like growth factor-2. [145] Many reports have discussed the effects of endothelial cells on cardiomyocyte function in the heart. Studies have shown that endothelial cells protect cardiomyocytes from apoptosis in culture, aid in myocyte organization, and play a role in cardiomyocyte hypertrophy [149,150]. However, cardiomyocyte-derived signaling in endothelial-cardiomyocyte crosstalk is less thoroughly studied. Interestingly, conditioned media from ferroptotic cardiomyocytes include cytokines involved in angiogenesis, suggesting that cardiomyocytes directly participate in the remodeling process post-MI through the regulation of angiogenesis. Our findings implicate cardiomyocytes as direct and potent regulators of endothelial activity.

3.2 Results

To identify the potential mechanisms involved in the decline of cardiac function in response to Fer-1 treatment, we began investigating the cell populations in the infarct of treated animals. As timely revascularization is crucial for mitigating damage from ischemic injury, we first sought to characterize the endothelial cell population in the infarct. Immunohistochemical staining of venous and capillary endothelial cell marker Endomucin (EMCN) [151] revealed that daily Fer-1 treatment at a dose of 2 mg/kg from the time of surgery significantly reduced the number of vascular endothelial cells in the infarct, decreasing from 17.07% in the DMSO treated hearts to 9.37% in the Fer-1 treated hearts. Interestingly, similar treatment with a dose of 1 mg/kg resulted in a non-significant but trending decrease in EMCN+ cells in the infarct of 14.36% (**Figure 3.1**). This pattern is consistent with a ferrostatin-1 dose-dependent response of the endothelial cell density in the infarct.

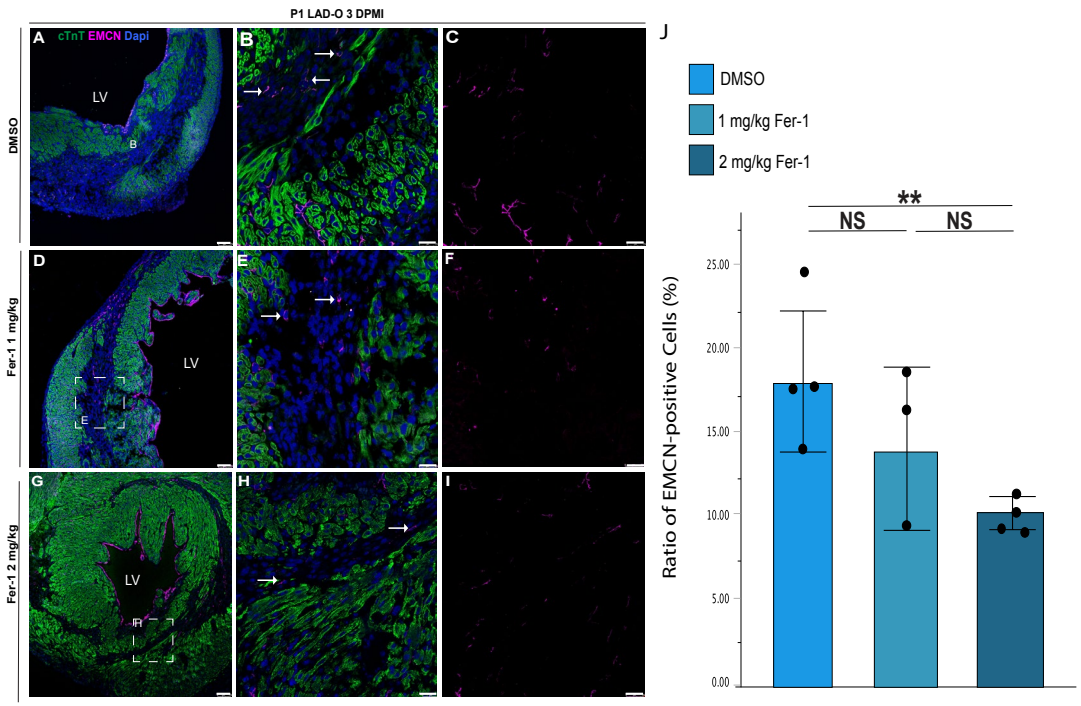

Figure 3.1 Inhibition of ferroptosis decreases endothelial cell density in the infarct in a dose-dependent manner. (**A**–**I**) At 3 days after P1 LAD-O, tissue sections from hearts treated with vehicle control (DMSO, (**A**–**C**B) and Fer-1 (**C-D**) were stained for Endomucin (EMCN) (purple) and cTnT (green). Arrows indicate positive EMCN staining in the infarct, quantified in **(J)** as the percent of total CMs per field. Percentage of EMCN-positive endothelial cells is significantly decreased in the Fer-1 treated mice (10.29%) compared to vehicle control mice (17.89%) (p = .009). Fer-1 treated hearts at the lower dose of 1 mg/kg exhibit a trending decrease of endothelial density in the infarct (13.86%).

We first sought to determine whether the decrease in endothelial cell population in the infarct was due to a decrease in proliferation. P1 3DPMI mouse hearts treated with either DMSO or Fer-1 were probed for expression of EMCN to label endothelial cells and phospho-histone H3, a marker of chromosomal condensation and mitotic activity [152,153], to label proliferating cells (**Figure 3.2A-D**). Double positive cells were identified as proliferating endothelial cells. In DMSO treated hearts, 0.29% of the endothelial population in the infarct stained positive for PH3. In Fer-1 treated hearts this number increases to 0.90%, although this increase is non-significant (**Figure 3.2**).

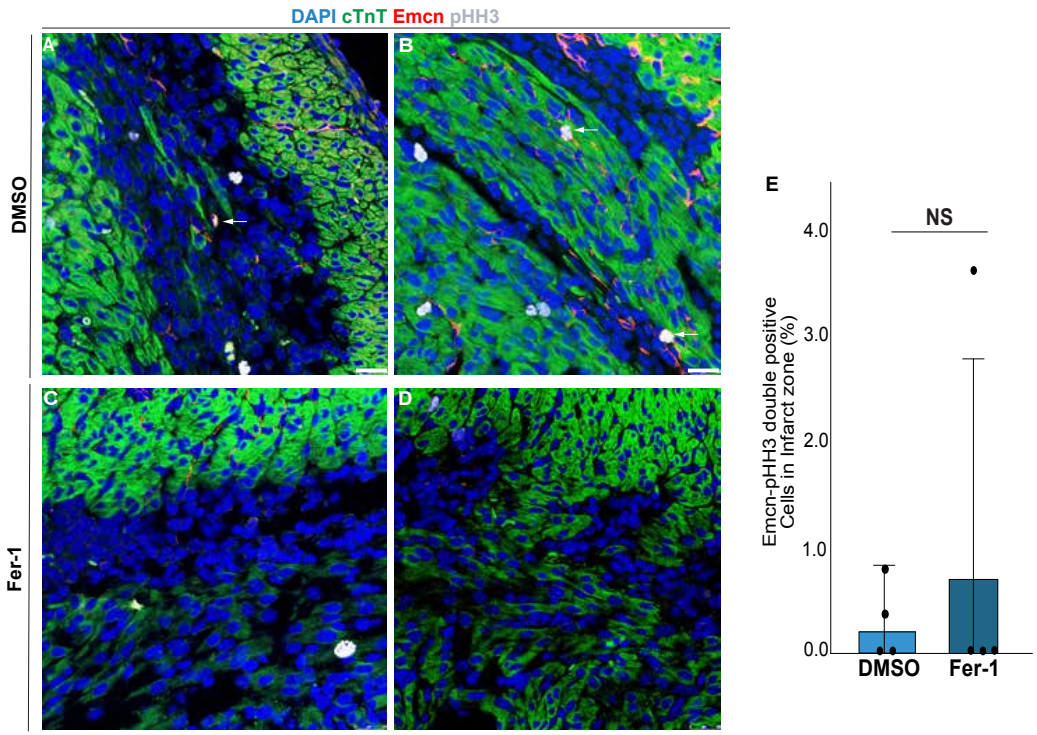

Figure 3.2 Fer-1 administration decreases does not significantly affect endothelial proliferation. At 3 days after P1 LAD-O, tissue sections from hearts treated with vehicle control (DMSO, (**A**–**C**B) and Fer-1 (**C-D**) were stained for Endomucin (EMCN) (red), phosphor histone H3 (PHH3) and cTnT (green). Double positive cells were labeled as proliferating endothelial cells, indicated by arrows and quantified in **(E)** as the percent of total EMCN-positive cells in the infarct. Percentage of PHH3-positive endothelial cells is trending upwards in the Fer-1 treated mice (10.29%) compared to vehicle control mice (17.89%) (p = .009). Fer-1 treated hearts at the lower dose of 1 mg/kg exhibit a trending decrease of endothelial density in the infarct (13.86%).

We then hypothesized that the decrease in endothelial cells in the infarct after Fer-1 administration could be due to increased apoptosis, as seen in the cardiomyocyte population (**Figure 2.5**). cCas3 staining was repeated in conjunction with EMCN to label apoptotic endothelial cells in the DMSO and Fer-1 treated P1 3DPMI hearts. In DMSO treated hearts 3.12% of endothelial cells were positive for cCas3, while in Fer-1 treated hearts 2.40% of endothelial cells were positive for cCas3, indicating a decrease in apoptosis. However, this decrease was not significant (**Figure 3.3**). These data indicate that the decreased endothelial population in the infarct is not due to decreased proliferation nor increased apoptosis.

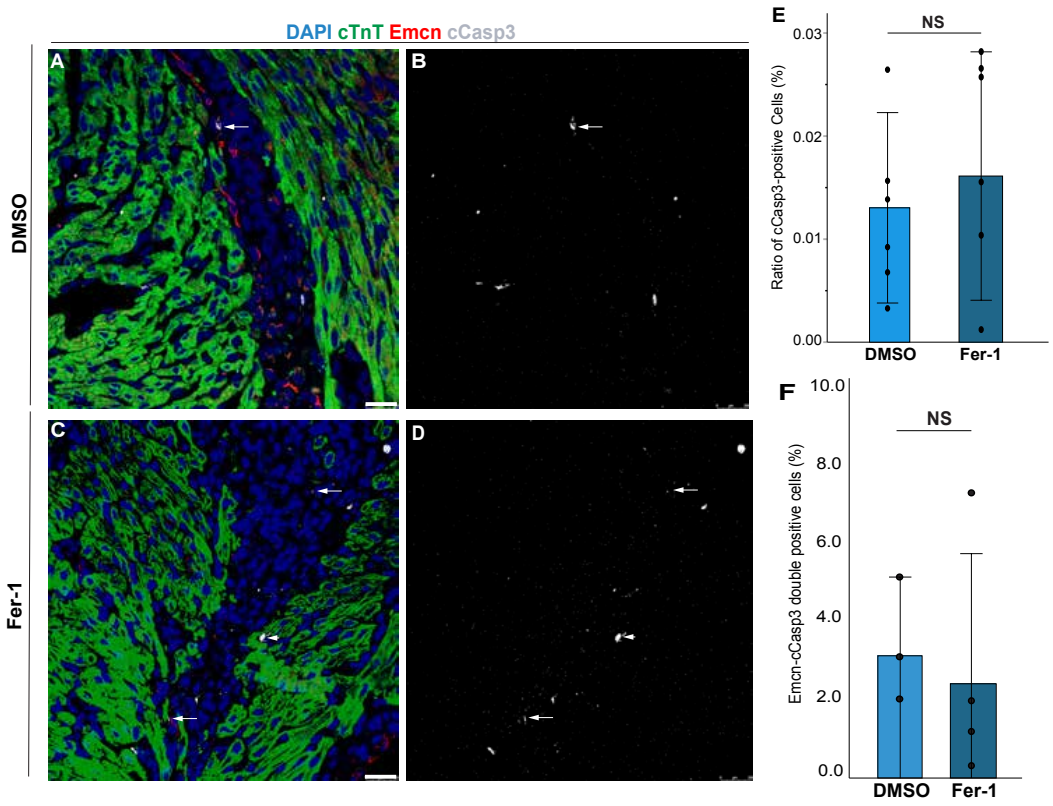

Figure 3.3 Fer-1 administration does not significantly affect the rate of endothelial apoptosis. At 3 days after P1 LAD-O, tissue sections from hearts treated with vehicle control (DMSO, (**A**–**C**B) and Fer-1 (**C-D**) were stained for Endomucin (EMCN) (red), cleaved caspase-3 (cCasp3) and cTnT (green). No significant change is observed between vehicle control (DMSO) (.013%) and Fer-1 (.016%) total apoptotic rate as percent of cCasp3-positive nuclei (p = .619), quantified in **(E)**. Double positive cells were labeled as apoptotic endothelial cells, indicated by arrows and quantified in **(F)** as the percent of total EMCN-positive cells in the infarct. Percentage of cCasp3-positive endothelial cells is trending downwards in the Fer-1 treated mice (2.40%) compared to vehicle control mice (3.12%) (p = .740).

To further investigate the specific effects of cardiomyocyte ferroptosis on the endothelial cell population, we generated conditioned media from cardiomyocytes using DMSO as the vehicle control, Erastin as an inducer of ferroptosis, and Staurosporine as an inducer of apoptosis [154]. This conditioned media was then used to treat Human Umbilical Vein Endothelial Cells (HUVECs) during a tube formation assay, an *in vitro* measure of the ability of the endothelial cells to form tube-like structures that mimic the formation of blood vessels in the heart [155-157] (**Figure 3.4**). Analysis revealed that conditioned media from ferroptotic cardiomyocytes supported tube formation as strongly as the control media in all metrics analyzed, including total mesh area, mean mesh size, number of nodes, junctions, extremities, total branching length, and total segments length. However, conditioned media from apoptotic cardiomyocytes was not capable of supporting tube formation. Further, these HUVECs were unable to survive until the final timepoint at 6 hours (**Figure 3.5**).

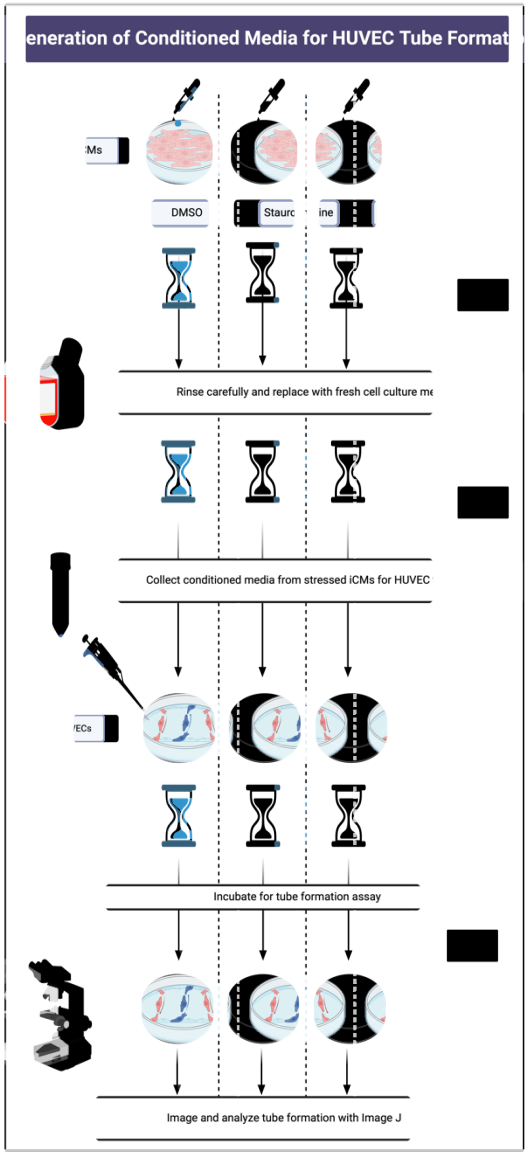

Figure 3.4 Diagram depicting experimental workflow to test the effects of ferroptotic cardiomyocyte-derived conditioned media on the angiogenic response. Human induced pluripotent stem cell-derived cardiomyocytes were cultured in 30µM Erastin as an inducer of ferroptosis, 1mM Staurosporine as an inducer of apoptosis, or DMSO control for 6 hours to induce cell stress. After 6 hours, treated media was removed, cells were washed gently but repeatedly with PBS to remove all traces of Erastin, Staurosporine, or DMSO, and fresh media was added. iCMs were allowed to recover overnight for a period of 16 hours, and conditioned media containing cytokines produced from stressed cardiomyocytes was collected. Conditioned media was then added to Human umbilical vein endothelial cells (HUVECs) in a 1:1 ratio of complete HUVEC media plated on growth-factor reduced Matrigel. Huvecs were imaged every 60 minutes for 6 hours to observe tube formation. Images were analyzed using Angiogenesis Analyzer from FIJI, a validated plugin from the NIH[158,159], to quantify the extent of tube formation.

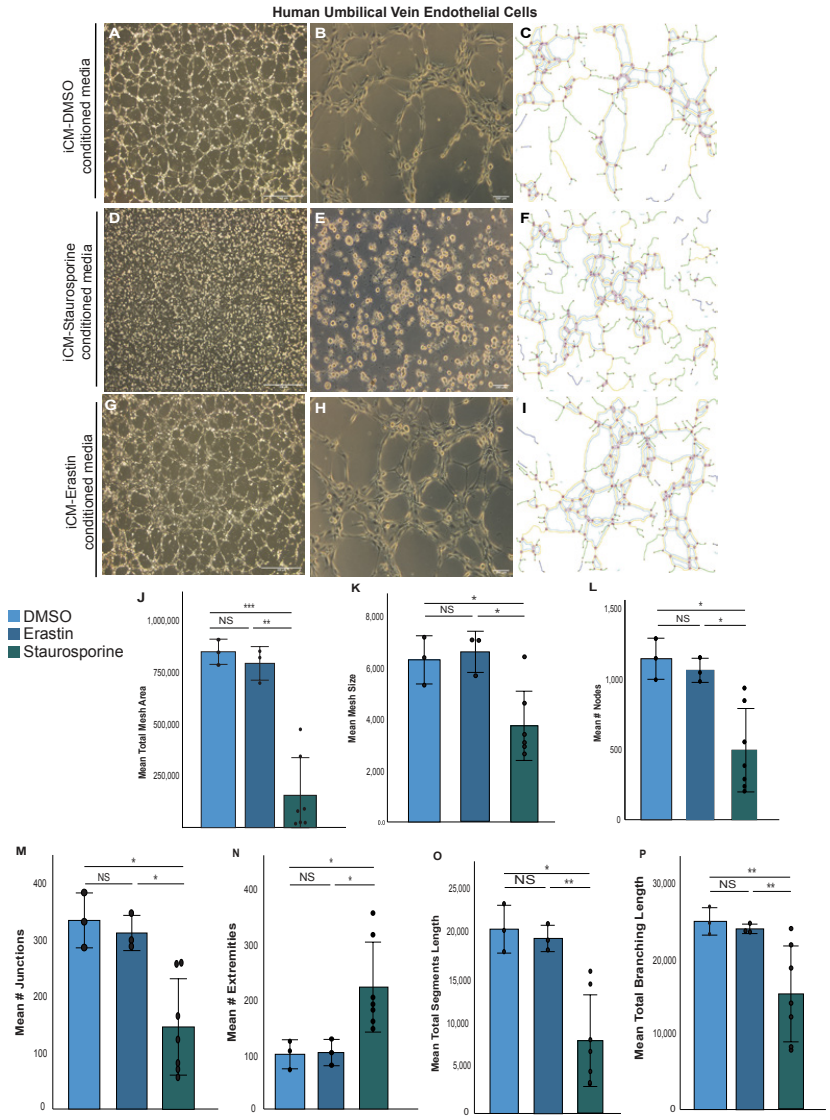

Figure 3.5 Ferroptotic Cardiomyocytes support endothelial tube formation. (A-I) Representative images of Huvecs treated with DMSO vehicle control **(A-C),** 30 μM Erastin **(D-F),** or 1 mM Staurosporine **(G-I)** after 6 hours incubation. **(C, F, I)** higher magnification images of the Angiogenesis Analyzer overlay showing branches (green lines), junctions (blue circles), nodes (red circles), segments (yellow lines), meshes (light blue lines), close master junctions (purple lines connecting two junctions), extremities (white lines pointing to yellow circles), and isolated segments (dark blue lines). **(J-P)** Quantification of tube formation metrics at 6 hours. Values were averaged and plotted as the fold change over the DMSO control value. * $P < 0.05$ ** $P < 0.01$. *** $P < 0.001$ NS., not significant.

While Fer-1 administration yielded striking results in the endothelial cell population in the infarct, subcutaneous injections are not specific to the myocardial tissue. The crosstalk between cell types has been thoroughly documented, and our lab has recently established that human cardiac fibroblasts protect cardiomyocytes from ferroptosis by sharing the iron burden. Thus, to test the specific effects of ferroptotic cardiomyocytes on the endothelial cell population, we moved to an in vitro system to determine whether cardiomyocytes undergoing ferroptosis significantly affect the angiogenic response.

To determine the impact of secreted factors from stressed cardiomyocytes on endothelial cell survival, we treated HUVECs with conditioned media from cardiomyocytes. Conditioned media from cardiomyocytes treated with DMSO, Staurosporine, and Erastin was utilized, as well as unconditioned cardiomyocyte media as a control. Supporting previous data from the tube formation assays, HUVECs survived at high rates in all categories except conditioned media from apoptotic cardiomyocytes. DMSO conditioned media treated HUVECs survived at an average rate of 84%, while Erastin conditioned media treated HUVECs survived at an average rate of 78%, with no significant difference between the two ($p = .324$). Conversely, the Staurosporine conditioned media treated HUVECs survived at an average rate of only 45% (**Figure 3.6A**), significantly decreased from all other categories. This confirms previous findings that apoptotic cardiomyocytes do not support endothelial survival or tube formation and instead actively promote endothelial cell death.

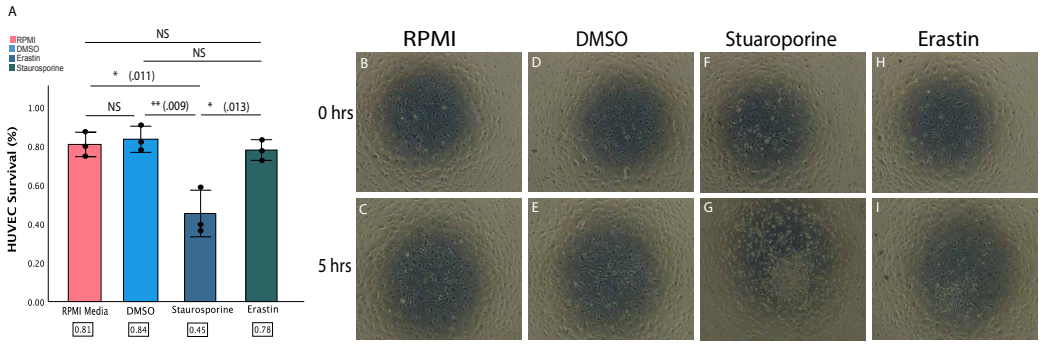

Figure 3.6 Conditioned media from stressed cardiomyocytes uniquely impacts endothelial survival. Conditioned media was generated as previously described. **(A)** Rates of HUVEC survival when incubated with conditioned media from iCMs treated with vehicle control (DMSO), staurosporine, or erastin. HUVECs were collected after 5 hours of incubation, imaged, and counted to determine survival rates with Trypan blue exclusion dye. Conditioned media from apoptotic iCMs resulted in significantly decreased survival compared to unconditioned CM media (p = .011), DMSO conditioned media (p = .009), and erastin conditioned media (p = .013). Representative images of HUVEC culture at time 0 **(B, D, F, H)** and again after a 5 hour incubation period **(C, E, G, I)**.

As neither increased apoptotic endothelial cell death nor decreased proliferation was identified in the infarcts of Fer-1 treated hearts, we performed scratch assays to investigate endothelial migration. HUVECs were treated with conditioned media, and a scratch was administered to create a gap and simulate an injury[160,161]. Cells were incubated for 24 hours to determine the immediate effects of conditioned media. HUVECs treated with DMSO conditioned media migrated into the gap and reduce the gap to, on average, 70% of the original gap size. HUVECs treated with Erastin conditioned media reduced the gap to 52% of the original gap size, on average, which was not significantly different from the DMSO group ($p = .117$). The Staurosporine conditioned media treated HUVECs once again did not survive and were therefore unable to repopulate the gap, instead increasing the size of the gap to nearly 400% its original size (**Figure 3.7G**), significantly increased compared to the DMSO ($p = 0.000074$) and Erastin ($p = 0.000013$) groups. These data together support a uniquely beneficial role of ferroptotic cardiomyocytes for endothelial cell survival, tube formation, and migration.

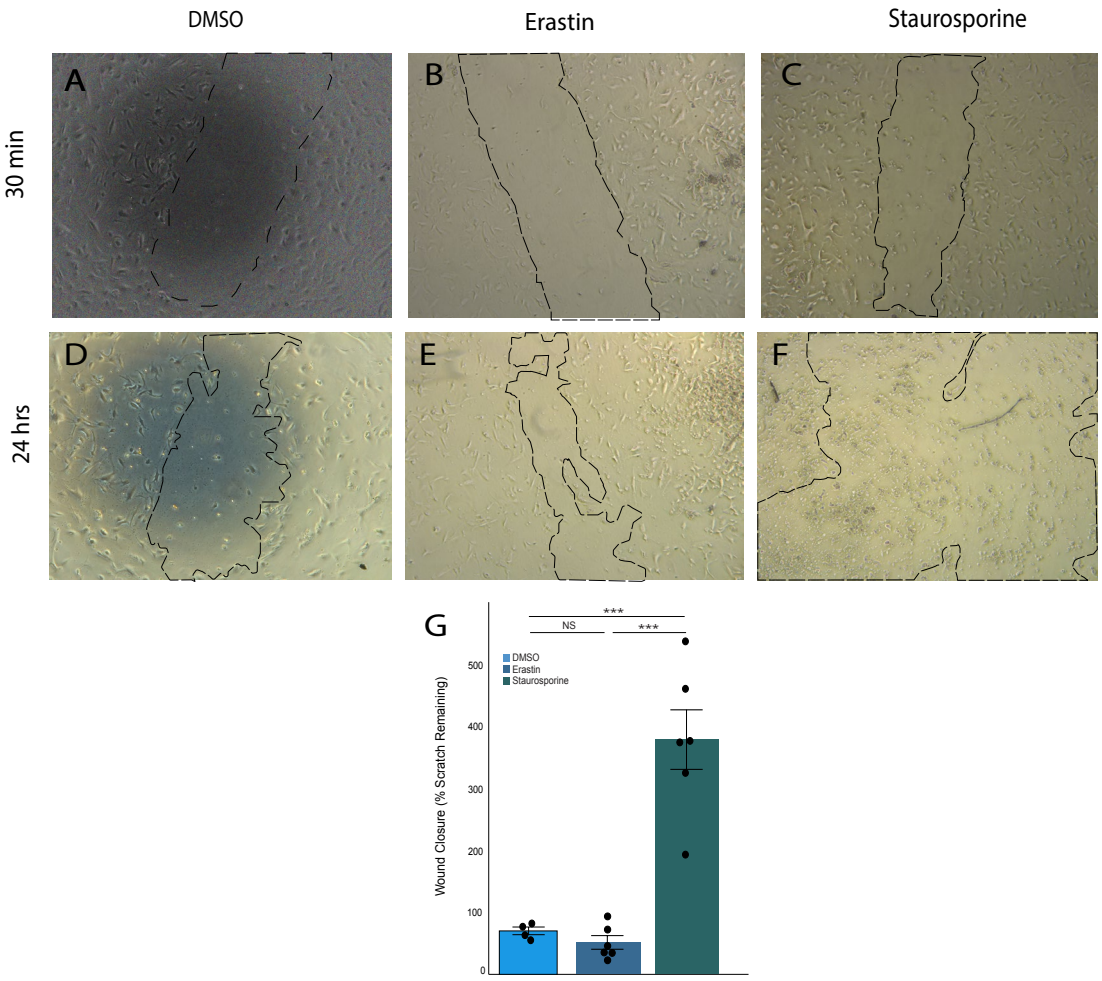

Figure 3.7 Conditioned media from stressed cardiomyocytes uniquely impacts endothelial migration and wound healing. Conditioned media was generated as previously described. Dashed lines indicate the borders of the simulated injury as measured. Representative images of HUVEC culture are shown at at 30 minutes **(A-C)** and again after a 24 hour incubation period **(D-F).** Rates of migration into the scratched area when incubated with conditioned media from iCMs treated with vehicle control (DMSO), staurosporine, or erastin are shown in **(G)**. HUVECs were re-imaged to determine new scratch borders at 24 hours and migration was quantified as percent area remaining of original scratch area. Conditioned media from apoptotic iCMs resulted in significantly decreased migration and survival compared to DMSO conditioned media ($p < .001$), and erastin conditioned media ($p < .001$).

3.3 Discussion

These studies present novel findings that implicate ferroptotic cardiomyocytes as strong supporters of endothelial cell populations in the heart post-MI. Previous work has implicated ferroptosis as the main mechanism of cell.

Our model of LAD-O followed by Fer-1 administration demonstrates a dose-dependent response in the endothelial cell population in the infarct (**Figure 3.1**). When administered at the lower dose of 1 mg/kg, we observed a trending decrease in endothelial cell density in the infarct. This percentage was significantly reduced when the dose administered was increased to 2 mg/kg. Previous studies that have utilized Fer-1 at the lower dose of 1 mg/kg showed reduced infarct size as a result of pretreatment in adult mice [65,162]. However, these studies did not report on cardiac function after Fer-1 treatment alone or investigate other processes involved in cardiac remodeling after I/R injury, such as angiogenesis[65]. We administered Fer-1 following the LAD-O procedure to more closely mimic the clinical setting. It is likely that our choice of timing combined with the higher dosage and younger mouse model is responsible for the conflicting results we report. As no significant decrease in infarct size was observed at the 2 mg/kg dose, the benefits of decreased ferroptotic cell death may be outweighed by the deleterious effects, such as reduced revascularization of the ischemic area.

Immunostaining of infarcted hearts treated with Fer-1 suggests that neither changes in endothelial cell proliferation (**Figure 3.2**) nor apoptosis (**Figure 3.3**) are robust enough to cause the decreased endothelial density in the infarct. However,

presented *in vitro* data both confirms this result and suggests that migration and tube formation are strongly contributing factors. To determine the impact of secreted factors from stressed cardiomyocytes on endothelial cell survival, we treated HUVECs with conditioned media from cardiomyocytes. Conditioned media from cardiomyocytes treated with DMSO, Staurosporine, and Erastin was utilized, as well as unconditioned cardiomyocyte media as a control. Assays of HUVECs treated with conditioned media showed that ferroptotic cardiomyocytes are uniquely able to support tube formation compared to apoptotic cardiomyocytes (**Figure 3.5**). This phenomenon was observed in all 3 *in vitro* assays. Supporting previous data from the tube formation assays, HUVECs survived at high rates in all categories except conditioned media from apoptotic cardiomyocytes. DMSO conditioned media treated HUVECs survived at an average rate of 84%, while Erastin conditioned media treated HUVECs survived at an average rate of 78%, with no significant difference between the two. Conversely, the Staurosporine conditioned media treated HUVECs survived at an average rate of only 45%. Conditioned media from apoptotic cardiomyocytes quickly resulted in endothelial cell death while ferroptotic cardiomyocytes supported both endothelial survival (**Figure 3.6**).

As neither increased apoptotic endothelial cell death nor decreased proliferation was identified in the infarcts of Fer-1 treated hearts, we performed scratch assays to investigate endothelial migration. HUVECs were treated with conditioned media, and a scratch was administered to create a gap and simulate an injury[160,161]. Cells were incubated for 24 hours to determine the immediate effects of conditioned media. HUVECs treated with DMSO conditioned media migrated into the gap and reduce the

gap to, on average, 70% of the original gap size. HUVECs treated with Erastin conditioned media reduced the gap to 52% of the original gap size, on average, which was not significantly different from the DMSO group ($p = 1.00$). The Staurosporine conditioned media treated HUVECs once again did not survive and were therefore unable to repopulate the gap, instead increasing the size of the gap to nearly 400% its original size (**Figure 3.7**), significantly increased compared to the DMSO ($p = 0.000074$) and Erastin ($p = 0.000013$) groups.

These data together support a uniquely beneficial role of ferroptotic cardiomyocytes for endothelial cell survival, tube formation, and migration. These studies suggest reduced endothelial migration as a plausible cause of the decreasing endothelial population in the infarcts of Fer-1 treated mice. Further investigation into the mechanisms involved in regulating the endothelial population in the Fer-1 treated heart could inform future therapeutic approaches for treating MI.

Inhibition of ferroptosis alters the immune response through cytokine signaling

4.1 Introduction

After an MI, multiple cell types must be activated, mobilized, and regulated for the purposes of cardiac remodeling[138,163,164]. A robust and early immune response is required to remove damaged cells and ECM that would otherwise pose a rupture risk[138,165]. This inflammatory phase is a required event for the initiation of the reparative phase[138,165]. However, the timely resolution of the inflammatory phase is critical for preventing adverse remodeling, expansion of the infarct, and declining cardiac function[138]. execution and resolution of the inflammatory response directly determines the degree of adverse cardiac remodeling[164]. Thus, immune cell involvement in MI is widely studied.

Macrophages are highly plastic and essential members of the innate immune system that possess tissue-specific functions [73,166]. Neonatal hearts depleted of macrophages are unable to regenerate[71]. Transcriptional profiling of macrophages isolated from the infarct revealed continuous metabolic reprogramming and changes in polarization over time as remodeling progressed, allowing them to exert a broad range of effects[74]. Macrophages may be polarized towards the M1 or M2 phenotypes, where M1 is pro-inflammatory and M2 is pro-regenerative[166,167]. Many studies have investigated the signaling between macrophages and other cell types, such as endothelial cells[168-170]. However, as cardiomyocytes have only recently been acknowledged as active contributors to infarct remodeling, the signaling between cardiomyocytes and macrophages has not been thoroughly investigated [137].

Our earlier work showed that ferroptotic cardiomyocytes secrete cytokines involved with the inflammatory response, interleukin signaling, and leukocyte activation. We hypothesize that these ferroptotic cardiomyocytes bolster the reparative phase of infarct remodeling by stimulating macrophage polarization towards the M2 phenotype through IL-19 signaling.

4.2 Results

We sought to investigate whether the macrophage population of the infarcted mouse heart was affected by the suppression of ferroptosis. To inhibit ferroptosis we continued to utilize Fer-1 administration directly after LAD-O, and every 24 hours following, until 3 days post-MI, for multiple levels of analysis (**Figure 4.1**). We then probed for Mac-3 and CD206 expressing macrophages in Fer-1 treated hearts. Mac-3 is a membrane surface glycoprotein that acts as a pan macrophage marker and is commonly used to identify macrophages [166,171]. CD206 is a membrane surface mannose receptor that acts as a marker of M2 macrophage polarization, and co-localization with Mac-3 was used to identify M2-like macrophages (**Figure 4.2A-D**) [166,172,173]. Fer-1 treatment post-MI lead to a reduction in the percentage of Mac-3 positive nuclei in the infarct from (**Figure 4.2E**). Additionally, Fer-1 treatment drastically reduced the percentage of M2-like macrophages in the infarct from an average of 62.51% to a striking 7.94% ($P < 0.001$) (**Figure 4.2F**). These findings indicate that

ferroptotic cardiomyocytes are instrumental in regulating the macrophage population in the infarct.

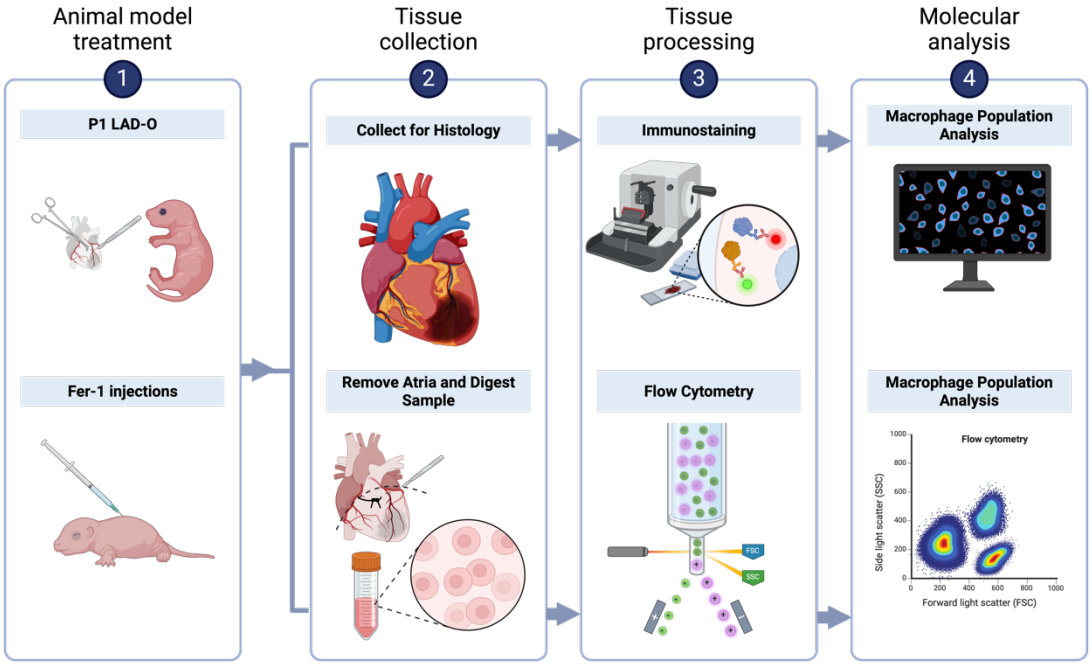

Figure 4.1 Graphic depicting experimental design for methods of investigating macrophage populations in Fer-1 treated LAD-O mice. Histological analysis maintains tissue architecture to allow specific examination in and around the infarct, while flow cytometry allows for the analysis of the larger macrophage population in the treated hearts. Diagram of experimental design showing timeline of Fer-1 or DMSO administration via subcutaneous injection immediately following LAD-O in P1 mice. Mice were treated with either Fer-1 or DMSO immediately after P1 LAD-O, and again every 24 hours until 3 days post-MI for histology or analysis with flow cytometry.

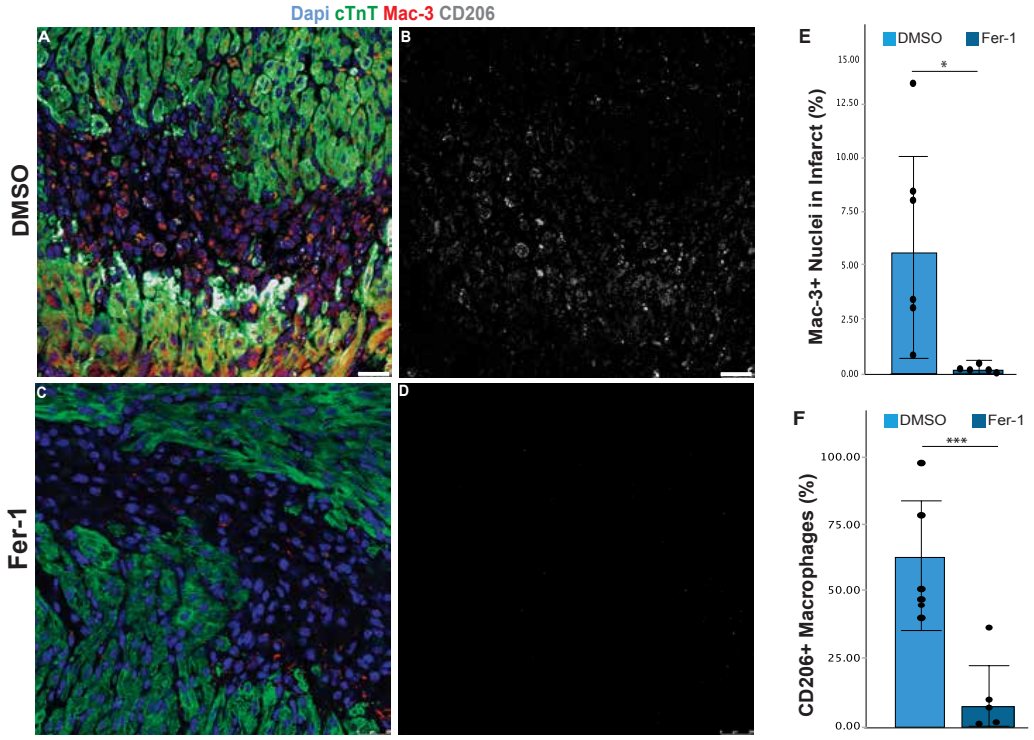

Figure 4.2 Inhibition of ferroptosis severely dampens the macrophage response in injured neonatal mouse hearts. At 3 days after P1 LAD-O, tissue sections from hearts treated with vehicle control (DMSO), (**A**–B) and Fer-1 (**C-D**) were stained for Mac-3 (red), CD206 (grey) and cTnT (green). **(E)** A significant decrease in the percentage of total macrophages in the infarct were observed in the Fer-1 treated hearts (0.16%) compared to the vehicle control (DMSO) hearts (5.56%), as calculated by Mac-3-positive nuclei per total Dapi in the infarct (p=.016). **(F)** Double positive cells were labeled as M2-like macrophages. Percentage of M2-like macrophages in the infarct sharply decreased from 62.51% to 7.94% ($P < 0.001$). N=6 per condition

We next sought to confirm the findings from immunohistochemistry via flow cytometry. We utilized multiple common gating strategies to identify various populations of macrophages present in total ventricular tissue from Fer-1 treated hearts at 3 days post-MI[166]. F4/80+CD206+ macrophages were labeled as M2-like, whereas F4/80+Ly6c+CD86+CD206- macrophages were labeled as M1-like[166](**Figure 4.3A-C**). Ly6C+, F4/80+, CD86+, and CD206- gating is frequently used as part of a panel to identify M1 macrophages in mice[166]. Analysis of the flow cytometry data supported immunohistochemical quantifications in the Fer-1 hearts, with the reduction of M2-like macrophages in the total ventricular tissue by nearly half in response to Fer-1 treatment, decreasing from 7.1% to 5.0% ($P = 0.032$)(**Figure 4.3D**). We also observed a trending increase in the M1-like macrophage population, increasing from 23.2% of the F4/80+Ly6c+ population to 29.45 (**Figure 4.3E**).

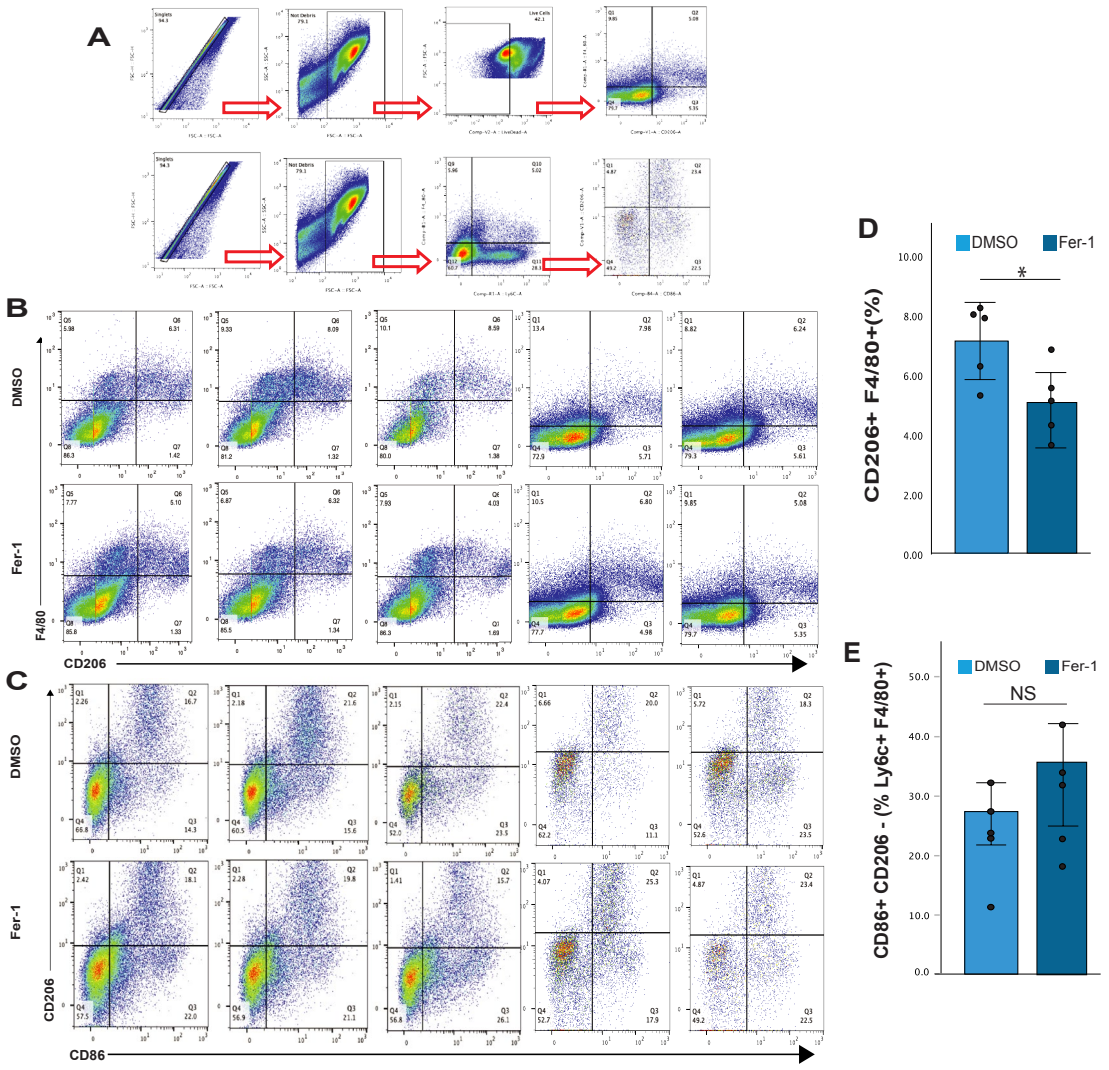

Figure 4.3 Ferrostatin-1 treatment alters the immune response. Flow cytometry of P1 3DPMI ventricular heart tissue collected after subcutaneous injection of either Fer-1 (2 mg/kg) or DMSO vehicle control at 0,1,2, and 3 days post-MI. **(A)** Gating strategy of flow cytometry study. Doublets were excludes based on FSC-A v FSC-H values, then dead cells excluded with live/dead dye staining. Lymphocytes were gated based on SSC-A and FSC-A. M2-like macrophages were gated based on F4/80+CD206+ expression. M1-like macrophages were gated based on F480+Ly6c+ CD206- CD86+ expression. **(B)** Density plots showing percentages of F4/80+CD206+ M2-like macrophages. Fer-1 treated ventricular tissue shows a decrease in the percentage of M2-like F4/80+ CD206+ macrophages compared to the DMSO treated hearts, quantified in **(D)**. **(C)** Density plots showing percentages of the total F480+Ly6c+ monocyte-derived macrophage population that are CD206- CD86+ M1-like macrophages. Fer-1 treated ventricular tissue exhibits an upward trend in the percentage of M1-like macrophages, quantified in **(E)**.

Based on the findings of impaired angiogenesis and altered macrophage populations in the hearts of Fer-1 treated animals, we re-examined the cytokine array data to identify any potential mechanisms by which ferroptotic cardiomyocytes might influence these processes. We identified interleukin-19 (IL-19) as a candidate target as IL-19 has been implicated in both angiogenesis and macrophage polarization, and is secreted by ferroptotic cardiomyocytes (**Figure 2.7**) [85,87,91,174]. Thus, we hypothesized that IL-19 plays a role in cardiomyocyte-derived signaling to other cell types in the infarcted heart.

To begin investigating the role of IL-19, we examined a publicly available single cell RNA-sequencing data set of mouse heart tissue after LAD-O or sham procedure to begin investigating the potential signaling pathways[175]. Cell clusters were called according to gene expression of known markers (**Figure 4.4, Table 1**).

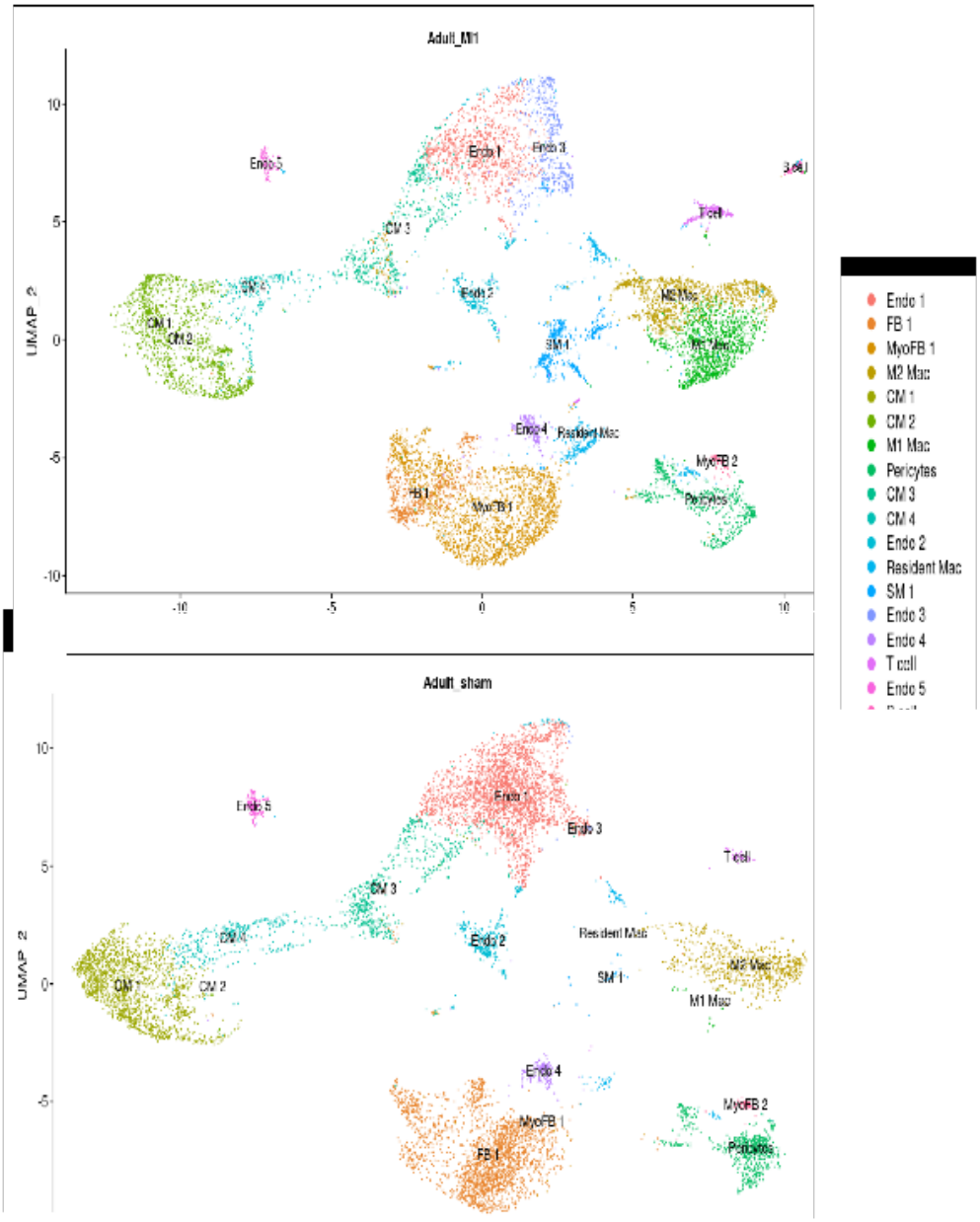

Figure 4.4: Analysis of publicly available single-cell RNA-sequencing data generated from LAD-O and Sham treated murine hearts shows 18 distinct cell clusters. GEO dataset GSE128628 was used for scRNA-seq analysis. Uniform Manifold Approximation and Projection (UMAP) was used for dimensional reduction and unsupervised clustering was carried out using the RunUMAP and FindClusters functions in Seurat, respectively. Clusters were annotated based on marker gene expression. UMAP showing the 18 color-coded cell clusters called based on RNA sequencing data in both the MI and Sham murine hearts.

Cell Type Called	Gene Name	Average log2FC
Endo1	Ptprm	2.07079294
	Ptprg	2.50197259
	Flt1	3.096270998
	Etl4	2.840831141
	Plcb4	2.436734021
	Egfl7	2.59040561
	Plcb1	2.843142702
	Cyyr1	3.002308826
	Adgrf5	2.752074268
	Adgrl4	2.813067895
	Itpkb	2.491803672
	Ablim1	1.753013783
	Stox2	2.34930434
	Ptprb	2.428276339
	Dach1	2.891802826
Endo4	Pcdh9	0.982685029
	Plcb1	0.825794305
	Kcnt2	0.941159269
	Flt1	0.641548969
	Tenm3	0.815921135
	Cyyr1	0.679619379
	Bicc1	0.870220403
	Adgrl4	0.772413142
	Egfl7	0.598941107
	Mecom	0.829939946
	Mir100hg	0.788071133
	Etl4	0.491378166
	Gulp1	0.839682764
	Rbms3	0.737791133
	Gpc6	0.658651143
CM1	Pde4d	3.46775483
	Cpeb3	3.030516621
	Mlip	2.963679856
	Rcan2	2.799432025
	Tnni3k	2.86060433

Cell Type Called	Gene Name	Average log2FC
	Coro6	2.630951885
	Pde4dip	2.616953807
	Rbm20	2.930056106
	Ryr2	2.894406662
	Mhrt	2.742512675
	Pde4b	2.594383299
	Pcdh7	2.526042876
	Dmd	2.901301445
	Palld	2.638175712
	Fhod3	2.672987313
FB1	Lama2	2.275215206
	Kcnt2	2.631368015
	Tnxb	3.184455375
	Celf2	1.852972097
	Abca8a	3.004951598
	Rora	1.700989007
	Pcdh9	2.444455536
	Bicc1	2.286819163
	Gpc6	1.597379414
	Ebf2	2.399954119
	Sox5	1.807504425
	Htra3	2.871684347
	Rbms3	1.558383577
	Gsn	2.627588637
	Mir100hg	2.0264955
M2 Macrophage	Pid1	2.379930765
	Slc9a9	2.863059025
	Arhgap15	2.51873245
	Runx1	2.21057816
	Dock2	2.253586282
	Inpp5d	2.25335691
	Dock8	2.358963841
	Zeb2	1.778124362
	Mctp1	3.005883478
	Ptprc	2.353255018

	Rbpj	3.519656195
	F13a1	3.660711531
	Mrc1	2.930147236
	Pip4k2a	1.875559993
	Fyb	2.25769707
FB1	Lama2	2.275215206
	Kcnt2	2.631368015
	Tnxb	3.184455375
	Celf2	1.852972097
	Abca8a	3.004951598
	Rora	1.700989007
	Pcdh9	2.444455536
	Bicc1	2.286819163
	Gpc6	1.597379414
	Ebf2	2.399954119
	Sox5	1.807504425
	Htra3	2.871684347
	Rbms3	1.558383577
	Gsn	2.627588637
	Mir100hg	2.0264955
SM1	Diaph3	3.445816821
	Mki67	3.007921977
	Hjurp	2.224502612
	Cenpp	2.727656453
	Top2a	2.663640735
	Rad51b	2.389674745
	Knl1	2.575106217
	Cit	2.059628329
	Ezh2	1.932005665
	Kif15	2.0769096
	Lockd	2.149606142
	Smc4	1.648249265
	Lmnb1	1.901664283
	Neil3	2.156657173
	Nsd2	1.812182
T Cell	Skap1	5.138233671
	Arhgap15	3.011221909
	Dock2	2.99758911
	Gm2682	4.919668195

	Grap2	3.799761509
	Ptprc	2.810810471
	Ikzf1	2.993181018
	Dock10	2.266065756
	Arhgap45	2.286096012
	Bcl2	2.927740927
	Inpp4b	2.827966294
	Mbnl1	1.630507908
	Lck	3.223857922
	Ankrd44	1.890637145
	Ripor2	2.90657602
Endo2	Cgnl1	3.461890006
	Tmem108	4.532379905
	Hmcn1	3.155879975
	Vwf	3.610004959
	Pecam1	2.192614934
	Heg1	1.867893822
	Cemip2	2.816639378
	Npr3	3.686472622
	Unc13b	2.303002282
	Chrm3	3.629582722
	Ptpn14	2.312215823
	Emcn	2.516364733
	Cdh11	2.892091994
	Prkg1	1.308380935
	Plxna4	1.883158362
Endo5	Reln	4.420755515
	Flt4	3.329145005
	Galnt18	2.675295991
	Prox1	3.297736486
	Pard6g	3.188126418
	Dock9	1.997181523
	Stox2	1.881498937
	Zfp521	1.910854614
	Lama4	1.987576239
	Mmrn1	3.311588179
	Ldb2	2.206788455
	Tshz2	1.858551985

	Ntn1	2.665771768
	Elk3	1.909002116
	Nxn	2.414080354
CM2	Fhl2	3.225659265
	Ryr2	2.880043138
	Ttn	2.513483751
	Sorbs1	2.507361266
	Ctnna3	2.946642745
	Rbm20	2.890783288
	Cacna1c	2.681587721
	Actn2	2.715681849
	Slc8a1	2.398101932
	Tnnt2	2.245160133
	Fhod3	2.797957959
	Ldb3	2.445871681
	Sorbs2	2.649735266
	Pde4dip	2.312041377
	Myom1	2.371069561
MyoFB1	Postn	3.149524201
	Col1a2	2.240892602
	Pdzrn3	2.559831852
	Col8a1	2.774454704
	Col3a1	2.150072705
	Kif26b	3.519313962
	Bnc2	2.560709918
	Rbms3	1.924331617
	Col1a1	2.067842252
	Col5a2	2.177375383
	Fstl1	1.944001659
	Gpc6	1.837286444
	Fn1	2.609833051
	Tenm3	2.089961814
	Fbn1	1.838081292
M1 Macrophages	Mertk	2.785018145
	Dock2	2.408763774
	Slc9a9	2.430750794
	Inpp5d	2.422027103
	Rreb1	2.085178114

	Ms4a7	2.968042235
	Runx1	2.115085393
	Rbm47	2.705269335
	Stab1	2.511739243
	Myo1f	2.696034372
	Arhgap15	2.06398561
	Zdhhc14	2.48223406
	Pid1	1.915647106
	Lrmda	1.806700258
	Abca1	2.274100081
MyoFB1	Postn	3.149524201
	Col1a2	2.240892602
	Pdzrn3	2.559831852
	Col8a1	2.774454704
	Col3a1	2.150072705
	Kif26b	3.519313962
	Bnc2	2.560709918
	Rbms3	1.924331617
	Col1a1	2.067842252
	Col5a2	2.177375383
	Fstl1	1.944001659
	Gpc6	1.837286444
	Fn1	2.609833051
	Tenm3	2.089961814
	Fbn1	1.838081292
Pericytes	Dlc1	2.987858121
	Prkg1	2.771345891
	Abcc9	4.258640541
	Plcl1	2.766647261
	Notch3	3.34463107
	Gucy1a2	2.980184649
	Mast4	1.857611344
	Gpc6	1.945881152
	Pdgfrb	2.865272997
	Trpc3	3.88142273
	Mrvi1	3.174813141
	Rgs5	3.150529307
	Ebf1	1.576600645
	Cald1	2.014776384

	Morrbid	2.501381242
Endo3	Magi1	1.887862839
	Pecam1	1.888165699
	Ldb2	2.30244036
	Apbb2	1.52549374
	Plekhg1	2.085432807
	Egfl7	1.726336139
	Rapgef5	2.076294391
	Ptprm	1.31130055
	Col4a1	1.695094794
	Ptprb	1.745934334
	Adamts9	2.143614037
	Col4a2	1.624945367
	Adgrl4	1.754514463
	Adgrl2	1.67415025
	Tcf4	1.274058348
CM4	Ttn	2.178704781
	Tnnt2	2.002027676
	Myh6	1.873091656
	Ryr2	2.09641084
	Pde4d	1.958355981
	Pde4dip	1.86013352
	Fhl2	2.018536164
	Cacna1c	1.917194365
	Rbm20	2.003739504
	Dmd	2.107085999
	Mybpc3	1.893850626
	Ctnna3	1.820543031
	Atp2a2	1.382836768
	Tnni3	1.734732138
	Malat1	0.6522065
CM3	Gm42418	1.751857337
	mt-Co1	2.960748083
	Mb	3.12093473
	Lars2	1.684809788
	mt-Co3	2.912503355
	Cmss1	1.65011816
	mt-Co2	2.98560453
	Tpm1	2.086039569

	Myh6	1.693761596
	Il31ra	1.829663599
	Gphn	1.557135706
	Myl2	2.497795951
	Camk1d	1.401545596
	Tnni3	2.221540031
	mt-Cytb	2.755129177
MyoFB2	Abcc9	2.719967961
	Dlc1	1.883209175
	Rgs5	2.412544678
	Pde8b	2.404165625
	Trpc3	2.438017922
	Pdgfrb	1.91150539
	Plcl1	1.814476667
	Notch3	1.978514136
	Lin7a	2.365048592
	Myo1b	1.802892156
	Prkg1	1.46868599
	Ano1	2.320499441
	Gucy1a2	1.935946027
	Ptprk	1.652124102
	Mrvi1	1.748288249
Resident Macrophages	Slc9a9	1.208058842
	Dock2	0.949598743
	Inpp5d	1.005085194
	Arhgap15	0.857940421
	Runx1	1.009320751
	Pid1	0.959476027
	Ptprc	0.842323395
	Fyb	1.005099104
	Stab1	1.096845922
	Mctp1	1.088724831
	Dock8	0.899645851
	Arhgap22	0.956029352
	Mertk	1.063121874
	Myo5a	0.978021517
	Rbm47	0.992551605
MyoFB2	Abcc9	2.719967961
	Dlc1	1.883209175

	Rgs5	2.412544678
	Pde8b	2.404165625
	Trpc3	2.438017922
	Pdgfrb	1.91150539
	Plcl1	1.814476667
	Notch3	1.978514136
	Lin7a	2.365048592
	Myo1b	1.802892156
	Prkg1	1.46868599
	Ano1	2.320499441
	Gucy1a2	1.935946027
	Ptprk	1.652124102
	Mrvi1	1.748288249
B Cell	Bank1	5.00905239
	Arhgap15	3.110745957
	Foxp1	2.176894182
	Aff3	3.853811226
	Bach2	3.376828331
	Dock2	2.664558014
	Prkcb	2.92078893
	Pax5	4.099760275
	Ripor2	3.906009758
	Ebf1	1.714160737
	Syk	2.798589847
	Gm15987	3.335354189
	Cd74	2.799911046
	Ccnd3	2.137678826
	Ralgps2	3.356868887

Table 4.1 Cell clusters called by gene expression of the top 15 genes expressed in each cluster. Cell clusters called in figure 4.4, with the top 15 most highly expressed genes in each cluster, corresponding with the UMAP showing the 18 color-coded cell clusters called based on RNA sequencing data in both the MI and Sham murine hearts.

After defining cell types by gene expression, we used CellChat to predict IL-19 signaling between cardiomyocytes, endothelial cells, and macrophages in response to ischemic injury based on published receptor-ligand data[175,176]. As IL-19 is known to signal through a heterodimer receptor comprised of IL20Rβ and IL20Rα, expression of these receptor subunits can be used to predict IL-19 signaling [86]. The circle plots are generated based on RNA expression data, where the size of the circle corresponding to each cell cluster is directly proportional to the number of cells in that cluster. The width of the line connecting two cell clusters is directly proportional to calculated interactions between the two clusters[177]. CellChat predicted strong interactions between subpopulations of cardiomyocytes, endothelial cells, and macrophages (**Figure 4.5**). Predicted signaling derived from resident macrophages are strongest towards Endo 3 and 4, and weaker towards Endo 1 (**Figure 4.5B**). Predicted signaling derived from cardiomyocyte subpopulations CMs 1 and 2 are strongest when directed towards the resident cardiac macrophage population. These signals similarly target M1 and M2 populations, albeit less robustly (**Figure 4.5C**). Endo 1-derived interactions are similarly strong when targeting Endo 3 and 4, along with resident macrophages. CMs 1 and 2 were predicted to engage strongly with Endo 1, 3, and 4, as well as with each other, while Endo 3 and 4 are predicted to engage strongly with each other as well as respond back with CMs 1 and 2 **(Figure 4.5D**).

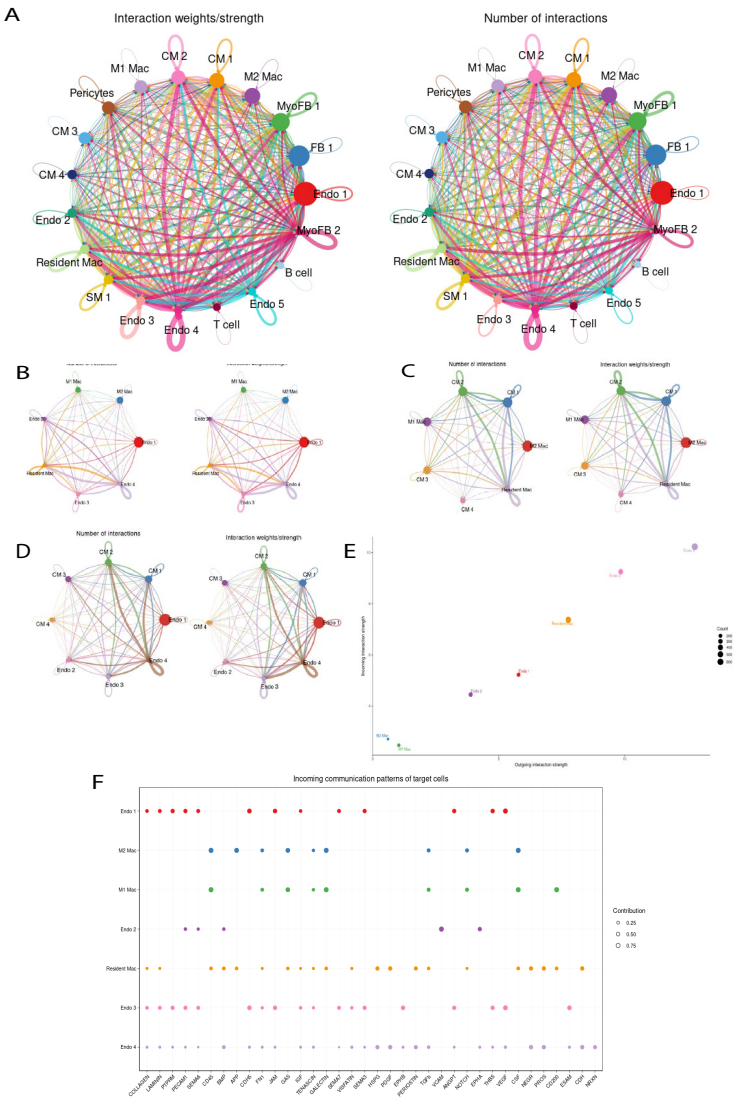

Figure 4.5 Single-cell RNA-Sequencing analysis predicts interactions between cardiac cell populations. The total number of predicted interactions, and the strength of those interactions, are displayed in circle plots in **(A-D)**. The size of the circle corresponding to each cell cluster is directly proportional to the number of cells in that cluster, and the width of the line connecting two cell clusters is directly proportional to calculated interactions between the two clusters. CM clusters 1 and 2 are predicted to interact strongly with resident cardiac macrophages, which is predicted to interact strongly with endothelial population 4 (Endo 4). The relative strength of the ingoing vs outgoing interactions is plotted in **(E)** to demonstrate which subpopulations are predicted to engage in a higher degree of signaling relative to each other. Similarly, common incoming signaling pathways, including collagen, VEGF, and TGFß, are graphed in **(F)**. Notably, the resident macrophage and endo 4 populations are both highly active.

To further investigate these predicted interactions, we investigated the expression of the receptor subunits IL20Rα and IL20Rβ in the sham and LAD-O mouse hearts. As IL-19 is part of the IL-10 family and is known to signal through a heterodimer receptor comprised of IL20Rβ and IL20Rα, expression of these receptor subunits can be used to predict IL-19 signaling [86,89,117]. The proportion of cells expressing IL20Rα remained consistently low between the Sham and MI conditions with few exceptions. Resident macrophage, MyoFB 1, SM 1, and T cell populations, which exhibited an increased expression of I IL20Rα in response to MI. Interestingly, Endo 1 and CM 1 exhibited increased I IL20Rα expression in the Sham hearts (**Figure 4.6A, C**). IL20Rβ expression is upregulated in response to MI in multiple cell types, but this change is more prominent in Resident macrophage, CM 3, SM 1, and MyoFB 2 populations, as well as all 5 subpopulations of endothelial cells **(Figure 4.6B-C).**

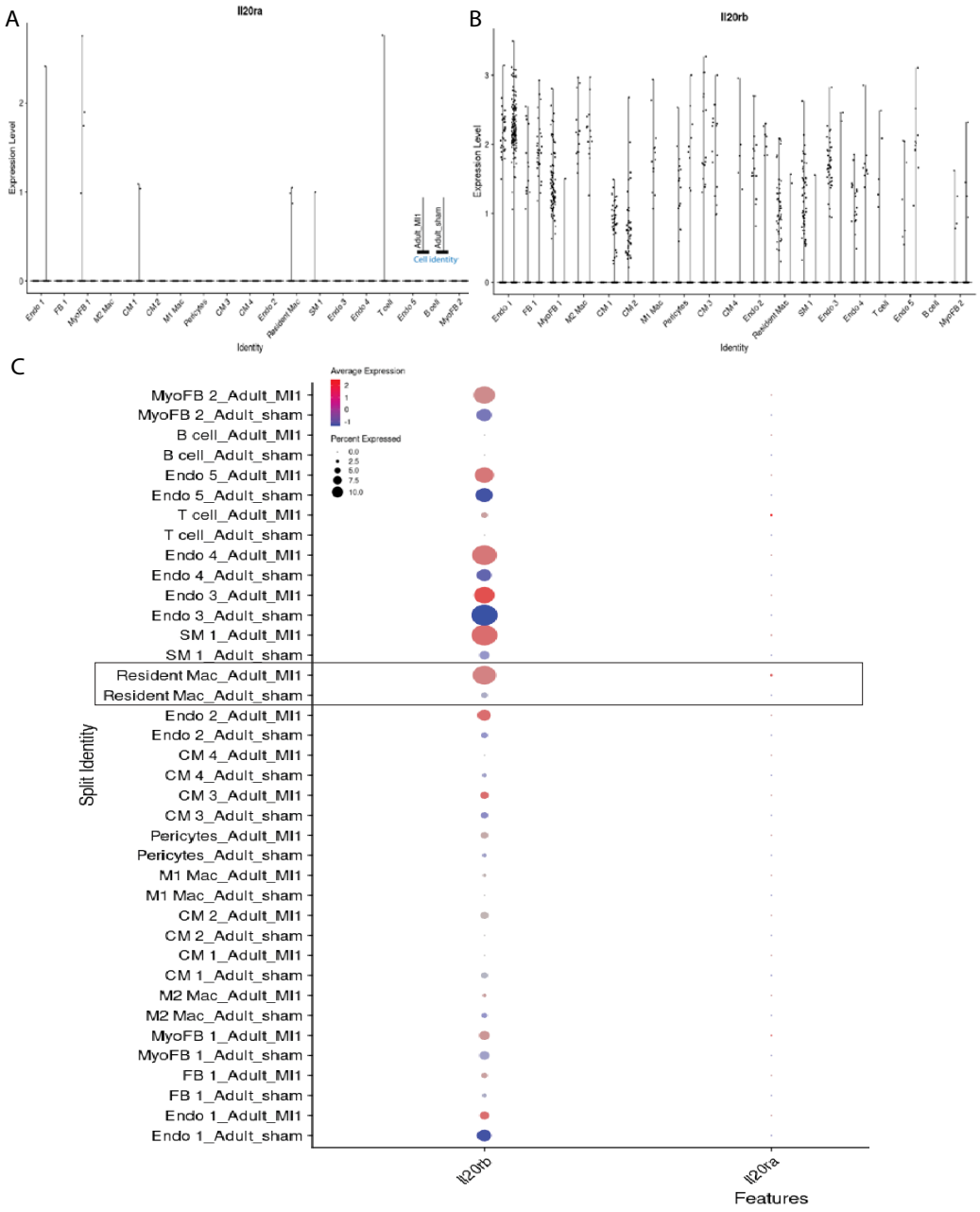

Figure 4.6 Expression of IL-19 receptors by cell type in Sham and LAD-O murine hearts as determined by single cell RNA-sequencing analysis. and Expression of IL20rb and IL20ra by sham vs MI Dot plot depicting the expression of IL20Rβ and IL20Rα. Boxes highlight the Resident Cardiac macrophage and Endo 1 populations that show the greatest upregulation in IL20Rα receptor subunit in response to MI, which corresponds to the feature plot shown in figure 6H. (G-H) Feature plot showing the RNA expression levels of each IL20 receptor subunit in each of the 18 cell clusters.

We next aimed to determine the effects of IL-19 on endothelial cells after injury. To test the effects of IL-19 on endothelial cell proliferation, we treated HUVECs with H2O2 to simulate the oxidative stress in the myocardium after ischemic injury. Recombinant IL-19 protein was added to the media and cells were probed for PH3 and Alpha-tubulin. PH3+ cells were counted and quantified as a percent of the total nuclei. A trending increase was observed in response to the addition of H_2O_2, (0.97%) and again in response to H_2O_2 and IL-19 protein administration (1.21%) (**Figure 4.7A**), although no significant increase was observed. These data may indicate that other cell types must be present to see the full effects of IL-19, although more experimentation and optimization should first confirm these results.

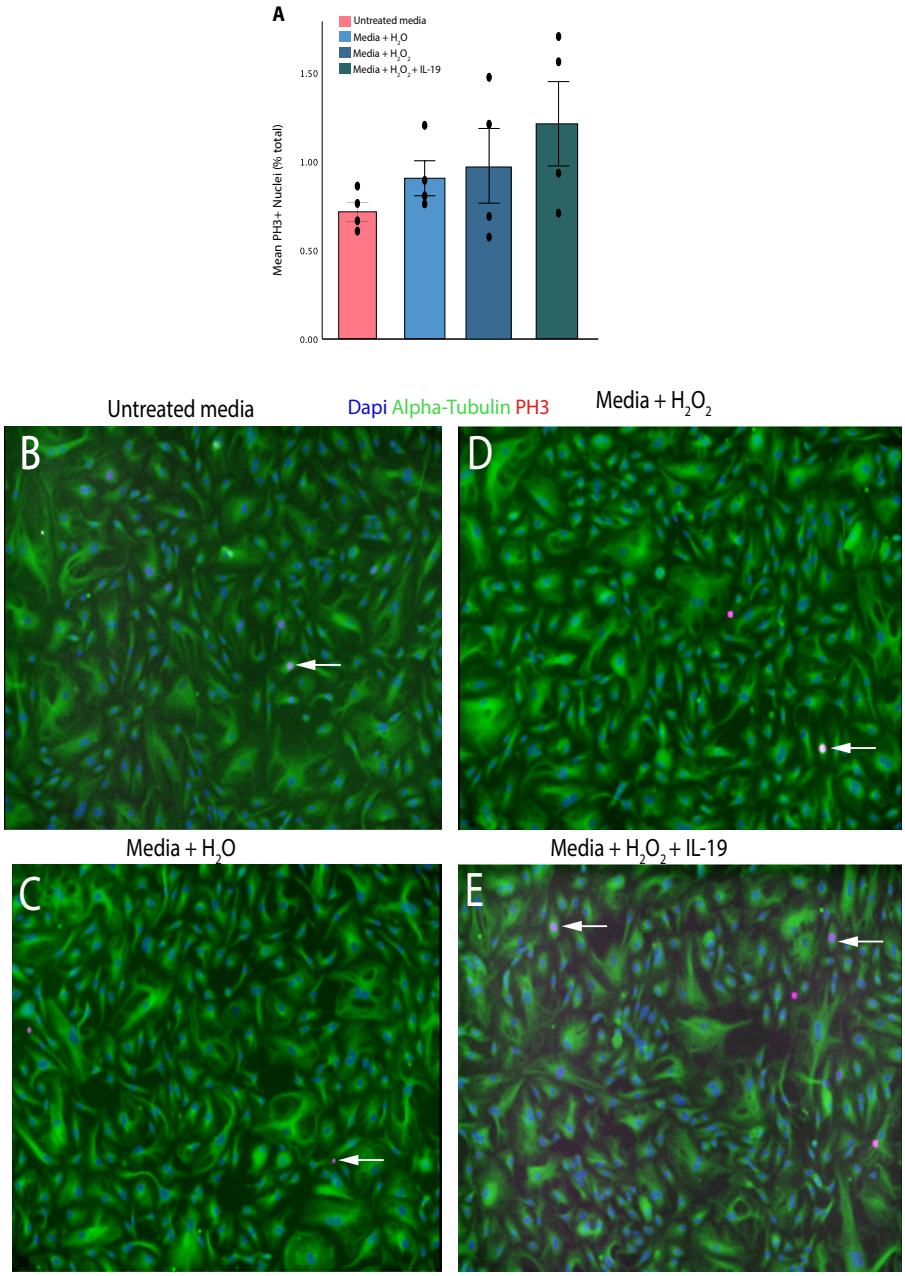

Figure 4.7- L-19 does not significantly improve proliferative rates of HUVECs in response to oxidative stress. HUVECs were treated with 500μM H_2O_2 to simulate oxidative stress, and 100ng/mL of exogenous recombinant IL-19 protein was added to investigate the effects of IL-19 on HUVEC proliferation under ROS-heavy conditions. Cells were incubated for 4 hours, then fixed and probed for alpha-tubulin (green) and PH3 (red). **(A)**. HUVECs treated with both H_2O_2 and IL-19 exhibited a trending increase in proliferation compared to H_2O_2 alone, increasing from 0.97% to 1.21% (N.S.) **(B-E)** Representative images show examples of proliferating HUVECs as depicted by double positive staining of Alpha-Tubulin and PH3 (arrows).

To further elucidate the function of IL-19 in the infarcted mouse heart, we moved to an *in vivo* analysis of IL-19. Mice were given either Sham or LAD-O procedure at the non-regenerative timepoint postnatal day 7 (P7) followed immediately by IL-19 or vehicle injection (**Figure 4.8A**). Hearts were then analyzed 21 days later to allow completion of the majority of infarct remodeling. IL-19 delivery alone did not alter myocardial structure or function in sham treated hearts (**Figure 4.8B-D**). In MI hearts, however, exogenous IL-19 delivery significantly improved outcomes at 21 days post MI compared to vehicle controls. We observed both preserved contractility as measured by echocardiography and decreased infarct size as measured by trichrome staining (**Figure 4.8E-H**). As we previously observed decreased endothelial density in the infarct with Fer-1 treatment, and IL-19 is an established pro-angiogenic cytokine, we evaluated endothelial density in the infarct after IL-19 administration. Immunostaining of EMCN revealed significantly improved endothelial density in response to IL-19 treatment at 21 days post-MI (**Figure 4.9A-C**).

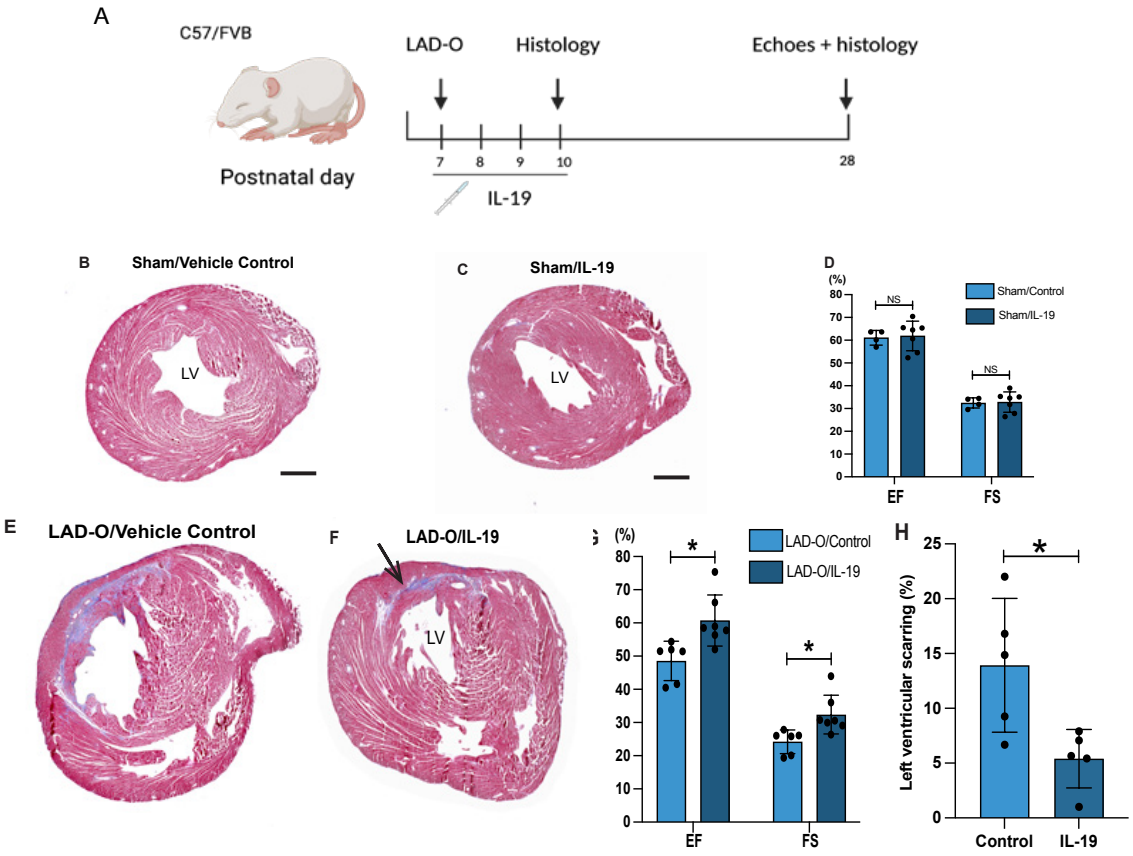

Figure 4.8 IL-19 administration ameliorates detrimental remodeling in P7 LAD-O hearts and improves cardiac function. (A) Experimental design of mouse model for panel B to H. Representative images of trichrome staining of heart sections at 21 days after sham procedure with vehicle control **(saline, B**) or IL-19 (**C**) treatment. Ejection fraction (EF) and fractional shorting (FS) of vehicle control and IL-19-treated mice were measured and graphed in (**D**), showing no difference in either measurement. (**E**–**H**) Representative trichrome images of heart sections at 21 days after LAD-O with vehicle control (**E**) or IL-19 (**F**) treatment. IL-19 treatment alone does not affect myocardial structure or function. EF and FS of vehicle control and IL-19-treated mice were measured and are plotted in (**G**). Infarct measurement is quantified in (**H**) as percent of left ventricular area.

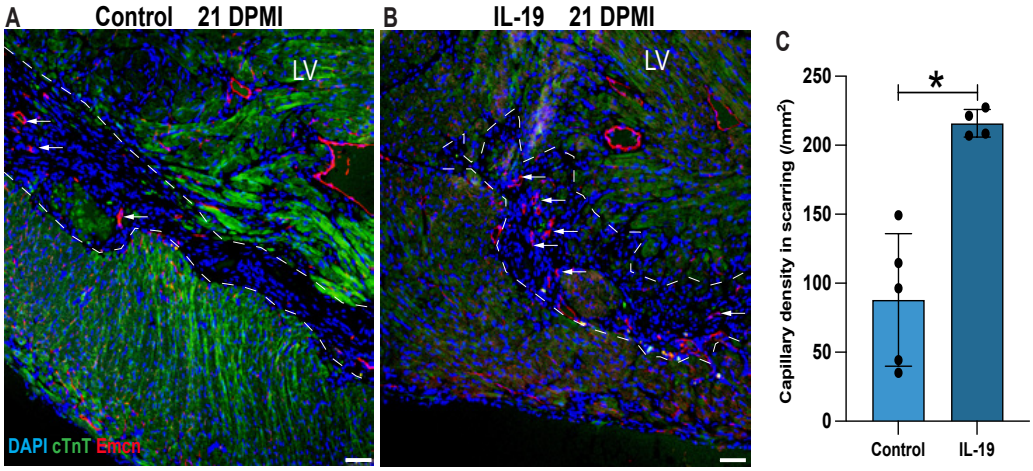

Figure 4.9 IL-19 treatment improves endothelial density in the infarct of P7 LAD-O hearts. At 21 days after P7 LAD-O, tissue sections from hearts treated with vehicle control (DMSO, (**A**–**C**B) or IL-19 (**C-D**) were stained for Endomucin (EMCN) (red) and cTnT (green). Dotted lines encircle the scarring in the left ventricle. Arrows indicate positive EMCN staining in the infarct, quantified in **(C)**. Percentage of EMCN-positive endothelial cells is significantly increased in the IL-19 treated mice compared to vehicle control mice.

We proceeded to examine the effect of IL-19 administration on P7 MI hearts at 3 days post-MI to characterize its role in the acute injury period associated with ferroptosis. Trichrome staining and subsequent analysis of the infarcted area revealed no changes in ischemic area (**Figure 4.10**). Immunostaining of EMCN similarly revealed no changed in endothelial cell density in the infarct. However, co-staining EMCN with PH3 showed that IL-19 treatment promoted cell cycle activity in endothelial cells. (**Figure 4.11**). Co-staining PH3 with MF20 showed no difference in cardiomyocyte cell cycle activity, reinforcing IL-19 as an angiogenic mediator. However, IL-19 administration did reduce the percentage of Ptgs2 positive cardiomyocytes in the infarct, indicating a reduction in oxidative stress. Notably, the localization of Ptgs2 positive cardiomyocytes suggests that IL-19 administration inhibits the spread of ferroptosis in cardiomyocytes along the border zone (**Figure 4.12**). Taken together, these data support a protective role for IL-19 in the post-MI, non-regenerative P7 mouse heart.

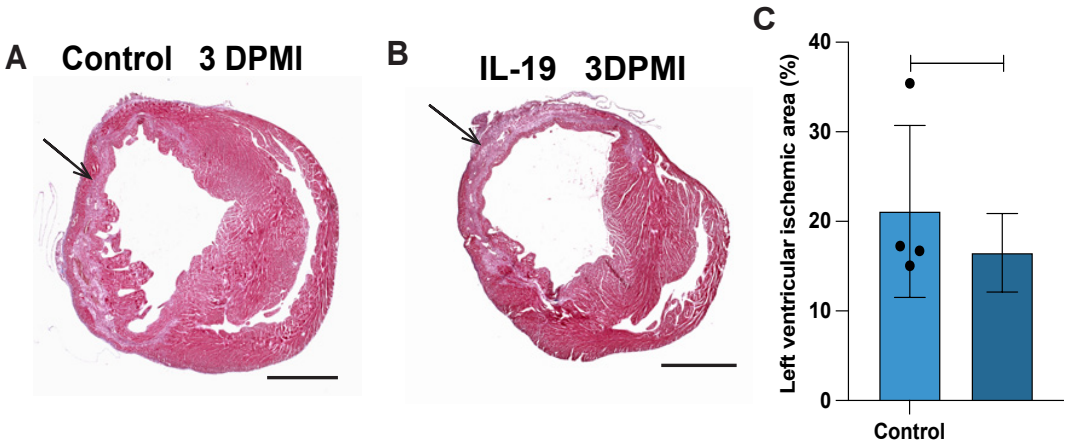

Figure 4.10 IL-19 does not alter ischemic area 3 days post-LAD-O in P7 hearts. Masson's trichrome staining to visualize infarcted/fibrotic area in blue (arrows) in heart sections of representative hearts from each group 3 days after P7 LAD-O with vehicle control **(A)** or IL-19 **(B)** treatment. Quantification of infarct size in DMSO and IL-19 treated hearts in P7 MI mice, as percent of total left ventricular area (**C**).

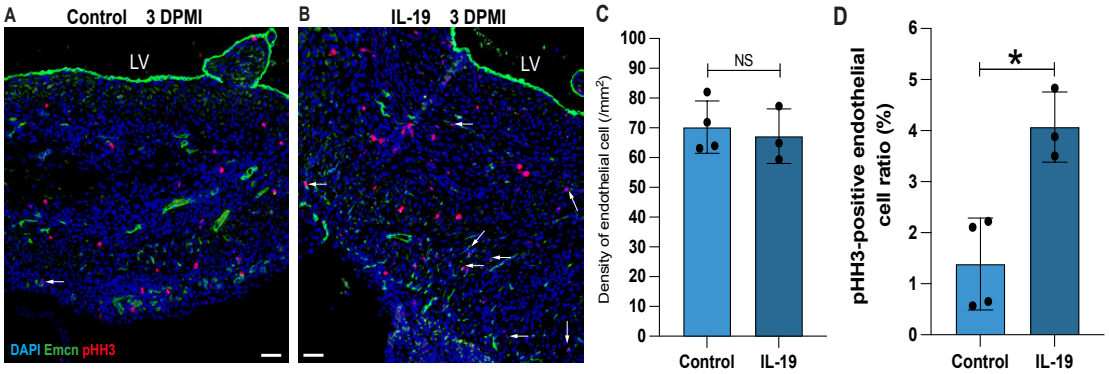

Figure 4.11 IL-19 administration improves proliferative rate in endothelial cells in the infarct of P7 mice. At 3 days after P7 LAD-O, tissue sections from hearts treated with vehicle control (DMSO, **A)** and IL-19 **(B)** were stained for Endomucin (EMCN) (green), PHH3 (green). Double positive cells were labeled as proliferating endothelial cells, indicated by arrows and quantified in **(D)** as the percent of total EMCN-positive cells in the infarct. Density of endothelial cells in scar zone is quantified in **(C)**. Notably, IL-19 improved proliferation rates in endothelial cell at this timepoint but not endothelial density in the infarct.

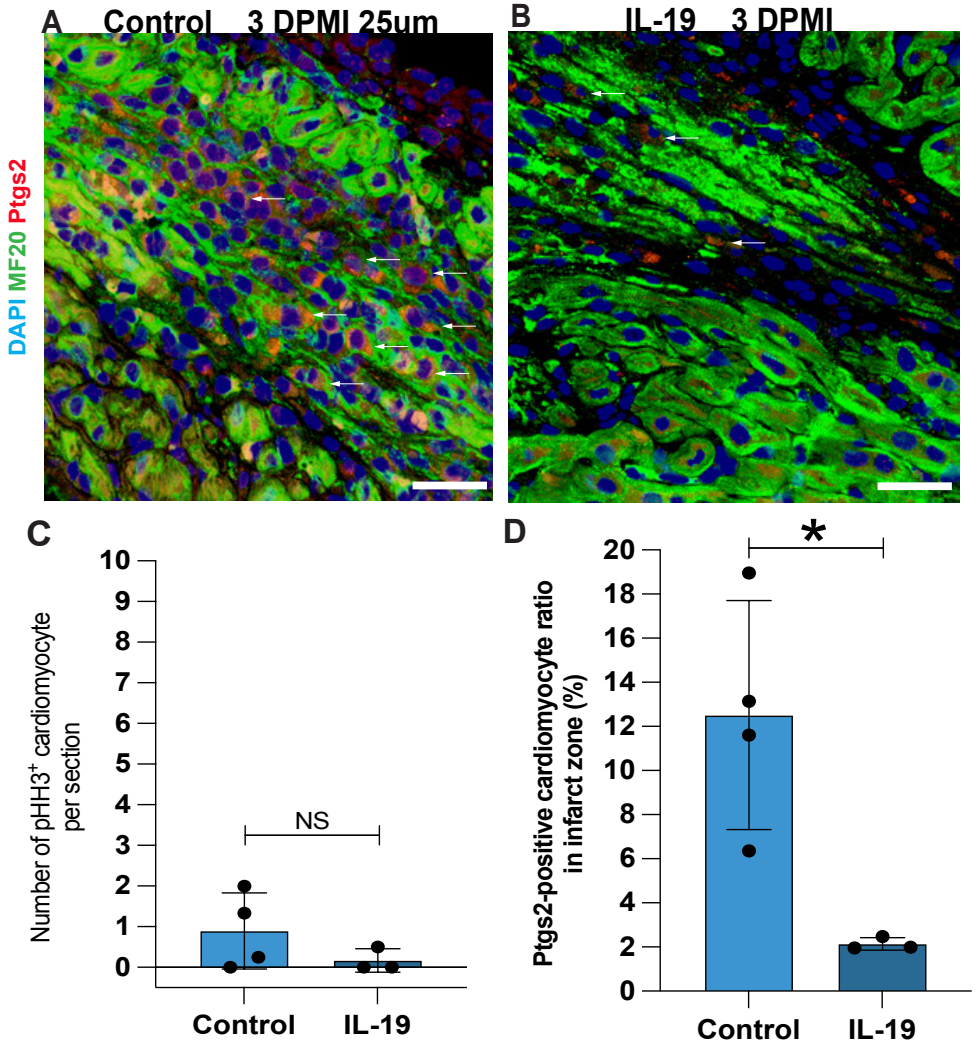

Figure 4.12 IL-19 does not inhibit cardiomyocyte ferroptosis. At 3 days after P7 LAD-O, tissue sections from hearts treated with vehicle control (DMSO, (**A**) or IL-19 (**B**) were stained for Ptgs2 (red), Dapi (blue), and MF20 (green). Arrows indicate positive Ptgs2 staining in the infarct, quantified in **(C)**, indicative of ferroptosis. Number of Ptgs-positive cardiomyocytes exhibits a trending, but significant decrease in percentage of ferroptotic cardiomyocytes in the infarct zone. Ratio of Ptgs2-positive cardiomyocytes in scar zone is quantified in (**D**). Interestingly, IL-19 delivery appears to limit spreading of ferroptosis in the border zone.

4.3 Discussion

This study presents novel data implicating secreted factors, including IL-19, derived from ferroptotic cardiomyocytes in macrophage polarization and infarct remodeling. Previous studies have focused only on the benefits of suppressing ferroptosis in the heart as a way to preserve the cardiomyocyte population and subsequently, cardiac function[178,179]. Here we highlight the importance of understanding the effects of RCD on the surrounding tissue. Additionally, we identify a mechanism of action that contributes to the beneficial effect ferroptotic cardiomyocytes exert on the immune system.

The process of cardiac repair in mice switches from inflammatory immune response to a reparative immune response around day 3[138]. While the clearance of apoptotic cardiomyocytes has been identified as a critical step in the transition to resolution of inflammation[138,180], ferroptosis in the infarcted mouse heart peaks at day 3 [98]. Considering the timing and prevalence of cardiomyocyte ferroptosis, and our observations in the infarcted mouse heart, it is likely to be similarly importance to the resolution of inflammation. As investigations continue, it seems increasingly plausible that cardiomyocytes play a more active role in the remodeling process than previously considered.

We reported a change in the macrophage population as a consequence of Fer-1 administration. Our immunofluorescence data show that the inhibition of ferroptosis via Fer-1 administration post-MI results in a decrease in total macrophage numbers in the

infarct (Figure 4.2). Those present in the infarct are significantly less polarized towards the M2 state (60 something % to like 9%) (**Figure 4.2**). While this effect is primarily limited to the infarct, the effects of Fer-1 are strong enough to be observed in flow cytometry of total ventricular tissue (**Figure 4.3**). We primarily utilized CD206 as an M2 marker; however, there are many recognized subgroups of the M2 macrophages, including M2a, M2b, M2c, M2d, and M2f [181,182]. CD206 is an established marker of M2a-c[181]. Each subtype has been recognized as possessing distinct functions. For example, M2a macrophages predominantly secrete factors that dampen the inflammatory response[182]. Macrophages are stimulated towards the M2a phenotype by IL-4 and IL-13, the first of which was the single most upregulated cytokine secreted by ferroptotic cardiomyocytes (**Figure 2.7**). M2a macrophages also secrete IL-10, which is capable of inducing M2c polarization[182]. M2c macrophages are primarily established as pro-regenerative, and contribute heavily to resolution of inflammation and matrix deposition[182]. However, M2b macrophages perform both pro- and anti-inflammatory functions. They are stimulated by LPS to produce anti-inflammatory cytokines such as IL-10 and promote the anti-inflammatory Th2 responses, but also produce pro-inflammatory cytokines such as TNF and IL-6 [183-185]. M2d macrophages are known to be pro-angiogenic and express factors such as VEGF and IL-10 [186]. Whether these macrophages also express CD206, or whether these subtypes are similarly expressed in vivo as they are in in vitro, remains unclear[181,187]. Cytokine array data suggests that ferroptotic cardiomyocytes may initially push macrophages towards the M2a

phenotype. However, the details of macrophage subtype polarization by ferroptotic cardiomyocytes warrant further investigation.

We utilized publicly available single-cell RNA sequencing data from adult mice given Sham or LAD-O surgery to further investigate the findings of altered angiogenesis and macrophage polarization, as well as the potential role of IL-19[175]. A total of 18 cell types were clustered in R with Seurat based on established cell type markers (**Table 1, Figures 4.5 and 4.6**)[188]. We then followed up by utilizing CellChat to produce quantitative inferences of communications between cell types based on established, complex ligand-receptor data[189]. This allows us to visualize the strength of the predicted signaling pathways between cell types. These analyses revealed strong signaling pathways between certain subgroups of cell types, predominantly involving CMs 1 and 2, Resident Macrophages, and Endo 1, 2, and 3. CMs 1 and 2 both established strong interactions with the resident macrophages, which likewise signaled back to both CMs 1 and 2. Less strong interactions were also predicted to originate from the Resident Macrophages and target the M1 and M2 macrophage populations. Resident cardiac macrophages also interacted strongly with endothelial subgroups Endo 3 and 4, and less strongly with Endo 1 and 2. Interestingly, strong interactions originating from Endo 3 and 4 connected all 4 endothelial cell groups in addition to the Resident Macrophage population. While it is not possible to observe the timing of predicted interactions, these models suggest that Endo 3 and 4 communicate strongly with the Resident Macrophages and continue to regulate the remaining endothelial cell populations. This agrees with previous publications that describe resident cardiac macrophages as direct

regulators of angiogenesis via endothelial cell interactions[78,190-192]. Finally, we observed strong signaling between Endo 3 and 4, as well as between CMs 1 and 2 and Endo 3 and 4 (**Figure 4.5**). Taken together, these predictions provide support for signaling networks that include CMs 1 and 2 signaling to Resident Macrophages and Endo 1 and 2, which then aid in coordinating the remaining endothelial cell population.

Based on our findings, ferroptotic cardiomyocytes may play a significant role in the resolution of inflammation. As angiogenesis and macrophage modulation were both significantly affected by Fer-1 administration, we investigated the expression of IL-19, a cytokine known to regulate both processes[85,87,91]. Through our analysis of published single-cell RNA sequencing data, we found that IL20Ra and IL20RB, the subunits that comprise the IL-19 receptor, were more highly expressed after MI (**Figure 4.6**). However, IL20RA was expressed in fewer cell types post-MI, including myofibroblasts, resident macrophages, T cells, and smooth muscle cells. Interestingly, IL20RA expression was increased in Sham but decreased post-MI in endothelial group Endo 1, and in cardiomyocyte group CM 1 (**Figure 4.6**). Western blotting confirmed the upregulation of IL-19 protein in ferroptotic cardiomyocyte-derived conditioned media (**Figure 4.7**).

To test the ability of IL-19 to increase cell cycle activity in endothelial cells, we added H2O2 to HUVEC culture to mimic oxidative stress *in vivo* and added recombinant IL-19 protein. These cells were then probed for PH3 as a marker of proliferation. Interestingly, only a trending increase was observed in response to the addition of both H2O2 and IL-19 **(Figure 4.8**). It has been shown that IL-19 signals through the p44/42 MAPK pathway in HUVECs[90], the same pathway activated by H2O2 in HUVECs[193]. IL-

19 has also been shown to improve both tube formation and migration in endothelial cells[193]. We see a similar trend in the amount of cell spreading in H2O2+IL-19 treated HUVECs (**Figure 4.8**). For future studies, the amount of IL-19 protein should tested at varying amounts to identify the amount needed to see a significant increase in HUVEC spreading, and to record any dose-dependent increases in cell size.

We proceeded to utilize exogenous IL-19 delivery in our P7, non-regenerative LAD-O mouse model of MI (**Figure 4.9**). While no changes were seen in the sham hearts, the LAD-O + IL-19 hearts exhibited both a decrease in infarct size as well as an increase in cardiac function at 21 days post-MI (**Figure 4.10**). A 21 days post-MI, at which point infarct remodeling should be stable, we observed a significant increase in the endothelial cell density in the infarct (**Figure 4.11**). This confirms the lasting effects of IL-19 injection beyond when IL-19 administration ceased at 4 days post-MI. To observe the short-term effects of IL-19 on the infarcted mouse heart, we repeated the experiments, but instead observed the heart at 3 days post-MI. At this timepoint there was no significant change in infarct size, indicating that the role of IL-19 is not reducing the ischemic area (**Figure 4.12**).

As IL-19 is involved in angiogenesis, we investigated the endothelial population at 3 days post-MI. Interestingly, there was no significant difference in the endothelial cell density at this point; however, the percent of PH3+ endothelial cells was significantly increased (**Figure 4.13**). This partially explains the discrepancy in the endothelial cell population the 3- and 21-days post-MI mice. As IL-19 is involved more so in the remodeling of the left ventricle after injury, the delayed response of the

endothelial population fits. At 3 days post-MI, the endothelial population in the heart is in the earlier phases of responding to IL-19 treatment and cell cycle activity begins to increase, leading to the delayed improvement in angiogenesis seen.

Finally, we investigated whether IL-19 treatment improved cardiomyocyte proliferation or survival. Expectedly, we saw no improvement in the number of PH3 positive cardiomyocytes. The trend was decreasing rather than increasing (**Figure 4.13**). However, the Ptgs2 positive cardiomyocytes in the infarct significantly decreased in response to IL-19 treatment. Interestingly, the pattern of positive staining indicated that the expansion of oxidative stress in the infarct may be stopped from expanding the along the border zone. The finding that IL-19 seems to prevent the spread of ferroptosis in cardiomyocytes along the border zone of the infarct is of particular interest. Recently, Nishizawa, H., et al reported that cells exposed to Erastin are capable of spreading lipid peroxidation resulting in ferroptosis to neighboring cells independently of Erastin[194]. Shortly after, Kawasaki, N. K., et al reported that RSL3 induced ferroptosis expanded in the heart from cell to cell along myofibers[179]. This expansion of cell death is seemingly limited by IL-19, but more investigation is needed [179,194].

Collectively, the data we present here show that ferroptosis play a strong beneficial role in recruiting and polarizing the macrophage population in the infarct. Computational modeling predicts strong interactions between subpopulations of macrophages, cardiomyocytes, and endothelial cells. These interactions are at least partially mediated by IL-19 signaling, which is a key component of left ventricular remodeling post-MI through regulation of angiogenesis. We implicate cytokines

secreted by ferroptotic cardiomyocytes in angiogenesis both directly and via macrophage polarization, a novel finding that provides crucial insights into the development of future therapeutics.

Discussion and Future Directions

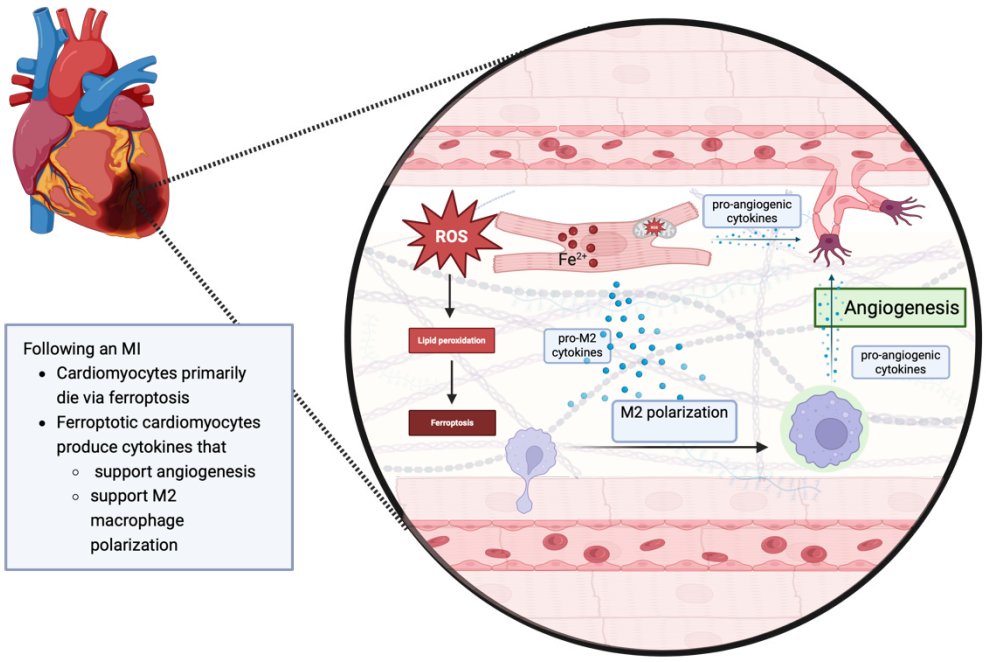

Figure 5.1: Graphical abstract of hypothesized mechanism. Here, we examine the effects of cardiomyocyte ferroptosis on the infarcted heart using ferrostatin-1 to inhibit ferroptosis and Erastin to induce ferroptosis in mouse models of MI and human iPSC-derived cell culture. Our analysis revealed that ferroptotic cardiomyocytes play a supportive role in the wound healing and tissue remodeling environment, which may partially explain why cardiomyocytes preferentially undergo ferroptosis as opposed to other types of regulated cell death in the infarcted heart. These affects occur at least partially through IL-19 signaling. These findings show that inhibiting ferroptosis in the regenerating mouse heart has consequences on the immune system and the angiogenic response, as well as highlight the importance of understanding the effects of cell death in regeneration when developing novel therapeutics.

Cardiovascular diseases (CVDs) are the leading cause of death in the United States, with a heart attack occurring every 40 seconds. [1,119]. CVDs contribute heavily to both premature mortality and rising health care costs, representing an economic burden of over $400 billion in the US alone [1,3]. Globally, ischemic heart disease has remained the number one cause of death for decades [4]. The prevalence of risk factors associated with heart disease is unfortunately projected to increase markedly over the next several decades[5]. Altogether, heart disease represents a significant public health crisis. MI is predominantly caused by a rupture of an atherosclerotic plaque that results in clot formation in the coronary arteries[6]. Therapies such as percutaneous coronary intervention (PCI) and thrombolytic therapy have led to improved outcomes, but pose their own unique challenges[6]. Discrepancies in reports on current therapies serve to highlight how urgently new therapies that go beyond current myocardial injury mitigation strategies are needed.

During an MI, blood flow is first occluded to the cardiac muscle tissue, and clinical standards are to re-perfuse the hypoxic tissue as quickly as possible to mitigate damage[10]. This rapid reoxygenation causes a burst of ROS production, resulting in further damage and cardiomyocyte death[11]. Mature human cardiomyocytes are unable to regenerate following injury due to the low annual turnover of between 0.2-2% in adults [12]. This limitation inhibits recovery for MI patients as lost cardiomyocytes cannot be replaced to support cardiac function.

Previous work from our lab demonstrated that ferroptosis is the primary mechanism of cardiomyocyte death in the P1 and P7 mouse heart post-MI[98].

Ferroptosis is an iron-dependent form of cell death characterized by the accumulation of cytotoxic lipid peroxides. Since its initial characterization by the Stockwell lab in 2012, ferroptosis has been observed in a many organs and injury states, including many cardiovascular diseases [51,66]. This dissertation work focused on several main questions to address existing gaps in knowledge on ferroptosis post-MI:

1. Does inhibiting ferroptosis in the early postnatal mouse heart post-MI improve cardiac function?
2. How do ferroptotic cardiomyocytes affect the angiogenic response?
3. What is the role of ferroptotic cardiomyocytes in immune regulation?

Addressing these questions will guide ongoing and future research into ferroptosis inhibitors as a potential therapeutic option for patients experiencing an MI.

To address the first question, we used both *in vivo* and *in vitro* methods. Initially, we hypothesized that Fer-1 would cause similar improvements in the P7 heart that have been published in mature mouse models[65]. We began by using Fer-1 as an established inhibitor of ferroptosis in the P1 and P7 mouse model of MI. As the P1 mouse heart is a regenerative model, we did not expect to see much, if any, improvement [15]. Surprisingly, we saw cardiac function, but not infarct size, decline in the P7 mouse hearts in response to Fer-1 treatment. Cell death profiling of the CMs revealed in increase in CM apoptosis. Switching to the iCM cell culture model, we treated iCMs with

Erastin as an inducer of ferroptosis or Staurosporine as an inducer of apoptosis and collected conditioned media, then characterized the secretome of ferroptotic cardiomyocytes with a commercially available cytokine array. Gene ontology analysis of the upregulated cytokines revealed enrichment in enrichment in the immune response, endothelial cell apoptotic process, and Interleukin-10 signaling. Taken together, these data suggest that ferroptotic cardiomyocytes contribute to beneficial ventricular remodeling processes.

These data contradict previously established paradigms that Fer-1 administration leads to decreased infarct size[65]. However, this study administered Fer-1 at a lower dose, and as a pretreatment to the I/R injury. The pretreatment model is not clinically relevant for I/R injury from MI as medication cannot be administered prior to the injury. The closest model might be to treat a patient after experiencing an MI but before undergoing PCI. This has been tested clinically using Deferoxamine (DFO), an iron chelator, in patients with ST-segment elevation-myocardial infarction (STEMI). That study concluded that despite confirming a reduction in both serum iron and oxidative stress, DFO administration before PCI did not improve cardiac function nor infarct size[195]. Hence, the pretreatment model may represent a more practical application for Doxorubicin-induced cardiomyopathy, which was also investigated in the same study, or I/R injury caused by heart transplantation[66]. The dosage used in the pretreatment study was also lower at 1 mg/kg. Our data show no significant reduction in endothelial cell density in the infarcts of mice treated with the 1 mg/kg Fer-1 dose. It seems plausible that inhibiting ferroptosis to a lesser degree could provide more benefit than

detriment to the injured heart by suppressing CM death enough to preserve more cardiac tissue while still allowing for the release of beneficial remodeling factors. Future studies to determine which factors released by ferroptotic iCMs are required for beneficial remodeling could inform further trials and experimentation with Fer-1 as a therapeutic.

To answer the second question and investigate the potential causes of Fer-1 induced impaired cardiac function post-MI, we hypothesized that inhibition of ferroptosis impaired angiogenesis. We examined the endothelial cell population and apoptotic rates of Fer-1 treated P1 3DPMI LAD-O hearts. Data revealed a significant decrease in endothelial cell density in the infarct that could not be explained by a decreased proliferative rate or an increased apoptotic rate. Conditioned media from iCMs treated with inducers of cell death were used for a variety of *in vitro* HUVEC assays to characterize the endothelial response to CM-derived secreted factors. In measurements of survival, migration and tube formation, ferroptotic CM conditioned media treated HUVECs were similar to controls, while apoptotic CM conditioned media treated HUVECs consistently did not survive until the experimental endpoints. These data support the hypothesis that ferroptotic CMs are uniquely able support a pro-angiogenic microenvironment.

The lack of evidence to explain the decreased endothelial population in the infarct as a result of changed proliferation or apoptosis leaves room for future investigation. Our *in vitro* data suggests that endothelial migration and Endothelial–mesenchymal transition (EndMT) are both promising candidates. EndMT contributes to

neovascularization after ischemic injury, as endothelial cells acquire a mesenchymal phenotype during migration [196-198]. Published single-cell RNA sequencing data of infarcted murine hearts shows that a majority subset of endothelial cells exhibit an increase of mesenchymal markers at 3 days post-MI, indicative of EndMT [196,199]. This coincides with the timepoint at which ferroptosis peaks after MI. Additionally, endothelial migration can be stimulated by angiogenin[200], ICAM-1[201] , and Cripto-1 [202], all of which are produced by ferroptotic cardiomyocytes. Taken together, it seems plausible that Fer-1 inhibits revascularization in part by suppressing EndMT. However, angiogenesis is triggered through multiple pathways, one of the largest being hypoxic signaling. Hypoxia stimulates the stabilization of HIF1a, which increases transcription of VEGF, a potent angiogenic factor [26,203]. Notably, we showed that cardiomyocytes treated with Erastin release increased amounts of VEGF. It is likely that signaling derived from ferroptotic cardiomyocytes stimulates revascularization of the ischemic area through a mechanism including multiple pathways. Our studies suggest that endothelial migration is a contributing factor. Further investigation into the mechanisms involved in regulating the endothelial population in the Fer-1 treated heart could inform future therapeutic approaches for treating MI.

To address our third question, we hypothesized that ferroptotic CM- derived cytokines regulate macrophage polarization and angiogenesis. We observed a striking reduction in both macrophage density and percentage of M2-like macrophages in the infarct in Fer-1 treated hearts, which we confirmed via flow cytometry analysis of ventricular tissue. Our cytokine array combined with western blotting of conditioned

media indicated that ferroptotic CMs secreted increased amounts of IL-19, which is known to support both angiogenesis and M2 macrophage polarization[85,87,89,91]. HUVECs were stimulated with H_2O_2 and IL-19 protein was added and a trending increase in proliferation was observed. However, *in vivo*, exogenous administration of IL-19 protein significantly improved cardiac function, infarct size, endothelial density, and endothelial cell cycle activity, along with decreasing the percentage of Ptgs2 positive CMs. Localization of Ptgs2 positive CMs suggested that IL-19 inhibits spreading of ferroptosis beyond the border zone. Finally, we utilized predictive computational modeling of single cell RNA-sequencing data to graph predicted interactions between cell subtypes in infarcted mouse hearts.

Flow cytometry of Fer-1 treated LAD-O hearts revealed a decrease in M2-like macrophage polarization, which was primarily determined via positive CD206 staining and negative CD86 staining. However, there are recognized subtypes of M2 macrophages with distinct functions, including M2a, M2b, M2c, M2d, and M2f [181,182]. For example, M2a macrophages predominantly secrete factors that dampen the inflammatory response[182]. Macrophages are stimulated towards the M2a phenotype by IL-4 and IL-13, the first of which was the single most upregulated cytokine secreted by ferroptotic cardiomyocytes. M2a macrophages also secrete IL-10, which is capable of inducing M2c polarization[182]. M2c macrophages are primarily established as pro-regenerative, and contribute heavily to resolution of inflammation and matrix deposition[182]. However, M2b macrophages perform both pro- and anti-inflammatory functions. They are stimulated by LPS to produce anti-inflammatory cytokines such as IL-

10 and promote the anti-inflammatory Th2 responses, but also produce pro-inflammatory cytokines such as TNF and IL-6 [183-185]. M2d macrophages are known to be pro-angiogenic and express factors such as VEGF and IL-10 [186]. Cytokine array data suggests that ferroptotic cardiomyocytes may initially push macrophages towards the M2a phenotype, but this merits further investigation to gain a more comprehensive understanding of the nuances of macrophage polarization in this context.

Analysis of RNA sequencing data can provide a higher resolution dataset to examine shifts in the both the endothelial and immune populations. IL-19 has been shown to stimulate endothelial spreading and migration [90]. However, other environmental factors that contribute to ferroptosis likely also play a role in regulating angiogenesis. Research shows that hypoxia-induced HIF1a signaling promotes a shift away from oxidative phosphorylation towards anaerobic glycolysis, which enables cytoskeletal remodeling and fuels contraction during EC migration [204,205]. Studies also suggest that fatty acid oxidation modulates proliferation in stalk cells, the proliferative endothelial cells moving behind the leading tip endothelial cells to produce sprout elongation during blood vessel growth[205]. Ferroptosis may also impact the immune response through regulation of endothelial metabolism. HIF1a is downregulated in response to fatty acid metabolism in endothelial cells, which promotes CXCL1-mediated macrophage recruitment in endothelial cells by increasing monocyte adhesion [204,206,207]. As ROS and fatty acids are key contributors to ferroptosis, it follows that regulating ferroptosis would impact these processes in endothelial cells. Future studies

could build on these experiments to investigate the subpopulations of cells and their metabolic profiles to identify niches most responsive to ferroptotic CMs.

This body of work demonstrates that pharmacological inhibition of ferroptosis does not improve cardiac function after myocardial infarction in the regenerative or non-regenerative mouse heart. Findings identify decreased angiogenic activity in the infarct of Fer-1 treated mice given LAD-O and characterize the secretome from cardiomyocytes undergoing differing types of cell death. Ferroptotic cardiomyocytes secrete factors that uniquely support endothelial cell survival and tube formation. This work elucidates a mechanism where ferroptotic cardiomyocytes secrete cytokines, including IL-19, that promote angiogenesis in addition to immune recruitment and macrophage polarization. It is our goal that future studies will expand and build upon these results to guide the development of novel therapeutics that target cell death and improve outcomes for myocardial infarction patients.

Methods and Materials

Mouse Strains

All animal protocols and procedures complied with the NIH guidelines and were approved by the Institutional Animal Care and Use Committee (IACUC) of the Medical University of South Carolina (Charleston, South Carolina 29425, USA). The *FVB* (JAX 001800) and *C57BL/6J* (JAX 000664) were purchased from the Jackson Laboratory (JAX, Bar Harbor, ME 04609, USA). Male *C57BL/6J* mice were crossbred with female *FVB* mice, and F1 offspring were used for the studies.

Left Anterior Descending Coronary Artery Occlusion

For all mouse survival surgeries, littermate controls were used whenever possible. Both male and female mice were distributed randomly among groups. All surgeries were done blinded to mouse treatment. Wild type mice were subjected to LAD-O at P1 or P7 [6]. Briefly, Briefly, mice were placed under ice to anesthetize. Nylon sutures (AD Surgical, S-G618R13-U) were used to occlude the left anterior descending artery (LAD). Occlusion was confirmed by blanching of the myocardium. VetBond tissue adhesive (Santa Cruz Biotechnology, NC0846393) was used to close the thoracic cavity. The entire procedure lasted approximately 10 minutes from hypothermia induction until recovery. Sham procedures were done identically without the occlusion of the coronary artery. Ferrostatin-1 (Fer-1, 2 mg/Kg, MilliporeSigma, SML0583) or DMSO vehicle control was administered subcutaneously at 0, 1, 2, and 3 days after surgery. Hearts were collected at 3 days post-surgery for histological examination. For analysis of cardiac function, mice

were subjected echocardiography 14 days post-surgery, then hearts were collected for histological examination.

Echocardiography

At 14 days after P1 LAD-O and 21 days after P7 LAD-O, echocardiography was performed using a Vevo 3100 ultrasound system (Fujifilm VisualSonics), equipped with a MX550S transducer. B-mode and M-mode data were acquired following the manufacturer's guidelines. Each measurement was performed three times per mouse.

Cell Culture

Human umbilical vein endothelial cells (HUVECs, ATCC® CRL-1730™) were cultured in Kaighn's Modification of Ham's F-12 Medium (ATCC, 30-2004), supplemented with 10% FBS (Corning, 35-011-CV), Endothelial Cell Growth Supplement (Corning, CB-40006), and Heparin (Sigma, H4784-250MG). Cells were passaged to passage 3 before being used in tube formation assays.

Differentiation of Human iPSCs to Cardiomyocytes

iPSCs (Cornell Institute for Medical Research, AICS-0048-039) were cultured in mTeSR1media (STEMCELL Technologies, 85850) on Matrigel (Gibco, A1413302)-coated plates. At 80% of confluency, iPSCs were differentiated into iCMs as previously described[208]. Briefly, the iPSCs were treated with 8μM CHIR-99021 (SelleckChem, S2924) in RPMI (Gibco, 11875093)-B27(no insulin) (Gibco, A1895601) from day 0-1.

Media was changed on day 2 and the cells were treated with 5 μM IWR1 (SelleckChem, S7086) in RPMI-B27(no insulin) from day 3-4. Starting from day 7, RPMI-B27 with insulin (Gibco, 17504044) media were given to iPSC-derived cardiomyocytes (iCMs). Two rounds of glucose starvation from day 12-15 and from day 20-23 were performed to eliminate non-cardiomyocyte cells. At day 30, iCMs were transferred to Matrigel-coated 24-well plates and maintained in RPMI-B27 with insulin for further use.

Conditioned Medium from iCMs

iCMs were transferred to Matrigel-coated 6-well plates, rinsed with PBS, then treated with 30 μM erastin (Sigma, E7781), 1mM Staurosporine (Sigma-Aldrich, S6942), or DMSO vehicle control diluted in 3 ml of RPMI-B27 with insulin per well. After 6 hours, media were removed, and iCMs were rinsed three times with PBS to remove all traces of erastin, Staurosporine, or DMSO. Fresh RPMI-B27 with insulin was added to the iCMs for an overnight conditioning period of 16 hours. Conditioned media was collected for cytokine array analysis and HUVEC tube formation experiments.

HUVEC Tube Formation Assay

HUVECs were seeded at a density of 7.5 x 10^4 cells per well in 24-well plates pre-coated with Matrigel. HUVECs were then treated with conditioned media from iCMs mixed 1:1 with complete HUVEC media for a total volume of 1 mL per well. Cells were incubated for 6 hours at 37 °C and 5% CO2 and imaged with a Leica DMi1 inverted phase contrast microscope every hour to document tube formation. Images were analyzed with the

Angiogenesis Analyzer plugin from FIJI [159,209]. For our application, the parameters evaluated were the number of junctions, nodes, and extremities, total branching length, total segments length, total mesh area, and mean mesh size. Each tube formation assay was performed as three independent experiments using at least three wells per condition.

Cytokine Array Assay

Conditioned media of iCM culture was applied to the Proteome Profiler Array Human XL Cytokine Array Kit (R&D Systems, ARY022B) according to manufacturer instructions. 3 ml of conditioned media from erastin- or DMSO-treated iCMs was concentrated down to 200 μl using MilliporeSigma's Protein Concentration Kit (Fisher Scientific, 50-525-36). Equal amount of total protein from each group (determined by a BCA protein assay) was loaded onto the cytokine array. Blotting signal was visualized in a ChemiDoc Touch Imaging System (Bio-Rad, 12003154). Blot analysis was performed using FIJI (NIH), and heatmap was generated with R-Studio. Gene Ontology analysis was performed using Metascape[210].

Dissociation of Ventricular Cardiac Cells

At 3 days after P1 LAD-O, the hearts were harvested and rinsed with ice cold HBSS (ThermoFisher, 14025092) in 60-mm cell culture dishes. The atrial tissue was removed, and the ventricular tissue was cut into 1 mm pieces and incubated in 5 ml of Collagenase solution containing 600 U/ml Collagenase type II (ThermoFisher, 17101015) and 60 U/ml

DNase I (Sigma-Aldrich, AMPD1) for 15 minutes at 37 °C and 5% CO2. Tissue was gently pipetted up and down to facilitate the digestion. Supernatant was collected and stored on ice to quench collagenase activity. 5 ml of fresh collagenase working solution was added to the remaining heart tissue for a second round of digestion. A total of 5 rounds of digestion were performed. Single cell suspensions collected at each step were consolidated in their corresponding 15 mL tubes and centrifuged at 300 g for 10 minutes. Supernatant was discarded and the pellet was dissociated with 2 ml of ice cold FACS Buffer (PBS + 1% BSA + 0.5 mM EDTA). Cell suspension was filtered using a 30-μm cell strainer, then subjected to a 2-minute incubation with Red Blood Cell Lysis Buffer (Miltenyi, 130-094-183) followed by centrifugation, resuspension, and cell counting with a hemocytometer.

Flow Cytometry

Isolated cardiac cells were resuspended in FACS buffer and incubated with FCR Blocking reagent (Miltenyi, 130-092-575) for 20 minutes at 4 °C to block the Fc receptor. Following washing with FACS buffer and resuspension, cells were stained with Viobility™ 405/520 Fixable Live/Dead Dye (1:1000 dilution, Miltenyi, 130-130-404) to exclude dead cells and debris. To prepare single channel controls for flow cytometry analysis and compensation, compensation beads (BioLegend, 424602) were prepared according to the manufacturer protocol and included in the surfaced marker antibody staining. To identify macrophages and their subtypes, cells were stained with the following surface marker antibodies for 20 minutes at 4 °C: Brilliant Violet 421-conjugated anti-CD206

(rat, 1:20 dilution, BioLegend, 141717); Alexa Fluor 488-conjugated anti-F4/80 (rat, 1:50 dilution, ThermoFisher, L34959); PECy7-conjugated anti-CD86 (rat, 1:10 dilution, Miltenyi, 130-105-135); and APC-conjugated anti-Ly6C (recombinant, 1:15 dilution, Miltenyi, 103-111-779). Flow cytometry was performed using a MACSQuant Analyzer 10 Flow Cytometer, and analyses were performed with FlowJo software v10.9 software (BD Life Sciences). Doublets were excludes based on FSC-A v FSC-H values, then dead cells excluded with live/dead dye staining. Lymphocytes were gated based on SSC-A and FSC-A.

Tissue Processing, Histology, and Immunohistochemistry

Hearts were fixed in 10% formalin (VWR, 10015-192) at room temperature overnight with continuous rocking. Tissue was then processed for paraffin embedding and sectioned at 7 μm thickness, deparaffinized in xylene, rehydrated, and subjected to histology or immunofluorescent staining. Tissue slides were incubated in humid chambers at 4 °C in primary antibody overnight in 1% BSA in PBS. On the second morning, slides were washed in PBS, then incubated in the dark at room temperature for 1 hour in secondary antibody in 1% BSA in PBS. Slides were washed with PBS and counterstained with DAPI (Sigma, D9542), then mounted in VECTASHIELD hard-set mounting medium (Vector Laboratories, H1400). Immunofluorescent images were acquired using a Leica SP8 confocal microscope (Leica Microsystems). Primary antibodies used include: cleaved Caspase 3 (1:200, Cell Signaling #9664), cardiac troponin T (cTnT) (1:400, Invitrogen #MA5-12960), cTnT (1:400, FISHER #ms-295p1abx),

MF20 (1:400, Developmental Studies Hybridoma Bank #AB_2147781), 4-HNE (1:400, Bioss #bs-6313R), EMCN (1:400, Santa Cruz #sc-65495), PH3 (1:200, Cell Signaling #9701), Mac-3 (1:100, Cedar Lane #CL8943AP), and CD206 (1:200, Bioss #bs-4727R). Secondary antibodies all used at a dilution of 1:400 and include: Thermo Invitrogen #A21200 Chicken anti mouse IgG 488, Thermo Invitrogen #A-21428 Goat anti-Rabbit IgG (H+L) Cross-Adsorbed Secondary Antibody, Alexa Fluor 555, Thermo Invitrogen #A-21247 Goat anti-Rat IgG (H+L) Cross-Adsorbed Secondary Antibody, Alexa Fluor 647, Thermo Invitrogen #A16034 Donkey anti-rabbit IgG (H+L) TRITC, Thermo Invitrogen #A21082 donkey anti goat IgG 633, and Thermo Invitrogen #A31573 donkey anti rabbit IgG 647. For measuring fibrotic scarring, a Masson's trichrome staining kit was used (Sigma, HT15). Tissue slides were deparaffinized, rehydrated, and washed with water, before staining in iron hematoxylin working solution for ten minutes. Slides were then rinsed in water, stained in scarlet acid fuchsin, rinsed in water, stained in phosphomolybdic-phosphotungstic acid solution, stained in aniline blue solution, rinsed in water, stained in 1% acetic acid solution, and rinsed in water before proceeding with rapid dehydration and clearing with xylenes. Tissue slides were mounted with Shurmount mounting medium (General Data, LC-A).

Single-Cell RNA Sequencing Analysis

GEO dataset GSE128628 was used for scRNA-Seq analysis [175]. Fastq files were aligned to mm10/GRCm38 reference transcriptome using the count function in Cell Ranger software (v7.1, 10x Genomics). The resulting gene expression matrix was further

analyzed in R using Seurat (v4.4.0) [188]. Thresholding was used to exclude low-quality cells. Uniform Manifold Approximation and Projection (UMAP) was used for dimensional reduction and unsupervised clustering was carried out using the RunUMAP and FindClusters functions in Seurat, respectively. Clusters were annotated based on marker gene expression. Cell interactions were inferred and visualized using the package[189].

Statistics

All quantitative experiments included at least 3 biological replicates. Animal studies included at least 3 mice per group. Statistical significance was determined via t-test. Equal variance was determined using Levene's Test. Outliers were determined by Grubb's test. All statistical work was done using IBM SPSS Statistics for Macintosh, Version 28.0.1.0. All bar graphs included scattered dots. All bar graphs represent mean ± SD. A P-value lower than 0.05 was considered statistically significant.

References

1. Martin, S.S.; Aday, A.W.; Almarzooq, Z.I.; Anderson, C.A.M.; Arora, P.; Avery, C.L.; Baker-Smith, C.M.; Barone Gibbs, B.; Beaton, A.Z.; Boehme, A.K.; et al. 2024 Heart Disease and Stroke Statistics: A Report of US and Global Data From the American Heart Association. *Circulation* **2024**, *149*, e347-e913, doi:10.1161/CIR.0000000000001209.

2. Tsao, C.W.; Aday, A.W.; Almarzooq, Z.I.; Anderson, C.A.M.; Arora, P.; Avery, C.L.; Baker-Smith, C.M.; Beaton, A.Z.; Boehme, A.K.; Buxton, A.E.; et al. Heart Disease and Stroke Statistics-2023 Update: A Report From the American Heart Association. *Circulation* **2023**, *147*, e93-e621, doi:10.1161/cir.0000000000001123.

3. Roth, G.A.; Mensah, G.A.; Johnson, C.O.; Addolorato, G.; Ammirati, E.; Baddour, L.M.; Barengo, N.C.; Beaton, A.Z.; Benjamin, E.J.; Benziger, C.P.; et al. Global Burden of Cardiovascular Diseases and Risk Factors, 1990-2019: Update From the GBD 2019 Study. *J Am Coll Cardiol* **2020**, *76*, 2982-3021, doi:10.1016/j.jacc.2020.11.010.

4. World health statistics 2024: monitoring health for the SDGs, sustainable development goals. **2024**.

5. Joynt Maddox, K.E.; Elkind, M.S.V.; Aparicio, H.J.; Commodore-Mensah, Y.; de Ferranti, S.D.; Dowd, W.N.; Hernandez, A.F.; Khavjou, O.; Michos, E.D.; Palaniappan, L.; et al. Forecasting the Burden of Cardiovascular Disease and Stroke in the United States Through 2050—Prevalence of Risk Factors and Disease: A Presidential Advisory From the American Heart Association. *Circulation* **2024**, *150*, e65-e88, doi:10.1161/CIR.0000000000001256.

6. Sachdeva, P.; Kaur, K.; Fatima, S.; Mahak, F.; Noman, M.; Siddenthi, S.M.; Surksha, M.A.; Munir, M.; Fatima, F.; Sultana, S.S.; et al. Advancements in Myocardial Infarction Management: Exploring Novel Approaches and Strategies. *Cureus* **2023**, *15*, e45578, doi:10.7759/cureus.45578.

7. Carrick, D.; Oldroyd, K.G.; McEntegart, M.; Haig, C.; Petrie, M.C.; Eteiba, H.; Hood, S.; Owens, C.; Watkins, S.; Layland, J.; et al. A randomized trial of deferred stenting versus immediate stenting to prevent no- or slow-reflow in acute ST-segment elevation myocardial infarction (DEFER-STEMI). *J Am Coll Cardiol* **2014**, *63*, 2088-2098, doi:10.1016/j.jacc.2014.02.530.

8. Koul, S.; Andell, P.; Martinsson, A.; Gustav Smith, J.; van der Pals, J.; Scherstén, F.; Jernberg, T.; Lagerqvist, B.; Erlinge, D. Delay From First Medical Contact to Primary PCI and All-Cause Mortality: A Nationwide Study of Patients With ST-Elevation Myocardial Infarction. *Journal of the American Heart Association 3*, e000486, doi:10.1161/JAHA.113.000486.

9. Hemmati, R.; Fathi, M.; Heidarian Moghadam, M.; Mohebbi, B.; Keshavarz, K.; Mohebbi, A.; Rahmani, A. Timing percutaneous coronary interventions and cardiovascular events in non-ST-elevation myocardial infarction patients. *Am J Cardiovasc Dis* **2024**, *14*, 40-46, doi:10.62347/ratb9072.

10. He, J.; Liu, D.; Zhao, L.; Zhou, D.; Rong, J.; Zhang, L.; Xia, Z. Myocardial ischemia/reperfusion injury: Mechanisms of injury and implications for management (Review). *Exp Ther Med* **2022**, *23*, 430, doi:10.3892/etm.2022.11357.

11. Xiang, Q.; Yi, X.; Zhu, X.-H.; Wei, X.; Jiang, D.-S. Regulated cell death in myocardial ischemia–reperfusion injury. *Trends in Endocrinology & Metabolism* **2024**, *35*, 219-234, doi:https://doi.org/10.1016/j.tem.2023.10.010.

12. Bergmann, O.; Bhardwaj, R.D.; Bernard, S.; Zdunek, S.; Barnabé-Heider, F.; Walsh, S.; Zupicich, J.; Alkass, K.; Buchholz, B.A.; Druid, H.; et al. Evidence for Cardiomyocyte Renewal in Humans. *Science* **2009**, *324*, 98-102, doi:10.1126/science.1164680.

13. Price, E.L.; Vieira, J.M.; Riley, P.R. Model organisms at the heart of regeneration. *Dis Model Mech* **2019**, *12*, doi:10.1242/dmm.040691.

14. Poss, K.D.; Wilson, L.G.; Keating, M.T. Heart regeneration in zebrafish. *Science* **2002**, *298*, 2188-2190, doi:10.1126/science.1077857.

15. Porrello, E.R.; Mahmoud, A.I.; Simpson, E.; Hill, J.A.; Richardson, J.A.; Olson, E.N.; Sadek, H.A. Transient regenerative potential of the neonatal mouse heart. *Science* **2011**, *331*, 1078-1080, doi:10.1126/science.1200708.

16. Bise, T.; Sallin, P.; Pfefferli, C.; Jaźwińska, A. Multiple cryoinjuries modulate the efficiency of zebrafish heart regeneration. *Scientific Reports* **2020**, *10*, 11551, doi:10.1038/s41598-020-68200-1.

17. Tao, G.; Kahr, P.C.; Morikawa, Y.; Zhang, M.; Rahmani, M.; Heallen, T.R.; Li, L.; Sun, Z.; Olson, E.N.; Amendt, B.A.; et al. Pitx2 promotes heart repair by activating the antioxidant response after cardiac injury. *Nature* **2016**, *534*, 119-123, doi:10.1038/nature17959.

18. Darehzereshki, A.; Rubin, N.; Gamba, L.; Kim, J.; Fraser, J.; Huang, Y.; Billings, J.; Mohammadzadeh, R.; Wood, J.; Warburton, D.; et al. Differential regenerative capacity of neonatal mouse hearts after cryoinjury. *Dev Biol* **2015**, *399*, 91-99, doi:10.1016/j.ydbio.2014.12.018.

19. Notari, M.; Ventura-Rubio, A.; Bedford-Guaus, S.J.; Jorba, I.; Mulero, L.; Navajas, D.; Martí, M.; Raya, Á. The local microenvironment limits the regenerative

potential of the mouse neonatal heart. *Sci Adv* **2018**, *4*, eaao5553, doi:10.1126/sciadv.aao5553.

20. Bryant, D.M.; O'Meara, C.C.; Ho, N.N.; Gannon, J.; Cai, L.; Lee, R.T. A systematic analysis of neonatal mouse heart regeneration after apical resection. *J Mol Cell Cardiol* **2015**, *79*, 315-318, doi:10.1016/j.yjmcc.2014.12.011.

21. Uygur, A.; Lee, Richard T. Mechanisms of Cardiac Regeneration. *Dev Cell* **2016**, *36*, 362-374, doi:10.1016/j.devcel.2016.01.018.

22. Sampaio-Pinto, V.; Rodrigues, S.C.; Laundos, T.L.; Silva, E.D.; Vasques-Nóvoa, F.; Silva, A.C.; Cerqueira, R.J.; Resende, T.P.; Pianca, N.; Leite-Moreira, A.; et al. Neonatal Apex Resection Triggers Cardiomyocyte Proliferation, Neovascularization and Functional Recovery Despite Local Fibrosis. *Stem Cell Reports* **2018**, *10*, 860-874, doi:10.1016/j.stemcr.2018.01.042.

23. Puente, B.N.; Kimura, W.; Muralidhar, S.A.; Moon, J.; Amatruda, J.F.; Phelps, K.L.; Grinsfelder, D.; Rothermel, B.A.; Chen, R.; Garcia, J.A.; et al. The oxygen-rich postnatal environment induces cardiomyocyte cell-cycle arrest through DNA damage response. *Cell* **2014**, *157*, 565-579, doi:10.1016/j.cell.2014.03.032.

24. Cadenas, S. ROS and redox signaling in myocardial ischemia-reperfusion injury and cardioprotection. *Free Radical Biology and Medicine* **2018**, *117*, 76-89, doi:https://doi.org/10.1016/j.freeradbiomed.2018.01.024.

25. Zuo, L.; Zhou, T.; Pannell, B.K.; Ziegler, A.C.; Best, T.M. Biological and physiological role of reactive oxygen species – the good, the bad and the ugly. *Acta Physiologica* **2015**, *214*, 329-348, doi:https://doi.org/10.1111/apha.12515.

26. Fukai, T.; Ushio-Fukai, M. Cross-Talk between NADPH Oxidase and Mitochondria: Role in ROS Signaling and Angiogenesis. *Cells* **2020**, *9*, doi:10.3390/cells9081849.

27. Gaschler, M.M.; Stockwell, B.R. Lipid peroxidation in cell death. *Biochem Biophys Res Commun* **2017**, *482*, 419-425, doi:10.1016/j.bbrc.2016.10.086.

28. Zhou, T.; Prather, E.R.; Garrison, D.E.; Zuo, L. Interplay between ROS and Antioxidants during Ischemia-Reperfusion Injuries in Cardiac and Skeletal Muscle. *Int J Mol Sci* **2018**, *19*, doi:10.3390/ijms19020417.

29. Brown, D.A.; Perry, J.B.; Allen, M.E.; Sabbah, H.N.; Stauffer, B.L.; Shaikh, S.R.; Cleland, J.G.F.; Colucci, W.S.; Butler, J.; Voors, A.A.; et al. Mitochondrial function as a therapeutic target in heart failure. *Nature Reviews Cardiology* **2017**, *14*, 238-250, doi:10.1038/nrcardio.2016.203.

30. Tamariz, L.; Hare, J.M. Xanthine oxidase inhibitors in heart failure: where do we go from here? *Circulation* **2015**, *131*, 1741-1744, doi:10.1161/circulationaha.115.016379.

31. Loboda, A.; Damulewicz, M.; Pyza, E.; Jozkowicz, A.; Dulak, J. Role of Nrf2/HO-1 system in development, oxidative stress response and diseases: an evolutionarily conserved mechanism. *Cell Mol Life Sci* **2016**, *73*, 3221-3247, doi:10.1007/s00018-016-2223-0.

32. Pei, J.; Pan, X.; Wei, G.; Hua, Y. Research progress of glutathione peroxidase family (GPX) in redoxidation. *Front Pharmacol* **2023**, *14*, 1147414, doi:10.3389/fphar.2023.1147414.

33. Chen, T.; Wei, X.; Chen, Z.; Morin, D.; Alvarez, S.V.; Yoon, Y.; Huang, Y. Designing energy-efficient separation membranes: Knowledge from nature for a sustainable future. *Advanced Membranes* **2022**, *2*, 100031, doi:https://doi.org/10.1016/j.advmem.2022.100031.

34. von Krusenstiern, A.N.; Robson, R.N.; Qian, N.; Qiu, B.; Hu, F.; Reznik, E.; Smith, N.; Zandkarimi, F.; Estes, V.M.; Dupont, M.; et al. Identification of essential sites of lipid peroxidation in ferroptosis. *Nat Chem Biol* **2023**, doi:10.1038/s41589-022-01249-3.

35. Tsubone, T.M.; Junqueira, H.C.; Baptista, M.S.; Itri, R. Contrasting roles of oxidized lipids in modulating membrane microdomains. *Biochimica et Biophysica Acta (BBA) - Biomembranes* **2019**, *1861*, 660-669, doi:https://doi.org/10.1016/j.bbamem.2018.12.017.

36. Chng, C.P.; Sadovsky, Y.; Hsia, K.J.; Huang, C. Site-Specific Peroxidation Modulates Lipid Bilayer Mechanics. *Extreme Mech Lett* **2021**, *42*, doi:10.1016/j.eml.2020.101148.

37. Tang, Y.; Wu, J.; Sun, X.; Tan, S.; Li, W.; Yin, S.; Liu, L.; Chen, Y.; Liu, Y.; Tan, Q.; et al. Cardiolipin oxidized by ROS from complex II acts as a target of gasdermin D to drive mitochondrial pore and heart dysfunction in endotoxemia. *Cell Reports* **2024**, *43*, doi:10.1016/j.celrep.2024.114237.

38. Trujillo-Rangel, W.; García-Valdés, L.; Méndez-Del Villar, M.; Castañeda-Arellano, R.; Totsuka-Sutto, S.E.; García-Benavides, L. Therapeutic Targets for Regulating Oxidative Damage Induced by Ischemia-Reperfusion Injury: A Study from a Pharmacological Perspective. *Oxid Med Cell Longev* **2022**, *2022*, 8624318, doi:10.1155/2022/8624318.

39. Zhou, T.; Chuang, C.-C.; Zuo, L. Molecular Characterization of Reactive Oxygen Species in Myocardial Ischemia-Reperfusion Injury. *BioMed Research International* **2015**, *2015*, 864946, doi:https://doi.org/10.1155/2015/864946.

40. Tang, D.; Chen, X.; Kang, R.; Kroemer, G. Ferroptosis: molecular mechanisms and health implications. *Cell Research* **2021**, *31*, 107-125, doi:10.1038/s41422-020-00441-1.

41. Peuhkurinen, K.J.; Takala, T.E.; Nuutinen, E.M.; Hassinen, I.E. Tricarboxylic acid cycle metabolites during ischemia in isolated perfused rat heart. *American Journal of Physiology-Heart and Circulatory Physiology* **1983**, *244*, H281-H288, doi:10.1152/ajpheart.1983.244.2.H281.

42. Chouchani, E.T.; Pell, V.R.; Gaude, E.; Aksentijević, D.; Sundier, S.Y.; Robb, E.L.; Logan, A.; Nadtochiy, S.M.; Ord, E.N.J.; Smith, A.C.; et al. Ischaemic accumulation of succinate controls reperfusion injury through mitochondrial ROS. *Nature* **2014**, *515*, 431-435, doi:10.1038/nature13909.

43. Chouchani, Edward T.; Pell, Victoria R.; James, Andrew M.; Work, Lorraine M.; Saeb-Parsy, K.; Frezza, C.; Krieg, T.; Murphy, Michael P. A Unifying Mechanism for Mitochondrial Superoxide Production during Ischemia-Reperfusion Injury. *Cell Metabolism* **2016**, *23*, 254-263, doi:10.1016/j.cmet.2015.12.009.

44. Prag, H.A.; Kula-Alwar, D.; Beach, T.E.; Gruszczyk, A.V.; Burger, N.; Murphy, M.P. Chapter 26 - Mitochondrial ROS production during ischemia-reperfusion injury. In *Oxidative Stress*, Sies, H., Ed.; Academic Press: 2020; pp. 513-538.

45. Zhu, X.; Zuo, L. Characterization of oxygen radical formation mechanism at early cardiac ischemia. *Cell Death & Disease* **2013**, *4*, e787-e787, doi:10.1038/cddis.2013.313.

46. Bugger, H.; Pfeil, K. Mitochondrial ROS in myocardial ischemia reperfusion and remodeling. *Biochimica et Biophysica Acta (BBA) - Molecular Basis of Disease* **2020**, *1866*, 165768, doi:https://doi.org/10.1016/j.bbadis.2020.165768.

47. Panov, A.V.; Dikalov, S.I. Cardiolipin, Perhydroxyl Radicals, and Lipid Peroxidation in Mitochondrial Dysfunctions and Aging. *Oxid Med Cell Longev* **2020**, *2020*, 1323028, doi:10.1155/2020/1323028.

48. Mohr, M.E.; Li, S.; Trouten, A.M.; Stairley, R.A.; Roddy, P.L.; Liu, C.; Zhang, M.; Sucov, H.M.; Tao, G. Cardiomyocyte-fibroblast interaction regulates ferroptosis and fibrosis after myocardial injury. *bioRxiv* **2023**, 2023.2002.2007.527364, doi:10.1101/2023.02.07.527364.

49. Zhou, L.; Sun, J.; Gu, L.; Wang, S.; Yang, T.; Wei, T.; Shan, T.; Wang, H.; Wang, L. Programmed Cell Death: Complex Regulatory Networks in Cardiovascular Disease. *Front Cell Dev Biol* **2021**, *9*, 794879, doi:10.3389/fcell.2021.794879.

50. Peng, F.; Liao, M.; Qin, R.; Zhu, S.; Peng, C.; Fu, L.; Chen, Y.; Han, B. Regulated cell death (RCD) in cancer: key pathways and targeted therapies. *Signal Transduction and Targeted Therapy* **2022**, *7*, 286, doi:10.1038/s41392-022-01110-y.

51. Dixon, S.J.; Lemberg, K.M.; Lamprecht, M.R.; Skouta, R.; Zaitsev, E.M.; Gleason, C.E.; Patel, D.N.; Bauer, A.J.; Cantley, A.M.; Yang, W.S.; et al. Ferroptosis: an iron-dependent form of nonapoptotic cell death. *Cell* **2012**, *149*, 1060-1072, doi:10.1016/j.cell.2012.03.042.

52. Nagata, S. Apoptosis and Clearance of Apoptotic Cells. *Annu Rev Immunol* **2018**, *36*, 489-517, doi:10.1146/annurev-immunol-042617-053010.

53. Zhu, L.; Zhang, B.; Luo, J.; Dong, S.; Zang, K.; Wu, Y. Ampelopsin-sodium induces apoptosis in human lung adenocarcinoma cell lines by promoting tubulin polymerization in vitro. *Oncol Lett* **2019**, *18*, 189-196, doi:10.3892/ol.2019.10288.

54. Wu, P.; Zhang, X.; Duan, D.; Zhao, L. Organelle-Specific Mechanisms in Crosstalk between Apoptosis and Ferroptosis. *Oxid Med Cell Longev* **2023**, *2023*, 3400147, doi:10.1155/2023/3400147.

55. Xie, Y.; Hou, W.; Song, X.; Yu, Y.; Huang, J.; Sun, X.; Kang, R.; Tang, D. Ferroptosis: process and function. *Cell Death & Differentiation* **2016**, *23*, 369-379, doi:10.1038/cdd.2015.158.

56. Park, E.; Chung, S.W. ROS-mediated autophagy increases intracellular iron levels and ferroptosis by ferritin and transferrin receptor regulation. *Cell Death Dis* **2019**, *10*, 822, doi:10.1038/s41419-019-2064-5.

57. Skouta, R.; Dixon, S.J.; Wang, J.; Dunn, D.E.; Orman, M.; Shimada, K.; Rosenberg, P.A.; Lo, D.C.; Weinberg, J.M.; Linkermann, A.; et al. Ferrostatins inhibit oxidative lipid damage and cell death in diverse disease models. *J Am Chem Soc* **2014**, *136*, 4551-4556, doi:10.1021/ja411006a.

58. Brown, C.W.; Amante, J.J.; Goel, H.L.; Mercurio, A.M. The α6β4 integrin promotes resistance to ferroptosis. *J Cell Biol* **2017**, *216*, 4287-4297, doi:10.1083/jcb.201701136.

59. Fang, X.; Cai, Z.; Wang, H.; Han, D.; Cheng, Q.; Zhang, P.; Gao, F.; Yu, Y.; Song, Z.; Wu, Q.; et al. Loss of Cardiac Ferritin H Facilitates Cardiomyopathy via Slc7a11-Mediated Ferroptosis. *Circ Res* **2020**, *127*, 486-501, doi:10.1161/CIRCRESAHA.120.316509.

60. Epstein, A.C.R.; Gleadle, J.M.; McNeill, L.A.; Hewitson, K.S.; O'Rourke, J.; Mole, D.R.; Mukherji, M.; Metzen, E.; Wilson, M.I.; Dhanda, A.; et al. C. elegans EGL-9 and Mammalian Homologs Define a Family of Dioxygenases that Regulate HIF by Prolyl Hydroxylation. *Cell* **2001**, *107*, 43-54, doi:https://doi.org/10.1016/S0092-8674(01)00507-4.

61. Galaris, D.; Barbouti, A.; Pantopoulos, K. Iron homeostasis and oxidative stress: An intimate relationship. *Biochimica et Biophysica Acta (BBA) - Molecular Cell Research* **2019**, *1866*, 118535, doi:https://doi.org/10.1016/j.bbamcr.2019.118535.

62. Wang, X.; Chen, X.; Zhou, W.; Men, H.; Bao, T.; Sun, Y.; Wang, Q.; Tan, Y.; Keller, B.B.; Tong, Q.; et al. Ferroptosis is essential for diabetic cardiomyopathy and is prevented by sulforaphane via AMPK/NRF2 pathways. *Acta Pharm Sin B* **2022**, *12*, 708-722, doi:10.1016/j.apsb.2021.10.005.

63. Li, W.; Feng, G.; Gauthier, J.M.; Lokshina, I.; Higashikubo, R.; Evans, S.; Liu, X.; Hassan, A.; Tanaka, S.; Cicka, M.; et al. Ferroptotic cell death and TLR4/Trif signaling initiate neutrophil recruitment after heart transplantation. *J Clin Invest* **2019**, *129*, 2293-2304, doi:10.1172/jci126428.

64. Li, N.; Wang, W.; Zhou, H.; Wu, Q.; Duan, M.; Liu, C.; Wu, H.; Deng, W.; Shen, D.; Tang, Q. Ferritinophagy-mediated ferroptosis is involved in sepsis-induced cardiac injury. *Free Radic Biol Med* **2020**, *160*, 303-318, doi:10.1016/j.freeradbiomed.2020.08.009.

65. Fang, X.; Wang, H.; Han, D.; Xie, E.; Yang, X.; Wei, J.; Gu, S.; Gao, F.; Zhu, N.; Yin, X.; et al. Ferroptosis as a target for protection against cardiomyopathy. *Proc Natl Acad Sci U S A* **2019**, *116*, 2672-2680, doi:10.1073/pnas.1821022116.

66. Fratta Pasini, A.M.; Stranieri, C.; Busti, F.; Di Leo, E.G.; Girelli, D.; Cominacini, L. New Insights into the Role of Ferroptosis in Cardiovascular Diseases. *Cells* **2023**, *12*, doi:10.3390/cells12060867.

67. Miotto, G.; Rossetto, M.; Di Paolo, M.L.; Orian, L.; Venerando, R.; Roveri, A.; Vučković, A.-M.; Bosello Travain, V.; Zaccarin, M.; Zennaro, L.; et al. Insight into the mechanism of ferroptosis inhibition by ferrostatin-1. *Redox Biology* **2020**, *28*, 101328, doi:https://doi.org/10.1016/j.redox.2019.101328.

68. Iuchi, K.; Takai, T.; Hisatomi, H. Cell Death via Lipid Peroxidation and Protein Aggregation Diseases. *Biology* **2021**, *10*, 399.

69. Gilbert, G.; Demydenko, K.; Dries, E.; Puertas, R.D.; Jin, X.; Sipido, K.; Roderick, H.L. Calcium Signaling in Cardiomyocyte Function. *Cold Spring Harb Perspect Biol* **2020**, *12*, doi:10.1101/cshperspect.a035428.

70. Peet, C.; Ivetic, A.; Bromage, D.I.; Shah, A.M. Cardiac monocytes and macrophages after myocardial infarction. *Cardiovasc Res* **2020**, *116*, 1101-1112, doi:10.1093/cvr/cvz336.

71. Aurora, A.B.; Porrello, E.R.; Tan, W.; Mahmoud, A.I.; Hill, J.A.; Bassel-Duby, R.; Sadek, H.A.; Olson, E.N. Macrophages are required for neonatal heart regeneration. *J Clin Invest* **2014**, *124*, 1382-1392, doi:10.1172/jci72181.

72. De Kleer, I.; Willems, F.; Lambrecht, B.; Goriely, S. Ontogeny of Myeloid Cells. *Frontiers in Immunology* **2014**, *5*, doi:10.3389/fimmu.2014.00423.

73. Chen, R.; Zhang, H.; Tang, B.; Luo, Y.; Yang, Y.; Zhong, X.; Chen, S.; Xu, X.; Huang, S.; Liu, C. Macrophages in cardiovascular diseases: molecular mechanisms and therapeutic targets. *Signal Transduction and Targeted Therapy* **2024**, *9*, 130, doi:10.1038/s41392-024-01840-1.

74. Mouton, A.J.; DeLeon-Pennell, K.Y.; Rivera Gonzalez, O.J.; Flynn, E.R.; Freeman, T.C.; Saucerman, J.J.; Garrett, M.R.; Ma, Y.; Harmancey, R.; Lindsey, M.L. Mapping macrophage polarization over the myocardial infarction time continuum. *Basic Res Cardiol* **2018**, *113*, 26, doi:10.1007/s00395-018-0686-x.

75. Bajpai, G.; Bredemeyer, A.; Li, W.; Zaitsev, K.; Koenig, A.L.; Lokshina, I.; Mohan, J.; Ivey, B.; Hsiao, H.-M.; Weinheimer, C.; et al. Tissue Resident CCR2− and CCR2+ Cardiac Macrophages Differentially Orchestrate Monocyte Recruitment and Fate Specification Following Myocardial Injury. *Circulation Research* **2019**, *124*, 263-278, doi:doi:10.1161/CIRCRESAHA.118.314028.

76. Zuo, W.; Sun, R.; Ji, Z.; Ma, G. Macrophage-driven cardiac inflammation and healing: insights from homeostasis and myocardial infarction. *Cell Mol Biol Lett* **2023**, *28*, 81, doi:10.1186/s11658-023-00491-4.

77. Zhuang, Q.; Li, M.; Hu, D.; Li, J. Recent advances in potential targets for myocardial ischemia reperfusion injury: Role of macrophages. *Molecular Immunology* **2024**, *169*, 1-9, doi:https://doi.org/10.1016/j.molimm.2024.02.007.

78. Revelo, X.S.; Parthiban, P.; Chen, C.; Barrow, F.; Fredrickson, G.; Wang, H.; Yücel, D.; Herman, A.; van Berlo, J.H. Cardiac Resident Macrophages Prevent Fibrosis and Stimulate Angiogenesis. *Circ Res* **2021**, *129*, 1086-1101, doi:10.1161/circresaha.121.319737.

79. Corker, A.; Neff, L.S.; Broughton, P.; Bradshaw, A.D.; DeLeon-Pennell, K.Y. Organized Chaos: Deciphering Immune Cell Heterogeneity's Role in Inflammation in the Heart. *Biomolecules* **2021**, *12*, doi:10.3390/biom12010011.

80. Peet, C.; Ivetic, A.; Bromage, D.I.; Shah, A.M. Cardiac monocytes and macrophages after myocardial infarction. *Cardiovasc Res* **2020**, *116*, 1101-1112, doi:10.1093/cvr/cvz336.

81. Viola, A.; Munari, F.; Sánchez-Rodríguez, R.; Scolaro, T.; Castegna, A. The Metabolic Signature of Macrophage Responses. *Frontiers in Immunology* **2019**, *10*, doi:10.3389/fimmu.2019.01462.

82. Wang, N.; Liang, H.; Zen, K. Molecular mechanisms that influence the macrophage m1-m2 polarization balance. *Front Immunol* **2014**, *5*, 614, doi:10.3389/fimmu.2014.00614.

83. Voss, S.; Krüger, S.; Scherschel, K.; Warnke, S.; Schwarzl, M.; Schrage, B.; Girdauskas, E.; Meyer, C.; Blankenberg, S.; Westermann, D.; et al. Macrophage Migration Inhibitory Factor (MIF) Expression Increases during Myocardial Infarction and Supports Pro-Inflammatory Signaling in Cardiac Fibroblasts. *Biomolecules* **2019**, *9*, doi:10.3390/biom9020038.

84. Talman, V.; Kivelä, R. Cardiomyocyte-Endothelial Cell Interactions in Cardiac Remodeling and Regeneration. *Front Cardiovasc Med* **2018**, *5*, 101, doi:10.3389/fcvm.2018.00101.

85. Gabunia, K.; Autieri, M.V. Interleukin-19 can enhance angiogenesis by Macrophage Polarization. *Macrophage (Houst)* **2015**, *2*, e562, doi:10.14800/macrophage.562.

86. Oral, H.B.; Kotenko, S.V.; Yılmaz, M.; Mani, O.; Zumkehr, J.; Blaser, K.; Akdis, C.A.; Akdis, M. Regulation of T cells and cytokines by the interleukin-10 (IL-10)-family cytokines IL-19, IL-20, IL-22, IL-24 andIL-26. *European Journal of Immunology* **2006**, *36*, 380-388, doi:https://doi.org/10.1002/eji.200425523.

87. Richards, J.; Gabunia, K.; Kelemen, S.E.; Kako, F.; Choi, E.T.; Autieri, M.V. Interleukin-19 increases angiogenesis in ischemic hind limbs by direct effects on both endothelial cells and macrophage polarization. *J Mol Cell Cardiol* **2015**, *79*, 21-31, doi:10.1016/j.yjmcc.2014.11.002.

88. Guo, J.; Wang, H.; Li, L.; Yuan, Y.; Shi, X.; Hou, S. Treatment with IL-19 improves locomotor functional recovery after contusion trauma to the spinal cord. *Br J Pharmacol* **2018**, *175*, 2611-2621, doi:10.1111/bph.14193.

89. Yan, X.; Sano, M. God gives IL-19 with both hands: Anti-inflammatory but pro-angiogenic. *Journal of Molecular and Cellular Cardiology* **2015**, *80*, 20-22, doi:https://doi.org/10.1016/j.yjmcc.2014.12.012.

90. Jain, S.; Gabunia, K.; Kelemen, S.E.; Panetti, T.S.; Autieri, M.V. The anti-inflammatory cytokine interleukin 19 is expressed by and angiogenic for human

endothelial cells. *Arterioscler Thromb Vasc Biol* **2011**, *31*, 167-175, doi:10.1161/atvbaha.110.214916.

91. Kako, F.; Gabunia, K.; Ray, M.; Kelemen, S.E.; England, R.N.; Kako, B.; Scalia, R.G.; Autieri, M.V. Interleukin-19 induces angiogenesis in the absence of hypoxia by direct and indirect immune mechanisms. *Am J Physiol Cell Physiol* **2016**, *310*, C931-941, doi:10.1152/ajpcell.00006.2016.

92. Leigh, T.; Scalia, R.G.; Autieri, M.V. Resolution of inflammation in immune and nonimmune cells by interleukin-19. *Am J Physiol Cell Physiol* **2020**, *319*, C457-c464, doi:10.1152/ajpcell.00247.2020.

93. An, W.; Yu, Y.; Zhang, Y.; Zhang, Z.; Yu, Y.; Zhao, X. Exogenous IL-19 attenuates acute ischaemic injury and improves survival in male mice with myocardial infarction. *Br J Pharmacol* **2019**, *176*, 699-710, doi:10.1111/bph.14549.

94. Xu, S.; Zhang, J.; Liu, J.; Ye, J.; Xu, Y.; Wang, Z.; Yu, J.; Ye, D.; Zhao, M.; Feng, Y.; et al. The role of interleukin-10 family members in cardiovascular diseases. *International Immunopharmacology* **2021**, *94*, 107475, doi:https://doi.org/10.1016/j.intimp.2021.107475.

95. Qi, L.; Zhang, J.; Wu, K.; Shi, S.; Ji, Q.; Miao, H.; Que, B. IL-19 as a Biomarker for the Severity of Acute Myocardial Infarction. *Archives of Medical Research* **2020**, *51*, 160-166, doi:https://doi.org/10.1016/j.arcmed.2020.01.007.

96. Riching, A.S.; Song, K. Cardiac Regeneration: New Insights Into the Frontier of Ischemic Heart Failure Therapy. *Frontiers in Bioengineering and Biotechnology* **2021**, *8*, doi:10.3389/fbioe.2020.637538.

97. Lopaschuk, G.D.; Collins-Nakai, R.L.; Itoi, T. Developmental changes in energy substrate use by the heart. *Cardiovasc Res* **1992**, *26*, 1172-1180, doi:10.1093/cvr/26.12.1172.

98. Mohr, M.E.; Li, S.; Trouten, A.M.; Stairley, R.A.; Roddy, P.L.; Liu, C.; Zhang, M.; Sucov, H.M.; Tao, G. Cardiomyocyte-fibroblast interaction regulates ferroptosis and fibrosis after myocardial injury. *iScience* **2024**, *27*, 109219, doi:10.1016/j.isci.2024.109219.

99. Friedmann Angeli, J.P.; Schneider, M.; Proneth, B.; Tyurina, Y.Y.; Tyurin, V.A.; Hammond, V.J.; Herbach, N.; Aichler, M.; Walch, A.; Eggenhofer, E.; et al. Inactivation of the ferroptosis regulator Gpx4 triggers acute renal failure in mice. *Nat Cell Biol* **2014**, *16*, 1180-1191, doi:10.1038/ncb3064.

100. Stockwell, B.R.; Friedmann Angeli, J.P.; Bayir, H.; Bush, A.I.; Conrad, M.; Dixon, S.J.; Fulda, S.; Gascón, S.; Hatzios, S.K.; Kagan, V.E.; et al. Ferroptosis: A Regulated

Cell Death Nexus Linking Metabolism, Redox Biology, and Disease. *Cell* **2017**, *171*, 273-285, doi:10.1016/j.cell.2017.09.021.

101. Young, R.C.; Ozols, R.F.; Myers, C.E. The anthracycline antineoplastic drugs. *N Engl J Med* **1981**, *305*, 139-153, doi:10.1056/nejm198107163050305.

102. Singal, P.K.; Iliskovic, N. Doxorubicin-induced cardiomyopathy. *N Engl J Med* **1998**, *339*, 900-905, doi:10.1056/nejm199809243391307.

103. Christidi, E.; Brunham, L.R. Regulated cell death pathways in doxorubicin-induced cardiotoxicity. *Cell Death Dis* **2021**, *12*, 339, doi:10.1038/s41419-021-03614-x.

104. Minotti, G.; Ronchi, R.; Salvatorelli, E.; Menna, P.; Cairo, G. Doxorubicin irreversibly inactivates iron regulatory proteins 1 and 2 in cardiomyocytes: evidence for distinct metabolic pathways and implications for iron-mediated cardiotoxicity of antitumor therapy. *Cancer Res* **2001**, *61*, 8422-8428.

105. Xiao, Z.; Kong, B.; Fang, J.; Qin, T.; Dai, C.; Shuai, W.; Huang, H. Ferrostatin-1 alleviates lipopolysaccharide-induced cardiac dysfunction. *Bioengineered* **2021**, *12*, 9367-9376, doi:10.1080/21655979.2021.2001913.

106. Chiong, M.; Wang, Z.V.; Pedrozo, Z.; Cao, D.J.; Troncoso, R.; Ibacache, M.; Criollo, A.; Nemchenko, A.; Hill, J.A.; Lavandero, S. Cardiomyocyte death: mechanisms and translational implications. *Cell Death & Disease* **2011**, *2*, e244-e244, doi:10.1038/cddis.2011.130.

107. Li, R.L.; Fan, C.H.; Gong, S.Y.; Kang, S. Effect and Mechanism of LRP6 on Cardiac Myocyte Ferroptosis in Myocardial Infarction. *Oxid Med Cell Longev* **2021**, *2021*, 8963987, doi:10.1155/2021/8963987.

108. Wu, Y.-T.; Zhang, G.-Y.; Hua, Y.; Fan, H.-J.; Han, X.; Xu, H.-L.; Chen, G.-H.; Liu, B.; Xie, L.-P.; Zhou, Y.-C. Ferrostatin-1 suppresses cardiomyocyte ferroptosis after myocardial infarction by activating Nrf2 signaling. *Journal of Pharmacy and Pharmacology* **2023**, *75*, 1467-1477, doi:10.1093/jpp/rgad080.

109. Gan, B. How erastin assassinates cells by ferroptosis revealed. *Protein & Cell* **2023**, *14*, 84-86, doi:10.1093/procel/pwac007.

110. dos Santos, L.; Salles, T.A.; Arruda-Junior, D.F.; Campos, L.C.G.; Pereira, A.C.; Barreto, A.L.T.; Antonio, E.L.; Mansur, A.J.; Tucci, P.J.F.; Krieger, J.E.; et al. Circulating Dipeptidyl Peptidase IV Activity Correlates With Cardiac Dysfunction in Human and Experimental Heart Failure. *Circulation: Heart Failure* **2013**, *6*, 1029-1038, doi:10.1161/CIRCHEARTFAILURE.112.000057.

111. Xu, J.Y.; Xiong, Y.Y.; Tang, R.J.; Jiang, W.Y.; Ning, Y.; Gong, Z.T.; Huang, P.S.; Chen, G.H.; Xu, J.; Wu, C.X.; et al. Interleukin-5-induced eosinophil population improves

cardiac function after myocardial infarction. *Cardiovasc Res* **2022**, *118*, 2165-2178, doi:10.1093/cvr/cvab237.

112. He, X.; Du, T.; Long, T.; Liao, X.; Dong, Y.; Huang, Z.P. Signaling cascades in the failing heart and emerging therapeutic strategies. *Signal Transduct Target Ther* **2022**, *7*, 134, doi:10.1038/s41392-022-00972-6.

113. Angrisano, T.; Varrone, F.; Ragozzino, E.; Fico, A.; Minchiotti, G.; Brancaccio, M. Cripto Is Targeted by miR-1a-3p in a Mouse Model of Heart Development. *International Journal of Molecular Sciences* **2023**, *24*, doi:10.3390/ijms241512251.

114. Bakhshian Nik, A.; Alvarez-Argote, S.; O'Meara, C.C. Interleukin 4/13 signaling in cardiac regeneration and repair. *Am J Physiol Heart Circ Physiol* **2022**, *323*, H833-h844, doi:10.1152/ajpheart.00310.2022.

115. Naba, A.; Clauser, K.R.; Hoersch, S.; Liu, H.; Carr, S.A.; Hynes, R.O. The matrisome: in silico definition and in vivo characterization by proteomics of normal and tumor extracellular matrices. *Mol Cell Proteomics* **2012**, *11*, M111.014647, doi:10.1074/mcp.M111.014647.

116. Subramanian, A.; Tamayo, P.; Mootha, V.K.; Mukherjee, S.; Ebert, B.L.; Gillette, M.A.; Paulovich, A.; Pomeroy, S.L.; Golub, T.R.; Lander, E.S.; et al. Gene set enrichment analysis: A knowledge-based approach for interpreting genome-wide expression profiles. *Proceedings of the National Academy of Sciences* **2005**, *102*, 15545-15550, doi:10.1073/pnas.0506580102.

117. Ouyang, W.; O'Garra, A. IL-10 Family Cytokines IL-10 and IL-22: from Basic Science to Clinical Translation. *Immunity* **2019**, *50*, 871-891, doi:10.1016/j.immuni.2019.03.020.

118. Autieri, M.V. IL-19 and Other IL-20 Family Member Cytokines in Vascular Inflammatory Diseases. *Frontiers in Immunology* **2018**, *9*, doi:10.3389/fimmu.2018.00700.

119. Tsao, C.W.; Aday, A.W.; Almarzooq, Z.I.; Anderson, C.A.M.; Arora, P.; Avery, C.L.; Baker-Smith, C.M.; Beaton, A.Z.; Boehme, A.K.; Buxton, A.E.; et al. Heart Disease and Stroke Statistics—2023 Update: A Report From the American Heart Association. *Circulation* **2023**, *147*, e93-e621, doi:10.1161/CIR.0000000000001123.

120. Seow, K.S.; Ling, A.P.K. Mesenchymal stem cells as future treatment for cardiovascular regeneration and its challenges. *Ann Transl Med* **2024**, *12*, 73, doi:10.21037/atm-23-1936.

121. Miotto, G.; Rossetto, M.; Di Paolo, M.L.; Orian, L.; Venerando, R.; Roveri, A.; Vučković, A.M.; Bosello Travain, V.; Zaccarin, M.; Zennaro, L.; et al. Insight into the mechanism of ferroptosis inhibition by ferrostatin-1. *Redox Biol* **2020**, *28*, 101328, doi:10.1016/j.redox.2019.101328.

122. Tsikas, D. Assessment of lipid peroxidation by measuring malondialdehyde (MDA) and relatives in biological samples: Analytical and biological challenges. *Analytical Biochemistry* **2017**, *524*, 13-30, doi:https://doi.org/10.1016/j.ab.2016.10.021.

123. Moldogazieva, N.T.; Mokhosoev, I.M.; Mel'nikova, T.I.; Porozov, Y.B.; Terentiev, A.A. Oxidative Stress and Advanced Lipoxidation and Glycation End Products (ALEs and AGEs) in Aging and Age-Related Diseases. *Oxid Med Cell Longev* **2019**, *2019*, 3085756, doi:10.1155/2019/3085756.

124. Yang, F.; Liu, Y.-H.; Yang, X.-P.; Xu, J.; Kapke, A.; Carretero, O.A. Myocardial Infarction and Cardiac Remodelling in Mice. *Experimental Physiology* **2002**, *87*, 547-555, doi:https://doi.org/10.1113/eph8702385.

125. Walsh, S.; Pontén, A.; Fleischmann, B.K.; Jovinge, S. Cardiomyocyte cell cycle control and growth estimation in vivo—an analysis based on cardiomyocyte nuclei. *Cardiovasc Res* **2010**, *86*, 365-373, doi:10.1093/cvr/cvq005.

126. O'Neill, T.J.t.; Mack, C.P.; Taylor, J.M. Germline deletion of FAK-related non-kinase delays post-natal cardiomyocyte mitotic arrest. *J Mol Cell Cardiol* **2012**, *53*, 156-164, doi:10.1016/j.yjmcc.2012.04.007.

127. Thayyullathil, F.; Chathoth, S.; Hago, A.; Patel, M.; Galadari, S. Rapid reactive oxygen species (ROS) generation induced by curcumin leads to caspase-dependent and -independent apoptosis in L929 cells. *Free Radical Biology and Medicine* **2008**, *45*, 1403-1412, doi:https://doi.org/10.1016/j.freeradbiomed.2008.08.014.

128. Kizhakkayil, J.; Thayyullathil, F.; Chathoth, S.; Hago, A.; Patel, M.; Galadari, S. Glutathione regulates caspase-dependent ceramide production and curcumin-induced apoptosis in human leukemic cells. *Free Radical Biology and Medicine* **2012**, *52*, 1854-1864, doi:https://doi.org/10.1016/j.freeradbiomed.2012.02.026.

129. Neitemeier, S.; Jelinek, A.; Laino, V.; Hoffmann, L.; Eisenbach, I.; Eying, R.; Ganjam, G.K.; Dolga, A.M.; Oppermann, S.; Culmsee, C. BID links ferroptosis to mitochondrial cell death pathways. *Redox Biol* **2017**, *12*, 558-570, doi:10.1016/j.redox.2017.03.007.

130. Talkhabi, M.; Aghdami, N.; Baharvand, H. Human cardiomyocyte generation from pluripotent stem cells: A state-of-art. *Life Sciences* **2016**, *145*, 98-113, doi:https://doi.org/10.1016/j.lfs.2015.12.023.

131. Li, J.; Feng, X.; Wei, X. Modeling hypertrophic cardiomyopathy with human cardiomyocytes derived from induced pluripotent stem cells. *Stem Cell Res Ther* **2022**, *13*, 232, doi:10.1186/s13287-022-02905-0.

132. Lambeir, A.M.; Durinx, C.; Scharpé, S.; De Meester, I. Dipeptidyl-peptidase IV from bench to bedside: an update on structural properties, functions, and clinical aspects of the enzyme DPP IV. *Crit Rev Clin Lab Sci* **2003**, *40*, 209-294, doi:10.1080/713609354.

133. Rios-Navarro, C.; Gavara, J.; Vidal, V.; Bonanad, C.; Racugno, P.; Bayes-Genis, A.; Miñana, G.; Husser, O.; Oltra, R.; Nuñez, J.; et al. Characterization and implications of the dynamics of eosinophils in blood and in the infarcted myocardium after coronary reperfusion. *PLoS One* **2018**, *13*, e0206344, doi:10.1371/journal.pone.0206344.

134. Kim, N.H.; Kang, P.M. Apoptosis in cardiovascular diseases: mechanism and clinical implications. *Korean Circ J* **2010**, *40*, 299-305, doi:10.4070/kcj.2010.40.7.299.

135. Hu, X.; li, J.; Fu, M.; Zhao, X.; Wang, W. The JAK/STAT signaling pathway: from bench to clinic. *Signal Transduction and Targeted Therapy* **2021**, *6*, 402, doi:10.1038/s41392-021-00791-1.

136. Kilian, L.S.; Frank, D.; Rangrez, A.Y. RhoA Signaling in Immune Cell Response and Cardiac Disease. *Cells* **2021**, *10*, doi:10.3390/cells10071681.

137. Ninh, V.K.; Brown, J.H. The contribution of the cardiomyocyte to tissue inflammation in cardiomyopathies. *Curr Opin Physiol* **2021**, *19*, 129-134, doi:10.1016/j.cophys.2020.10.003.

138. Prabhu, S.D.; Frangogiannis, N.G. The Biological Basis for Cardiac Repair After Myocardial Infarction: From Inflammation to Fibrosis. *Circ Res* **2016**, *119*, 91-112, doi:10.1161/circresaha.116.303577.

139. Martín-Bórnez, M.; Falcón, D.; Morrugares, R.; Siegfried, G.; Khatib, A.M.; Rosado, J.A.; Galeano-Otero, I.; Smani, T. New Insights into the Reparative Angiogenesis after Myocardial Infarction. *Int J Mol Sci* **2023**, *24*, doi:10.3390/ijms241512298.

140. Blanco, R.; Gerhardt, H. VEGF and Notch in tip and stalk cell selection. *Cold Spring Harb Perspect Med* **2013**, *3*, a006569, doi:10.1101/cshperspect.a006569.

141. Guo, Y.; Zhang, S.; Wang, D.; Heng, B.C.; Deng, X. Role of cell rearrangement and related signaling pathways in the dynamic process of tip cell selection. *Cell Communication and Signaling* **2024**, *22*, 24, doi:10.1186/s12964-023-01364-1.

142. Mouton, A.J.; Ma, Y.; Rivera Gonzalez, O.J.; Daseke, M.J.; Flynn, E.R.; Freeman, T.C.; Garrett, M.R.; DeLeon-Pennell, K.Y.; Lindsey, M.L. Fibroblast polarization over the myocardial infarction time continuum shifts roles from inflammation to angiogenesis. *Basic Res Cardiol* **2019**, *114*, 6, doi:10.1007/s00395-019-0715-4.

143. Lužnik, Z.; Anchouche, S.; Dana, R.; Yin, J. Regulatory T Cells in Angiogenesis. *J Immunol* **2020**, *205*, 2557-2565, doi:10.4049/jimmunol.2000574.

144. Krock, B.L.; Skuli, N.; Simon, M.C. Hypoxia-induced angiogenesis: good and evil. *Genes Cancer* **2011**, *2*, 1117-1133, doi:10.1177/1947601911423654.

145. Zheng, J.; Chen, P.; Zhong, J.; Cheng, Y.; Chen, H.; He, Y.; Chen, C. HIF-1α in myocardial ischemia-reperfusion injury (Review). *Mol Med Rep* **2021**, *23*, doi:10.3892/mmr.2021.11991.

146. Choudhry, H.; Harris, A.L. Advances in Hypoxia-Inducible Factor Biology. *Cell Metabolism* **2018**, *27*, 281-298, doi:10.1016/j.cmet.2017.10.005.

147. Lee, J.W.; Ko, J.; Ju, C.; Eltzschig, H.K. Hypoxia signaling in human diseases and therapeutic targets. *Exp Mol Med* **2019**, *51*, 1-13, doi:10.1038/s12276-019-0235-1.

148. Hu, K.; Babapoor-Farrokhran, S.; Rodrigues, M.; Deshpande, M.; Puchner, B.; Kashiwabuchi, F.; Hassan, S.J.; Asnaghi, L.; Handa, J.T.; Merbs, S.; et al. Hypoxia-inducible factor 1 upregulation of both VEGF and ANGPTL4 is required to promote the angiogenic phenotype in uveal melanoma. *Oncotarget* **2016**, *7*, 7816-7828, doi:10.18632/oncotarget.6868.

149. Hsieh, P.C.; Davis, M.E.; Lisowski, L.K.; Lee, R.T. Endothelial-cardiomyocyte interactions in cardiac development and repair. *Annu Rev Physiol* **2006**, *68*, 51-66, doi:10.1146/annurev.physiol.68.040104.124629.

150. Kivelä, R.; Hemanthakumar, K.A.; Vaparanta, K.; Robciuc, M.; Izumiya, Y.; Kidoya, H.; Takakura, N.; Peng, X.; Sawyer, D.B.; Elenius, K.; et al. Endothelial Cells Regulate Physiological Cardiomyocyte Growth via VEGFR2-Mediated Paracrine Signaling. *Circulation* **2019**, *139*, 2570-2584, doi:10.1161/CIRCULATIONAHA.118.036099.

151. Zhang, G.; Yang, X.; Gao, R. Research progress on the structure and function of endomucin. *Animal Model Exp Med* **2020**, *3*, 325-329, doi:10.1002/ame2.12142.

152. Li, D.W.; Yang, Q.; Chen, J.T.; Zhou, H.; Liu, R.M.; Huang, X.T. Dynamic distribution of Ser-10 phosphorylated histone H3 in cytoplasm of MCF-7 and CHO cells during mitosis. *Cell Research* **2005**, *15*, 120-126, doi:10.1038/sj.cr.7290276.

153. Kar, A.; Sable, M.; A, A.; Jena, S.K.; Tripathy, P.R.; Gaikwad, M. An Immunohistochemical Study of Proliferation of Human Fetal Heart Cardiomyocyte With Phospho-Histone H3 Antibody. *Cureus* **2023**, *15*, e41159, doi:10.7759/cureus.41159.

154. Belmokhtar, C.A.; Hillion, J.; Ségal-Bendirdjian, E. Staurosporine induces apoptosis through both caspase-dependent and caspase-independent mechanisms. *Oncogene* **2001**, *20*, 3354-3362, doi:10.1038/sj.onc.1204436.

155. DeCicco-Skinner, K.L.; Henry, G.H.; Cataisson, C.; Tabib, T.; Gwilliam, J.C.; Watson, N.J.; Bullwinkle, E.M.; Falkenburg, L.; O'Neill, R.C.; Morin, A.; et al. Endothelial cell tube formation assay for the in vitro study of angiogenesis. *J Vis Exp* **2014**, e51312, doi:10.3791/51312.

156. Xie, D.; Ju, D.; Speyer, C.; Gorski, D.; Kosir, M.A. Strategic Endothelial Cell Tube Formation Assay: Comparing Extracellular Matrix and Growth Factor Reduced Extracellular Matrix. *J Vis Exp* **2016**, doi:10.3791/54074.

157. Kubota, Y.; Kleinman, H.K.; Martin, G.R.; Lawley, T.J. Role of laminin and basement membrane in the morphological differentiation of human endothelial cells into capillary-like structures. *J Cell Biol* **1988**, *107*, 1589-1598, doi:10.1083/jcb.107.4.1589.

158. Carpentier, G.; Berndt, S.; Ferratge, S.; Rasband, W.; Cuendet, M.; Uzan, G.; Albanese, P. Angiogenesis Analyzer for ImageJ — A comparative morphometric analysis of “Endothelial Tube Formation Assay” and “Fibrin Bead Assay”. *Scientific Reports* **2020**, *10*, 11568, doi:10.1038/s41598-020-67289-8.

159. Marquez-Curtis, L.A.; Sultani, A.B.; McGann, L.E.; Elliott, J.A.W. Beyond membrane integrity: Assessing the functionality of human umbilical vein endothelial cells after cryopreservation. *Cryobiology* **2016**, *72*, 183-190, doi:https://doi.org/10.1016/j.cryobiol.2016.05.005.

160. Jonkman, J.E.; Cathcart, J.A.; Xu, F.; Bartolini, M.E.; Amon, J.E.; Stevens, K.M.; Colarusso, P. An introduction to the wound healing assay using live-cell microscopy. *Cell Adh Migr* **2014**, *8*, 440-451, doi:10.4161/cam.36224.

161. Pijuan, J.; Barceló, C.; Moreno, D.F.; Maiques, O.; Sisó, P.; Marti, R.M.; Macià, A.; Panosa, A. In vitro Cell Migration, Invasion, and Adhesion Assays: From Cell

Imaging to Data Analysis. *Front Cell Dev Biol* **2019**, *7*, 107, doi:10.3389/fcell.2019.00107.

162. Li, N.; Wang, W.; Zhou, H.; Wu, Q.; Duan, M.; Liu, C.; Wu, H.; Deng, W.; Shen, D.; Tang, Q. Ferritinophagy-mediated ferroptosis is involved in sepsis-induced cardiac injury. *Free Radical Biology and Medicine* **2020**, *160*, 303-318, doi:https://doi.org/10.1016/j.freeradbiomed.2020.08.009.

163. Sun, Y. Myocardial repair/remodelling following infarction: roles of local factors. *Cardiovasc Res* **2009**, *81*, 482-490, doi:10.1093/cvr/cvn333.

164. Li, T.; Yan, Z.; Fan, Y.; Fan, X.; Li, A.; Qi, Z.; Zhang, J. Cardiac repair after myocardial infarction: A two-sided role of inflammation-mediated. *Frontiers in Cardiovascular Medicine* **2023**, *9*.

165. Burke, R.M.; Burgos Villar, K.N.; Small, E.M. Fibroblast contributions to ischemic cardiac remodeling. *Cell Signal* **2021**, *77*, 109824, doi:10.1016/j.cellsig.2020.109824.

166. Ma, Y.; Mouton, A.J.; Lindsey, M.L. Cardiac macrophage biology in the steady-state heart, the aging heart, and following myocardial infarction. *Transl Res* **2018**, *191*, 15-28, doi:10.1016/j.trsl.2017.10.001.

167. Sun, X.; Li, Y.; Deng, Q.; Hu, Y.; Dong, J.; Wang, W.; Wang, Y.; Li, C. Macrophage Polarization, Metabolic Reprogramming, and Inflammatory Effects in Ischemic Heart Disease. *Front Immunol* **2022**, *13*, 934040, doi:10.3389/fimmu.2022.934040.

168. Carbone, M.L.; Failla, C.M. Interleukin role in the regulation of endothelial cell pathological activation. *Vascular Biology* **2021**, *3*, R96-R105, doi:10.1530/VB-21-0010.

169. Schelemei, P.; Wagner, E.; Picard, F.S.R.; Winkels, H. Macrophage mediators and mechanisms in cardiovascular disease. *The FASEB Journal* **2024**, *38*, e23424, doi:https://doi.org/10.1096/fj.202302001R.

170. Ouyang, W.; O'Garra, A. IL-10 Family Cytokines IL-10 and IL-22: from Basic Science to Clinical Translation. *Immunity* **2019**, *50*, 871-891, doi:10.1016/j.immuni.2019.03.020.

171. Ho, M.K.; Springer, T.A. Tissue distribution, structural characterization, and biosynthesis of Mac-3, a macrophage surface glycoprotein exhibiting molecular weight heterogeneity. *J Biol Chem* **1983**, *258*, 636-642.

172. Stein, M.; Keshav, S.; Harris, N.; Gordon, S. Interleukin 4 potently enhances murine macrophage mannose receptor activity: a marker of alternative

immunologic macrophage activation. *J Exp Med* **1992**, *176*, 287-292, doi:10.1084/jem.176.1.287.

173. Gordon, S.; Martinez, F.O. Alternative Activation of Macrophages: Mechanism and Functions. *Immunity* **2010**, *32*, 593-604, doi:10.1016/j.immuni.2010.05.007.

174. Gabunia, K.; Ellison, S.; Kelemen, S.; Kako, F.; Cornwell, W.D.; Rogers, T.J.; Datta, P.K.; Ouimet, M.; Moore, K.J.; Autieri, M.V. IL-19 Halts Progression of Atherosclerotic Plaque, Polarizes, and Increases Cholesterol Uptake and Efflux in Macrophages. *Am J Pathol* **2016**, *186*, 1361-1374, doi:10.1016/j.ajpath.2015.12.023.

175. Zhang, Y.; Gago-Lopez, N.; Li, N.; Zhang, Z.; Alver, N.; Liu, Y.; Martinson, A.M.; Mehri, A.; MacLellan, W.R. Single-cell imaging and transcriptomic analyses of endogenous cardiomyocyte dedifferentiation and cycling. *Cell Discovery* **2019**, *5*, 30, doi:10.1038/s41421-019-0095-9.

176. Almet, A.A.; Cang, Z.; Jin, S.; Nie, Q. The landscape of cell-cell communication through single-cell transcriptomics. *Curr Opin Syst Biol* **2021**, *26*, 12-23, doi:10.1016/j.coisb.2021.03.007.

177. Almet, A.A.; Cang, Z.; Jin, S.; Nie, Q. The landscape of cell–cell communication through single-cell transcriptomics. *Current Opinion in Systems Biology* **2021**, *26*, 12-23, doi:https://doi.org/10.1016/j.coisb.2021.03.007.

178. Kumfu, S.; Sripetchwandee, J.; Thonusin, C.; Sumneang, N.; Maneechote, C.; Arunsak, B.; Chunchai, T.; Oo, T.T.; Kongkaew, A.; Chattipakorn, S.C.; et al. Ferroptosis inhibitor improves cardiac function more effectively than inhibitors of apoptosis and necroptosis through cardiac mitochondrial protection in rats with iron-overloaded cardiomyopathy. *Toxicology and Applied Pharmacology* **2023**, *479*, 116727, doi:https://doi.org/10.1016/j.taap.2023.116727.

179. Kawasaki, N.K.; Suhara, T.; Komai, K.; Shimada, B.K.; Yorichika, N.; Kobayashi, M.; Baba, Y.; Higa, J.K.; Matsui, T. The role of ferroptosis in cell-to-cell propagation of cell death initiated from focal injury in cardiomyocytes. *Life Sciences* **2023**, *332*, 122113, doi:https://doi.org/10.1016/j.lfs.2023.122113.

180. Wan, E.; Yeap, X.Y.; Dehn, S.; Terry, R.; Novak, M.; Zhang, S.; Iwata, S.; Han, X.; Homma, S.; Drosatos, K.; et al. Enhanced efferocytosis of apoptotic cardiomyocytes through myeloid-epithelial-reproductive tyrosine kinase links acute inflammation resolution to cardiac repair after infarction. *Circ Res* **2013**, *113*, 1004-1012, doi:10.1161/circresaha.113.301198.

181. Abdelaziz, M.H.; Abdelwahab, S.F.; Wan, J.; Cai, W.; Huixuan, W.; Jianjun, C.; Kumar, K.D.; Vasudevan, A.; Sadek, A.; Su, Z.; et al. Alternatively activated

macrophages; a double-edged sword in allergic asthma. *J Transl Med* **2020**, *18*, 58, doi:10.1186/s12967-020-02251-w.

182. O'Rourke, S.A.; Dunne, A.; Monaghan, M.G. The Role of Macrophages in the Infarcted Myocardium: Orchestrators of ECM Remodeling. *Front Cardiovasc Med* **2019**, *6*, 101, doi:10.3389/fcvm.2019.00101.

183. Sironi, M.; Martinez, F.O.; D'Ambrosio, D.; Gattorno, M.; Polentarutti, N.; Locati, M.; Gregorio, A.; Iellem, A.; Cassatella, M.A.; Van Damme, J.; et al. Differential regulation of chemokine production by Fcγ receptor engagement in human monocytes: association of CCL1 with a distinct form of M2 monocyte activation (M2b, Type 2). *Journal of Leukocyte Biology* **2006**, *80*, 342-349, doi:10.1189/jlb.1005586.

184. Berger, A. Th1 and Th2 responses: what are they? *Bmj* **2000**, *321*, 424, doi:10.1136/bmj.321.7258.424.

185. Chang-Hoon, L.; Eun Young, C. Macrophages and Inflammation. *J Rheum Dis* **2018**, *25*, 11-18, doi:10.4078/jrd.2018.25.1.11.

186. Li, P.; Ma, C.; Li, J.; You, S.; Dang, L.; Wu, J.; Hao, Z.; Li, J.; Zhi, Y.; Chen, L.; et al. Proteomic characterization of four subtypes of M2 macrophages derived from human THP-1 cells. *J Zhejiang Univ Sci B* **2022**, *23*, 407-422, doi:10.1631/jzus.B2100930.

187. Nikovics, K.; Favier, A.L. Macrophage Identification In Situ. *Biomedicines* **2021**, *9*, doi:10.3390/biomedicines9101393.

188. Hao, Y.; Hao, S.; Andersen-Nissen, E.; Mauck, W.M., 3rd; Zheng, S.; Butler, A.; Lee, M.J.; Wilk, A.J.; Darby, C.; Zager, M.; et al. Integrated analysis of multimodal single-cell data. *Cell* **2021**, *184*, 3573-3587.e3529, doi:10.1016/j.cell.2021.04.048.

189. Jin, S.; Guerrero-Juarez, C.F.; Zhang, L.; Chang, I.; Ramos, R.; Kuan, C.-H.; Myung, P.; Plikus, M.V.; Nie, Q. Inference and analysis of cell-cell communication using CellChat. *Nature Communications* **2021**, *12*, 1088, doi:10.1038/s41467-021-21246-9.

190. Chen, C.; Wang, J.; Liu, C.; Hu, J. Cardiac resident macrophages: key regulatory mediators in the aftermath of myocardial infarction. *Front Immunol* **2023**, *14*, 1207100, doi:10.3389/fimmu.2023.1207100.

191. Dick, S.A.; Macklin, J.A.; Nejat, S.; Momen, A.; Clemente-Casares, X.; Althagafi, M.G.; Chen, J.; Kantores, C.; Hosseinzadeh, S.; Aronoff, L.; et al. Self-renewing resident cardiac macrophages limit adverse remodeling following myocardial infarction. *Nat Immunol* **2019**, *20*, 29-39, doi:10.1038/s41590-018-0272-2.

192. Bizou, M.; Itier, R.; Majdoubi, M.; Abbadi, D.; Pichery, E.; Dutaur, M.; Marsal, D.; Calise, D.; Garmy-Susini, B.; Douin-Echinard, V.; et al. Cardiac macrophage subsets differentially regulate lymphatic network remodeling during pressure overload. *Scientific Reports* **2021**, *11*, 16801, doi:10.1038/s41598-021-95723-y.

193. Kim, Y.M.; Kim, K.E.; Koh, G.Y.; Ho, Y.-S.; Lee, K.-J. Hydrogen Peroxide Produced by Angiopoietin-1 Mediates Angiogenesis. *Cancer Research* **2006**, *66*, 6167-6174, doi:10.1158/0008-5472.CAN-05-3640.

194. Nishizawa, H.; Matsumoto, M.; Chen, G.; Ishii, Y.; Tada, K.; Onodera, M.; Kato, H.; Muto, A.; Tanaka, K.; Igarashi, K. Lipid peroxidation and the subsequent cell death transmitting from ferroptotic cells to neighboring cells. *Cell Death & Disease* **2021**, *12*, 332, doi:10.1038/s41419-021-03613-y.

195. Chan, W.; Taylor, A.J.; Ellims, A.H.; Lefkovits, L.; Wong, C.; Kingwell, B.A.; Natoli, A.; Croft, K.D.; Mori, T.; Kaye, D.M.; et al. Effect of Iron Chelation on Myocardial Infarct Size and Oxidative Stress in ST-Elevation–Myocardial Infarction. *Circulation: Cardiovascular Interventions* **2012**, *5*, 270-278, doi:10.1161/CIRCINTERVENTIONS.111.966226.

196. Aisagbonhi, O.; Rai, M.; Ryzhov, S.; Atria, N.; Feoktistov, I.; Hatzopoulos, A.K. Experimental myocardial infarction triggers canonical Wnt signaling and endothelial-to-mesenchymal transition. *Dis Model Mech* **2011**, *4*, 469-483, doi:10.1242/dmm.006510.

197. Gerhardt, H.; Golding, M.; Fruttiger, M.; Ruhrberg, C.; Lundkvist, A.; Abramsson, A.; Jeltsch, M.; Mitchell, C.; Alitalo, K.; Shima, D.; et al. VEGF guides angiogenic sprouting utilizing endothelial tip cell filopodia. *J Cell Biol* **2003**, *161*, 1163-1177, doi:10.1083/jcb.200302047.

198. Gao, H.; Zhang, J.; Liu, T.; Shi, W. Rapamycin prevents endothelial cell migration by inhibiting the endothelial-to-mesenchymal transition and matrix metalloproteinase-2 and -9: an in vitro study. *Mol Vis* **2011**, *17*, 3406-3414.

199. Tombor, L.S.; John, D.; Glaser, S.F.; Luxán, G.; Forte, E.; Furtado, M.; Rosenthal, N.; Baumgarten, N.; Schulz, M.H.; Wittig, J.; et al. Single cell sequencing reveals endothelial plasticity with transient mesenchymal activation after myocardial infarction. *Nat Commun* **2021**, *12*, 681, doi:10.1038/s41467-021-20905-1.

200. Kim, H.-M.; Kang, D.-K.; Kim, H.Y.; Kang, S.S.; Chang, S.-I. Angiogenin-induced protein kinase B/Akt activation is necessary for angiogenesis but is independent of nuclear translocation of angiogenin in HUVE cells. *Biochemical and Biophysical Research Communications* **2007**, *352*, 509-513, doi:https://doi.org/10.1016/j.bbrc.2006.11.047.

201. Bui, T.M.; Wiesolek, H.L.; Sumagin, R. ICAM-1: A master regulator of cellular responses in inflammation, injury resolution, and tumorigenesis. *J Leukoc Biol* **2020**, *108*, 787-799, doi:10.1002/jlb.2mr0220-549r.

202. Watanabe, K.; Bianco, C.; Strizzi, L.; Hamada, S.; Mancino, M.; Bailly, V.; Mo, W.; Wen, D.; Miatkowski, K.; Gonzales, M.; et al. Growth Factor Induction of Cripto-1 Shedding by Glycosylphosphatidylinositol-Phospholipase D and Enhancement of Endothelial Cell Migration *. *Journal of Biological Chemistry* **2007**, *282*, 31643-31655, doi:10.1074/jbc.M702713200.

203. Knutson, A.K.; Williams, A.L.; Boisvert, W.A.; Shohet, R.V. HIF in the heart: development, metabolism, ischemia, and atherosclerosis. *J Clin Invest* **2021**, *131*, doi:10.1172/jci137557.

204. Wong, B.W.; Marsch, E.; Treps, L.; Baes, M.; Carmeliet, P. Endothelial cell metabolism in health and disease: impact of hypoxia. *Embo j* **2017**, *36*, 2187-2203, doi:10.15252/embj.201696150.

205. Zecchin, A.; Kalucka, J.; Dubois, C.; Carmeliet, P. How Endothelial Cells Adapt Their Metabolism to Form Vessels in Tumors. *Front Immunol* **2017**, *8*, 1750, doi:10.3389/fimmu.2017.01750.

206. Ullah, K.; Wu, R. Hypoxia-Inducible Factor Regulates Endothelial Metabolism in Cardiovascular Disease. *Front Physiol* **2021**, *12*, 670653, doi:10.3389/fphys.2021.670653.

207. Akhtar, S.; Hartmann, P.; Karshovska, E.; Rinderknecht, F.-A.; Subramanian, P.; Gremse, F.; Grommes, J.; Jacobs, M.; Kiessling, F.; Weber, C.; et al. Endothelial Hypoxia-Inducible Factor-1α Promotes Atherosclerosis and Monocyte Recruitment by Upregulating MicroRNA-19a. *Hypertension* **2015**, *66*, 1220-1226, doi:10.1161/HYPERTENSIONAHA.115.05886.

208. Lian, X.; Zhang, J.; Azarin, S.M.; Zhu, K.; Hazeltine, L.B.; Bao, X.; Hsiao, C.; Kamp, T.J.; Palecek, S.P. Directed cardiomyocyte differentiation from human pluripotent stem cells by modulating Wnt/β-catenin signaling under fully defined conditions. *Nat Protoc* **2013**, *8*, 162-175, doi:10.1038/nprot.2012.150.

209. Carpentier, G.; Berndt, S.; Ferratge, S.; Rasband, W.; Cuendet, M.; Uzan, G.; Albanese, P. Angiogenesis Analyzer for ImageJ - A comparative morphometric analysis of "Endothelial Tube Formation Assay" and "Fibrin Bead Assay". *Sci Rep* **2020**, *10*, 11568, doi:10.1038/s41598-020-67289-8.

210. Zhou, Y.; Zhou, B.; Pache, L.; Chang, M.; Khodabakhshi, A.H.; Tanaseichuk, O.; Benner, C.; Chanda, S.K. Metascape provides a biologist-oriented resource for

the analysis of systems-level datasets. *Nature Communications* **2019**, *10*, 1523, doi:10.1038/s41467-019-09234-6.